TÉCNICO LISBOA

Modeling the kinetics of light cuts catalytic cracking

Development of a predictive tool

Tiago Miguel Porfírio Fonseca

Thesis to obtain the Master of Science Degree in

Chemical Engineering

Supervisors: Prof. Carla Isabel Costa Pinheiro
Doctor Joana de Lis Raposo Fernandes

Examination Committee

Chairperson: Prof. Sebastião Manuel Tavares Silva Alves
Supervisor: Prof. Carla Isabel Costa Pinheiro
Member of the Committee: Prof. Maria Amélia Nortadas Duarte de Almeida Lemos

October 2014

This page was intentionally left blank.

It is harder to crack prejudice than an atom.

Albert Einstein

This page was intentionally left blank.

Acknowledgments

The present work is the end of a cycle. The collaboration of some people was essential to achieve it, to whom I express a word of thankfulness.

First of all, I wish to express my gratitude to my both dissertation supervisors. A special word to Doctor Joana Fernandes for her patience, availability and encouragement to regard the verdicts by the positive way. Her experience thought providing me to think outside the box in technical and professional approaches. Also, I would like to thank my IST supervisor, Professor Carla Pinheiro, for her support and advices to pursue what I truly like to do. Moreover, I thank both of them for the final revision of this work.

I would like to thank to IFP Energies Nouvelles for give me the opportunity to make the dissertation, especially to Doctor Tiago Sozinho.

Also, I am grateful to Professor Filipa Ribeiro for all the help and support provided, not only in the last year of my course, but also during my internship.

A word of appreciation to my colleagues from IFPEN, who participated directly in the development of this work and helped me at all times.

To my colleagues from the university a huge thanks for your friendship, companionship and help during these five years. We shared good and bad moments and you encouraged me when I needed.

I am deeply grateful to my closest friends for being part of my life and for always being there for me.

Most important, a hug of thank to my entire family for their unconditional support, especially to my grandmother Josefina.

Last but not least, I would like to dedicate this work to my parents, *Teresinha* and José, and to my sister, Rita. They are my life pillars and without them, their love and support I could not achieve my objectives. A huge thank to my mum for her work and effort during these years.

Thanks. Merci. Obrigado.

This page was intentionally left blank.

Abstract

The propylene demand is quickly increasing. This product is an important intermediary for the production of several petrochemical derivatives such as polypropylene. For that reason the research for new techniques and on-purpose routes to produce propylene are rising.

FCC units produce propylene as a by-product. To achieve the market demand in terms of propylene has been proposed the creation of different upgrades on FCC. One of them consists in adding a second riser which is fed with light stream coming from the main riser or from other refinery units. With this configuration is possible to improve the propylene to over 12%.

To predict the yields for each type of feedstock, IFPEN is developing a simulator capable to predict the kinetic performance. The previous version of this simulator estimates with accuracy the yields for PONA composition. The model is shaped for catalytic gasoline and oligomer feeds with different sets of parameters.

The aim of the present work is the improvement of this predictive tool, by including isoparaffins, and also the estimation of a set of parameters for coker gasoline. For that, new components were considered and also the reactions involving isoparaffins: catalytic and thermal cracking and isomerization. Its implementation increased the execution time five to eleven times. It was possible to group in one set the parameters for gasolines. The oligomers are described in different sets of parameters.

Globally, it was not achieved better results comparing to 2012 data, but the first approach to introduce the new family was successfully accomplished.

Keywords

Propylene, fluid catalytic cracking, modeling, kinetics, second riser, isoparaffins

This page was intentionally left blank.

Resumo

A procura de propileno está a aumentar rapidamente. Esta componente é um importante intermediário na produção de diversos derivados petroquímicos. Por essa razão, a pesquisa de novas tecnologias está a crescer.

O processo de FCC produz propileno como subproduto. Para aumentar a produção em propileno, estão a ser propostas a criação de diferentes tecnologias sobre o FCC. Uma delas consiste na adição de um segundo riser, em que é alimentado pelo caudal de saída do riser principal, ou outro proveniente de outras unidades de refinação. Com esta configuração é possível aumentar o rendimento de propileno, atingindo valores superiores a 12%.

Para prever os rendimentos das diversas alimentações, o IFPEN está a desenvolver um simulador capaz de prever o desempenho cinético. A versão anterior deste simulador estima com precisão os rendimentos para a composição PONA. O modelo prevê a performance para cargas como gasolina catalítica e oligómeros, que são descritos por diferentes conjuntos de parâmetros cinéticos.

O presente trabalho tem como objectivo o melhoramento deste modelo, mais precisamente na introdução de isoparafinas, como estimar os rendimentos para a gasoline de coker. Para isso, foram introduzidos novos componentes e reacções que envolvem as isoparafinas: cracking catalitico e térmico e isomerização. Esta implementação aumentou o tempo de execução de cinco a onze vezes. As gasolinas foram agrupadas no mesmo conjunto de parâmetros. Enquanto os oligómeros são descritos por conjuntos distintos.

Globalmente, não foi possível obter melhores resultados que em 2012, mas a primeira abordagem para introduzir as isoparafinas foi realizada com sucesso.

Palavras-chave

Propileno, cracking catalítico em leito fluidizado, modelação, cinética, segundo riser, isoparafinas

This page was intentionally left blank.

Contents

Acknowledgments v

Abstract vii

Resumo ix

List of figures xiii

List of tables xvii

Nomenclature xix

Subscripts, Superscripts and Abbreviations xx

1. Introduction 1

1.1. Motivation 1

1.2. Objectives 2

1.3. Thesis outline 2

2. Literature review 3

2.1. Fluidized Catalytic Cracking process 3

2.2. Second riser configuration 4

2.2.1. Feedstocks 5

2.2.1. Products 6

2.2.2. Operating conditions 6

2.2.3. Catalyst 7

2.2.4. Catalytic Cracking Mechanism 11

2.3. Kinetic models overview 15

3. Experimental data 17

4. Second riser model and simulator 21

4.1. Reactive Species 21

4.2. Reaction network 22

4.3. Kinetic model 24

4.4. Model implementation 30

4.5. Model modifications 32

4.5.1. ZSM-5 effect review 32

4.5.2. LCO formation as a first order reaction 33

4.5.3. Isoparaffins implementation 33

4.6. Optimization 36
5. Results 39
5.1. Standard cuts yields prediction for all the feeds 43
5.2. Dry gas ($\boldsymbol{H2}$, $\boldsymbol{C1}$ and $\boldsymbol{C2}$) 44
5.2.1. Species distribution 46
5.3. LPG ($\boldsymbol{C3}$ and $\boldsymbol{C4}$) 50
5.3.1. Species distribution 52
5.4. Gasoline cut ($\boldsymbol{C5 - C12}$) 55
5.4.1. Olefin lump 57
5.4.2. Aromatic lump 59
5.4.3. Naphthene lump 64
5.4.4. Total paraffin lump 65
5.4.5. Isoparaffin lump 67
5.4.6. Isoparaffin and total paraffins ratio 68
5.5. LCO 71
5.6. Coke 73
6. Sensitivity analysis 77
7. Conclusions 79
8. Future work 81
References 83
Appendices 87
A1. Parity diagrams 87
A2. Absolute errors for other species 90
A3. Relative error for propylene and second riser cuts 93
A4. Mean squared error of prediction 94

List of figures

Figure 1 – Propylene world production distribution by type of route considering 75 million tons in 2010. The on-propose production technologies considered are: Metathesis, Olefins cracking, MeOH to propylene, C3 dehydrogenation (Dupraz, 2012) 1
Figure 2 – Conventional FCC process scheme (Fernandes, 2007) 3
Figure 3 - Reaction-regeneration integration (Gauthier, et al., 2000) 4
Figure 4 – Dual riser configuration scheme (Do, 2009) 5
Figure 5 – Possible sources of second riser feedstock: naphtha stream recycled from main riser (a) and oligomers from a oligomerization unit (b) (Do, 2009) 5
Figure 6 – FCC catalyst scheme (Sadeghbeigi, 2012) 7
Figure 7 – Effects of rare-earth on gasoline octane and yield, where RON is research octane number and MON is motor octane number (Sadeghbeigi, 2012) 8
Figure 8 – ZSM-5 effect in propylene and butylene yields (Fu, et al., 1998) 9
Figure 9 – Comparison of critical molecular parameters for the paraffins. $w - h$ is the average between the width and height for each paraffins that determine if the molecule can enter into the pore. iNCx is a linear alkane, iMCx is a methyl alkane, iECx is a ethyl alkane, ijDMCx is a dimethyl alkane, iMjECx is a methyl-ethyl alkane, ijyzTMCx is a trimethyl or tetramethyl alkane; where x is the carbon atoms number in principal chain and i, j, y, z the carbon number of the principal chain where the branched is located (Jiménez-Cruz & Laredo, 2004) 10
Figure 10 - β-scission (a) and protolytic cracking (b) mechanism for an alkane molecule (Rahimi & Karimzadeh, 2011) 12
Figure 11 – Preferential protonation and cracking of a 3-methylpentane molecule (Kotre, et al., 2000) 13
Figure 12 – Simplified reaction network for alkane cracking on zeolite catalysts (Guisnet & Gilson, 2002) 13
Figure 13 –Mechanism of coke formation, where Ol is oligomerization reaction, HT is hydrogen transfer and Cyc is cyclization (Cerqueira, et al., 2008) 14
Figure 14 – Coke formation from a) alkenes and aromatics and b) only aromatics, where Alk is alkylation reaction, HT is hydrogen transfer, Cyc is cyclization, ISOM is isomerization and DC is dehydrogenative coupling (Cerqueira, et al., 2008) 15
Figure 15 – Feedstocks PIONA composition in mass percentage 17
Figure 16 – Carbon atoms distribution for each feedstock 18
Figure 17 – R2R pilot unit scheme, where REG is the regenerator and C1 the fractionator column 18
Figure 18 – Representation of molecule structure function for catalytic cracking normalized with its maximum value 26
Figure 19 - ZSM-5 influence for kinetic rate of paraffins and olefins catalytic cracking in function of ZSM-5 content percentage 27
Figure 20 – Representation of $fht1$ normalized with its maximum value in function of i and j, the reactant carbon numbers 28

Figure 21 - ZSM-5 influence for kinetic rate of hydrogen transfer reaction (step 1) in function of ZSM-5 content percentage 28
Figure 22 – Representation of $fht3$ in function of i, the reactant carbon number 29
Figure 23 – Representation of $fth1$ and $fth2$ in function of i, the reactant carbon number 30
Figure 24 – Control volume scheme 31
Figure 25 – Comparison of ZSM-5 effect function in 2012 and its improvement in 2014 33
Figure 26 – Molecule structure function in catalytic cracking of normal and branched paraffins with 12 carbon atoms ($i = 12$). The values were normalized with the maximum value of both situations. 42
Figure 27 – Result representation of molecule structure function for isoparaffins catalytic cracking normalized with its maximum value 42
Figure 28 – Main cuts yields parity diagram for all the feeds 43
Figure 29 – Parity diagram of dry gas cut for catalytic and coker gasolines ($MSEPCatalytic\ gasol.2012 = 6 \times 10 - 4$; $MSEPCatalytic\ gasol.2014 = 5 \times 10 - 5$; $MSEPCoke\ gasol.2014 = 8 \times 10 - 5$) 44
Figure 30 - Parity diagram of dry gas cut for PolyC3C4 ($MSEP2012 = 3 \times 10 - 4$; $MSEP\ 2014 = 2 \times 10 - 4$) 45
Figure 31 - Parity diagram of dry gas cut for PolyC4 ($MSEP2012 = 2 \times 10 - 4$; $MSEP\ 2014 = 1 \times 10 - 4$) 45
Figure 32 – $P1$ parity diagram for catalytic and coker gasoline ($MSEPCatalytic\ gasol.2012 = 1 \times 10 - 4$; $MSEPCatalytic\ gasol.2014 = 6 \times 10 - 6$; $MSEPCoke\ gasol.2014 = 9 \times 10 - 5$) 46
Figure 33 - $P1$ parity diagram for PolyC3C4 ($MSEP2012 = 3 \times 10 - 5$; $MSEP\ 2014 = 4 \times 10 - 5$) 47
Figure 34 - $P1$ parity diagram for PolyC4 ($MSEP2012 = 6 \times 10 - 5$; $MSEP\ 2014 = 5 \times 10 - 5$) 47
Figure 35 – $P2$ parity diagram for catalytic and coker gasoline ($MSEPCatalytic\ gasol.2012 = 8 \times 10 - 6$; $MSEPCatalytic\ gasol.2014 = 1 \times 10 - 5$; $MSEPCoke\ gasol.2014 = 5 \times 10 - 5$) 48
Figure 36 – $P2$ parity diagram for PolyC3C4 ($MSEP2012 = 8 \times 10 - 5$; $MSEP\ 2014 = 3 \times 10 - 5$) 49
Figure 37 – $P2$ parity diagram for PolyC4 ($MSEP2012 = 9 \times 10 - 5$; $MSEP\ 2014 = 1 \times 10 - 4$) 49
Figure 38 - Parity diagram of LPG cut for catalytic and coker gasoline ($MSEPCatalytic\ gasol.2012 = 6 \times 10 - 4$; $MSEPCatalytic\ gasol.2014 = 4 \times 10 - 4$; $MSEPCoke\ gasol.2014 = 3 \times 10 - 3$) 50
Figure 39 - Parity diagram of LPG cut for PolyC3C4 ($MSEP2012 = 6 \times 10 - 4$; $MSEP\ 2014 = 3 \times 10 - 3$) 51
Figure 40 - Parity diagram of LPG cut for PolyC4 ($MSEP2012 = 5 \times 10 - 4$; $MSEP\ 2014 = 4 \times 10 - 4$) 51
Figure 41 – $O3$ parity diagram for catalytic and coker gasoline ($MSEPCatalytic\ gasol.2012 = 1 \times 10 - 4$; $MSEPCatalytic\ gasol.2014 = 9{,}7 \times 10 - 5$; $MSEPCoke\ gasol.2014 = 3 \times 10 - 4$) 52
Figure 42 - $O3$ parity diagram for PolyC3C4 ($MSEP2012 = 3 \times 10 - 4$; $MSEP\ 2014 = 1 \times 10 - 4$) 52
Figure 43 - $O3$ parity diagram for PolyC4 ($MSEP2012 = 1.6 \times 10 - 4$; $MSEP\ 2014 = 2.4 \times 10 - 4$) 53
Figure 44 – $O4$ parity diagram for catalytic and coker gasoline ($MSEPCatalytic\ gasol.2012 = 8 \times 10 - 5$; $MSEPCatalytic\ gasol.2014 = 1 \times 10 - 4$; $MSEPCoke\ gasol.2014 = 3 \times 10 - 4$) 54
Figure 45 - $O4$ parity diagram for PolyC3C4 ($MSEP2012 = 1.2 \times 10 - 3$; $MSEP\ 2014 = 9.7 \times 10 - 4$) 54
Figure 46 - $O4$ parity diagram for PolyC4 ($MSEP2012 = 1.7 \times 10 - 3$; $MSEP\ 2014 = 1.6 \times 10 - 3$) 55

Figure 47 - Parity diagram of gasoline cut for catalytic and coker gasolines ($MSEPCatalytic\ gasol.2012 = 8 \times 10 - 4$; $MSEPCatalytic\ gasol.2014 = 1 \times 10 - 3$; $MSEPCoke\ gasol.2014 = 5 \times 10 - 3$).....56
Figure 48 - Parity diagram of gasoline cut for PolyC3C4 ($MSEP2012 = 9 \times 10 - 4$; $MSEP\ 2014 = 2 \times 10 - 3$).....56
Figure 49 - Parity diagram of gasoline cut for PolyC4 ($MSEP2012 = 6.3 \times 10 - 4$; $MSEP\ 2014 = 6.4 \times 10 - 4$).....57
Figure 50 - Parity diagram of olefin lump in gasoline cut for catalytic and coker gasolines ($MSEPCatalytic\ gasol.2012 = 1 \times 10 - 4$; $MSEPCatalytic\ gasol.2014 = 2 \times 10 - 5$; $MSEPCoke\ gasol.2014 = 2 \times 10 - 4$).....58
Figure 51 - Parity diagram of olefin lump in gasoline cut for PolyC3C4 ($MSEP2012 = 1 \times 10 - 4$; $MSEP\ 2014 = 7 \times 10 - 5$).....58
Figure 52 - Parity diagram of olefin lump in gasoline cut for PolyC4 ($MSEP2012 = 4 \times 10 - 5$; $MSEP\ 2014 = 6 \times 10 - 5$).....59
Figure 53 - Parity diagram of $A6$ for catalytic and coker gasoline ($MSEPCatalytic\ gasol.2012 = 3 \times 10 - 4$; $MSEPCatalytic\ gasol.2014 = 5 \times 10 - 5$; $MSEPCoke\ gasol.2014 = 1 \times 10 - 4$).....59
Figure 54 - Parity diagram of $A6$ for PolyC3C4 ($MSEP2012 = 3 \times 10 - 4$; $MSEP\ 2014 = 1 \times 10 - 4$)..60
Figure 55 - Parity diagram of $A6$ for PolyC4 ($MSEP2012 = 2.8 \times 10 - 6$; $MSEP\ 2014 = 3 \times 10 - 6$)....60
Figure 56 - Parity diagram of $A7$ for catalytic and coker gasoline ($MSEPCatalytic\ gasol.2012 = 2 \times 10 - 4$; $MSEPCatalytic\ gasol.2014 = 9 \times 10 - 4$; $MSEPCoke\ gasol.2014 = 9 \times 10 - 4$).....61
Figure 57 - Parity diagram of $A7$ for PolyC3C4 ($MSEP2012 = 2 \times 10 - 5$; $MSEP\ 2014 = 2 \times 105$).....61
Figure 58 - Parity diagram of $A7$ for PolyC4 ($MSEP2012 = 3 \times 10 - 5$; $MSEP\ 2014 = 4 \times 10 - 5$) 62
Figure 59 - Parity diagram of $A8$ for catalytic and coker gasoline ($MSEPCatalytic\ gasol.2012 = 3 \times 10 - 4$; $MSEPCatalytic\ gasol.2014 = 1 \times 10 - 3$; $MSEPCoke\ gasol.2014 = 1 \times 10 - 3$).....62
Figure 60 - Parity diagram of $A8$ for PolyC3C4 ($MSEP2012 = 2.2 \times 10 - 4$; $MSEP\ 2014 = 1.6 \times 10 - 4$) 63
Figure 61 - Parity diagram of $A8$ for PolyC4 ($MSEP2012 = 6 \times 10 - 5$; $MSEP\ 2014 = 5 \times 10 - 5$) 63
Figure 62 - Parity diagram of naphthenes lump in gasoline cut for catalytic and coker gasolines ($MSEPCatalytic\ gasol.2012 = 2 \times 10 - 5$; $MSEPCatalytic\ gasol.2014 = 3 \times 10 - 5$; $MSEPCoke\ gasol.2014 = 1 \times 10 - 4$).....64
Figure 63 - Parity diagram of naphthenes lump in gasoline cut for PolyC3C4 ($MSEP2012 = 4 \times 10 - 5$; $MSEP\ 2014 = 9 \times 10 - 5$).....65
Figure 64 - Parity diagram of naphthenes lump in gasoline cut for PolyC4 ($MSEP2012 = 2 \times 10 - 7$; $MSEP\ 2014 = 5 \times 10 - 6$).....65
Figure 65 - Parity diagram of total paraffins lump in gasoline cut for catalytic and coker gasolines ($MSEPCatalytic\ gasol.2012 = 2 \times 10 - 4$; $MSEPCatalytic\ gasol.2014 = 4 \times 10 - 4$; $MSEPCoke\ gasol.2014 = 3 \times 10 - 4$).....66
Figure 66 - Parity diagram of total paraffins lump in gasoline cut for PolyC3C4 ($MSEP2012 = 1.8 \times 10 - 4$; $MSEP\ 2014 = 2.3 \times 10 - 4$).....66

Figure 67 - Parity diagram of total paraffins lump in gasoline cut for PolyC4 ($MSEP2012 = 2 \times 10 - 4$; $MSEP\ 2014 = 6 \times 10 - 5$).....67
Figure 68 - Parity diagram of isoparaffins lump ($C4$-$C12$) for catalytic and coker gasoline ($MSEPCatalytic\ gasol. = 2 \times 10 - 4$; $MSEPCoke\ gasol. = 1 \times 10 - 4$) 67
Figure 69 - Parity diagram of isoparaffins lump ($C4$-$C12$) for PolyC3C4 ($MSEP\ 2014 = 2 \times 10 - 4$).....68
Figure 70 - Parity diagram of isoparaffins lump ($C4$-$C12$) for PolyC4 ($MSEP\ 2014 = 1 \times 10 - 4$).....68
Figure 71 – Isoparaffin and total paraffin ratio for $C4$.....69
Figure 72 - Isoparaffin and total paraffin ratio for $C5$.....69
Figure 73 - Isoparaffin and total paraffin ratio for $C6$.....70
Figure 74 - Isoparaffin and total paraffin ratio for $C7$.....70
Figure 75 - Isoparaffin and total paraffin ratio for $C8$.....71
Figure 76 - Isoparaffin and total paraffin ratio for $C9$.....71
Figure 77 - Parity diagram of LCO cut for catalytic and coker gasolines ($MSEPCatalytic\ gasol.2012 = 2 \times 10 - 4$; $MSEPCatalytic\ gasol.2014 = 1 \times 10 - 4$; $MSEPCoke\ gasol.2014 = 2 \times 10 - 4$).....72
Figure 78 - Parity diagram of LCO cut for PolyC3C4 ($MSEP2012 = 1.6 \times 10 - 4$; $MSEP\ 2014 = 1.7 \times 10 - 4$).....72
Figure 79 - Parity diagram of LCO cut for PolyC4 ($MSEP2012 = 1 \times 10 - 4$; $MSEP\ 2014 = 4 \times 10 - 5$) 73
Figure 80 - Parity diagram of coke cut for catalytic and coker gasolines ($MSEPCatalytic\ gasol.2012 = 1 \times 10 - 4$; $MSEPCatalytic\ gasol.2014 = 9 \times 10 - 5$; $MSEPCoke\ gasol.2014 = 3 \times 10 - 4$).....73
Figure 81 - Parity diagram of coke cut for PolyC3C4 ($MSEP2012 = 3.3 \times 10 - 4$; $MSEP\ 2014 = 2.7 \times 10 - 4$).....74
Figure 82 - Parity diagram of coke cut for PolyC4 ($MSEP2012 = 5 \times 10 - 5$; $MSEP\ 2014 = 8 \times 10 - 5$) 74
Figure 83 – Parity diagram of aromatic lump in gasoline cut for catalytic and coker gasolines 87
Figure 84 - Parity diagram of aromatic lump in gasoline cut for PolyC3C4 87
Figure 85 - Parity diagram of aromatic lump in gasoline cut for PolyC4 88
Figure 86 - Parity diagram of total paraffins $C4$ for all feeds 88
Figure 87 - Isoparaffin and total paraffins ratio for $C10$ 88
Figure 88 - Isoparaffin and total paraffins ratio for $C11$ 89
Figure 89 - Isoparaffin and total paraffins ratio for $C12$ 89

List of tables

Table 1 – FCC products, their boiling point and characteristics (Fahim, et al., 2010) 6
Table 2 – Critical diameter for some paraffins and olefins (Sigma Aldrich) 10
Table 3 – Main reactions in FCC process (Grace Davison, 1996) 11
Table 4 – Operating conditions summary 19
Table 5 – Properties values ratio between E-cat A and B 19
Table 6 – Experimental yields obtained at the highest contact time and 590°C 20
Table 7 – Activation energies values used in the model 37
Table 8 – Kinetic parameters distribution by reaction 37
Table 9 – Characteristics and execution time for the models of 2012 and 2014 39
Table 10 – Results for the sets of pre-exponential constants for the different feeds normalized with the correspondent value for gasolines feeds 40
Table 11 – Absolute error tolerance intervals of main cuts.....43
Table 12 – Absolute error tolerance intervals of dry gas cut for all feeds 45
Table 13 – Relative error precision intervals of dry gas cut for all feeds.....46
Table 14 – Absolute error tolerance intervals of $P1$ for all feeds.....47
Table 15 – Absolute error tolerance intervals of $P2$ for all feeds.....49
Table 16 – Absolute error tolerance intervals of LPG cut for the different feeds 51
Table 17 – Absolute error tolerance intervals of $O3$ for all feeds.....53
Table 18 – Absolute error tolerance intervals of $O4$ for all feeds.....55
Table 19 – Absolute error tolerance intervals of gasoline cut for the different feeds.....57
Table 20 – Absolute error tolerance intervals of $A6$ for all feeds.....60
Table 21 - Absolute error tolerance intervals of $A7$ for all feeds 62
Table 22 - Absolute error tolerance intervals of $A8$ for all feeds 63
Table 23 - Absolute error tolerance intervals of LCO cut for the different feeds 73
Table 24 - Absolute error tolerance intervals of coke cut for the different feeds.....74
Table 25 – Sensitivity analysis results for ±10% and ±20% deviation of activation energies values 77
Table 26 – Tolerance intervals of $O5$ for all feeds 90
Table 27 – Tolerance intervals of $O6$ for all feeds 90
Table 28 – Tolerance intervals of $O7$ for all feeds 90
Table 29 – Tolerance intervals of $O8$ for all feeds 90
Table 30 – Tolerance intervals of $O9$ for all feeds 90
Table 31 – Tolerance intervals of $N6$ for all feeds 91
Table 32 – Tolerance intervals of $N7$ for all feeds 91
Table 33 – Tolerance intervals of $N8$ for all feeds 91
Table 34 – Tolerance intervals of $iP4$ for all feeds 91
Table 35 – Tolerance intervals of $iP5$ for all feeds 91
Table 36 – Tolerance intervals of $iP6$ for all feeds 92
Table 37 – Tolerance intervals of $iP7$ for all feeds 92

Table 38 – Tolerance intervals of $iP8$ for all feeds 92
Table 39 – Tolerance intervals of $iP9$ for all feeds 92
Table 40 - Relative error precision intervals of LPG cut for all feeds 93
Table 41 - Relative error precision intervals of gasoline cut for all feeds 93
Table 42 –Relative error precision intervals of LCO cut for all feeds 93
Table 43 - Relative error precision intervals of coke for all feeds 93
Table 44 – Relative error precision intervals of $O3$for all feeds 93
Table 45 – MSEP results summary 94
Table 46 - MSEP results summary (continuation) 95

Nomenclature

Symbols

A_x	Aromatic with x carbon atoms
C_x	Hydrocarbon with x carbon atoms
CO_2	Carbon dioxide
C_p	Specific heat capacity ($J.kg^{-1}.K^{-1}$)
C/O	Cat to oil ratio
Ea	Activation energy ($J\ mol^{-1}$)
G_r	Gibbs free energy ($J\ mol^{-1}$)
H_2O	Water
H_2S	Hydrogen sulfide
H_2	Hydrogen
H_2^*	Hydride
H_f	Enthalpy of formation ($J\ mol^{-1}$)
iP_x	Isoparaffin with x carbon atoms
K	Rate constant ($Pa\ s^{-1}$)
K^0	Pre-exponential factor ($Pa\ s^{-1}$)
K_{eq}	Equilibrium constant
N_x	Naphthene with x carbon atoms
N_{comp}	Naphetenes group with five or more than six carbon atoms
Ni	Nickel
NO_x	Nitrogen oxide
O_x	Olefin with x carbon atoms
Pp	Partial pressure (Pa)
P_x	Paraffin with x carbon atoms
R	Universal gas constant ($J.mol^{-1}.K^{-1}$)
T	Temperature (K)
S_f	Entropy of formation ($J.mol^{-1}.K^{-1}$)
SO_x	Sulfur oxide
V	Vanadium
W_x	Weight of specie x on objective function

$y_{experimental}$	Experimental yield (%)
$y_{calculated}$	Calculated yield (%)
y_{LCO}	Number of hydrogen atoms considered for LCO
y_{Coke}	Number of hydrogen atoms considered for coke
x_{LCO}	Number of carbon atoms considered for LCO
x_{Coke}	Number of carbon atoms considered for coke
Z/M	Zeolite to matrix ratio

Greek letters

α	dependence factor on the reactant's carbon number, a.u.
β	symmetry governing factor, affecting product distribution, a.u.

Subscripts, Superscripts and Abbreviations

Cycli	Cyclization
E-cat	Equilibrium catalyst
Eq.	Equation
FCC	Fluid Catalytic Cracking
gasol	Gasoline
GC	Gas chromatograph
HCN	Heavy cracked naphtha
HCO	Heavy cycle oil
ht1	Step 1 of hydrogen transfer
ht2	Step 2 of hydrogen transfer
ht3	Step 3 of hydrogen transfer
Iso	Isoparaffin
Isom	Isomerization
LCN	Light cracked naphtha
LCO	Light cycle oil
LPG	Liquefied petroleum gases
Ocr	Olefins catalytic cracking
Oligom	Oligomerization
Pcr	Paraffins catalytic cracking
Ref	reference

REO	Rare-earth oxides
th1	Olefins thermal cracking
th2	Paraffins thermal cracking

This page was intentionally left blank.

1. Introduction

The propylene is an important intermediary for the production of petrochemicals such as polypropylene, propylene oxide and cumene. The propylene production is achieved mainly by non-catalytic steam cracking of natural gas liquids, naphtha, or gas oil naphtha (Nizamoff, 2013). Generally, the steam cracking objective is to increase the ethylene production. When using naphtha as the feedstock, the process usually gives an ethylene/propylene ratio of 2:1 (Nizamoff, 2013). Moreover, the abundance of shale gas has caused gas price to decrease relatively to oil price. Therefore, the cracker operators are driven to use more ethane instead of heavier feeds, which are more expansive. However, the use of ethane as steam cracker feedstock produces less propylene and consequently the propylene price has risen. With propylene demand growing faster than ethylene, combined with the building of more ethane crackers rather than naphtha crackers, the research of new techniques and on-purpose routes are rising (Wan, 2012).

1.1. Motivation

The Fluidized Catalytic Cracking (FCC) process is not an on-purpose process to produce propylene, however it represents the second biggest contributor for propylene production as by-product.

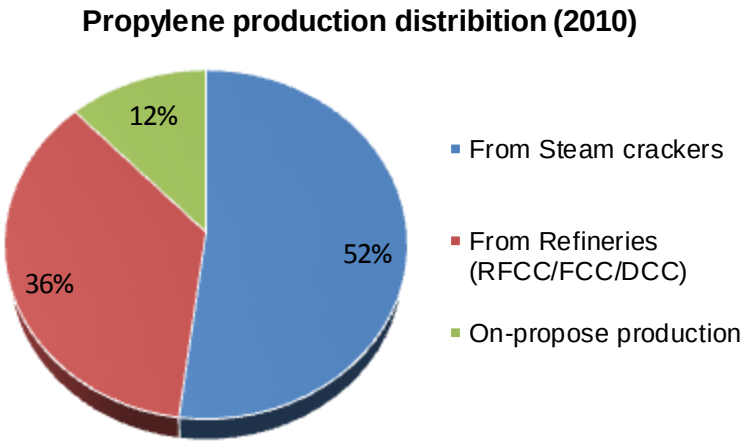

Figure 1 – Propylene world production distribution by type of route considering 75 million tons in 2010. The on-propose production technologies considered are: Metathesis, Olefins cracking, MeOH to propylene, C3 dehydrogenation (Dupraz, 2012)

Besides, the FCC is a highly adaptable conversion process enabling to adjust propylene/gasoline/diesel production according to market demand (Do, 2009). Therefore, concerning the demand increase in diesel and the corresponding decrease of gasoline, and also the demand increase of propylene, the FCC process has been the object of several studies for maximizing the propylene production (Concawe, 2013). This can be achieved with the conventional FCC with high severity operation and optimal ZSM-5 content in catalyst, leading to propylene yields of 8 to 13% depending on the FCC feed. In addition to the use of ZSM-5 to boost propylene production, other ways to maximize propylene have been studied. One of them is the dual riser configuration in FCC, which is studied in the present work.

In the dual riser configuration a second riser is added to the conventional FFC system. This second riser is dedicated to the cracking of a naphtha boiling range type of feed coming from the main riser or from another source available in the refinery. The propylene yield attained with this type of configuration depends on both the main and second riser feeds. For example, with residue feed cracked in the main riser and the recycle of light cracked naphtha (LCN) to the second riser the propylene yield can go up to 12 to 15%. If instead of a LCN an oligomer is fed to the second riser propylene production will be even higher.

To better integrate this new technology in refineries configuration and to test the different possible feeds combinations, in order to maximize propylene production, the modeling of this dual riser technology is extremely important.

1.2. Objectives

Since 2008, a simulator is being developed by IFP Energies Nouvelles (IFPEN) to predict the yields and performances in the second riser of a dual riser FCC configuration. A molecular lumping strategy was implemented where the compounds are divided in four families: paraffins, olefins, naphthenes and aromatics. Later on, the reaction network was modified in 2010 and 2012 by adding new reactions to achieve better results. The effect of ZSM-5 percentage was also introduced in the model in 2012 in order to improve the predictions.

The aim of this work is the model improvement for a better description of reaction kinetics. For this purpose the distinction between normal and branched paraffins will be done. For that, it is necessary to modify the reaction network to take into account the new components. Others changes will be also studied, namely the ZSM-5 effect in hydrogen transfer reaction.

1.3. Thesis outline

This thesis is organized as follows. Chapter 2 is introduced briefly the FCC as well as the second riser configuration, where it is explained their operation, feedstocks, operation conditions and catalyst. It is also shortly presented the catalytic cracking mechanism, and an overview of the kinetic models. Chapter 3 describes how the experimental data was obtained and what conditions are used. Further, chapter 4 is dedicated to a detailed description of the model and the proposed improvements. In chapter 5, the results are presented and analyzed. Finally, this dissertation ends with the final conclusions section and the future work concerning the remaining improvements that should be integrated in the model.

2. Literature review

2.1. Fluidized Catalytic Cracking process

The Fluidized Catalytic Cracking (FCC) is one of the most important conversion processes in refineries. This process is used to convert heavy fractions into lighter and more valuable products such as naphtha, LCO and light olefins (propylene and butylene). The FCC process has been in operation for over 60 years during which, a great deal of developments has occurred. Major improvements have occurred mainly in the structure of the catalysts and in the design of the reactor and regenerator (Fahim, et al., 2010). Several feeds are possible in FCC such as atmospheric distillates and residue, coking distillates, visbreaking distillates, vacuum gas oil (VGO) and vacuum residue. The FCC catalyst[1] is a Y-faujasite type with a matrix and additives.

The conventional process comprises three zones: reaction, separation and catalyst regeneration.

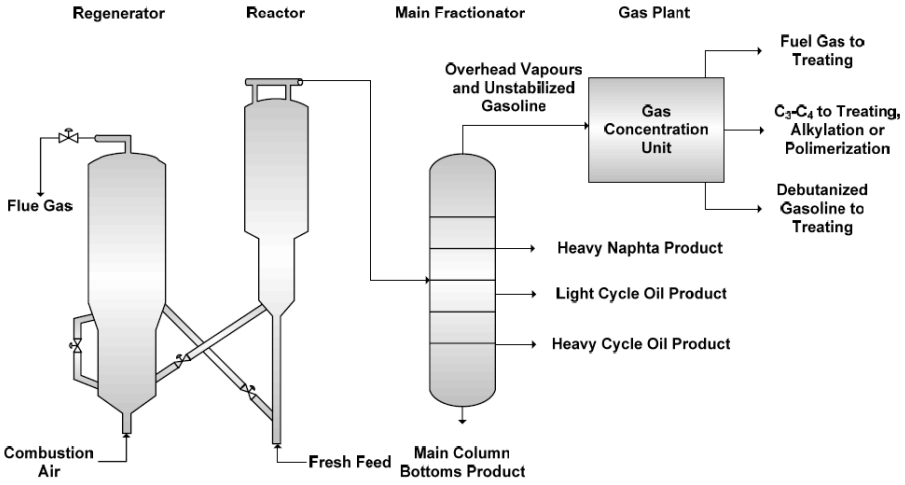

Figure 2 – Conventional FCC process scheme (Fernandes, 2007)

In the reaction zone, the feed is pre-heated up to 300°C and it vaporizes in the bottom of the riser with steam. The regenerated catalyst is also introduced in the riser's bottom with a higher temperature, around 650-760°C. The volume expansion of the generated vapors and the addiction of steam are the main driving forces to transport the catalyst and the feed up the riser, which contact time vary from 2 to 10 s. The riser is the main reactor in which the endothermic reactions take place (mainly cracking reactions).

The separation zone starts in the top of the riser, where the catalyst and the products are separated by a set of cyclones. The products are sent to a fractionator to obtain the different products cuts. The catalyst collected is sent to the stripper zone by gravity. Steam is injected into the stripper section to remove the hydrocarbons that still remain in the catalyst. The separation zone is designed to minimize the contact of catalyst with vapors and the occurrence of secondary reaction.

[1] In the sub-chapter 2.2.3, the catalyst is described with more detailed.

In the regeneration zone, the catalyst from separation zone is deactivated with coke that was formed in the riser. The coke is burned off in this zone by introducing excess air which is used to ensure the efficient combustion of coke. This procedure produces CO, CO_2, H_2O, SO_x and NO_x which are called flue gas. The flue gas is emitted at such a high temperature that can be sent to the power recovery unit to produce superheated steam. The regenerated catalyst returns to the riser to close the cycle.

The formation of coke is an important aspect once it enables the process to operate in heat balance. The heat produced in catalyst regeneration zone by coke combustion is enough to rise the temperature of the feed, and to compensate the energy needed for endothermic reactions, vaporization and stripping superheat steam, as well as the heat losses in the process (Leprince, 2001 and Gauthier, et al., 2000).

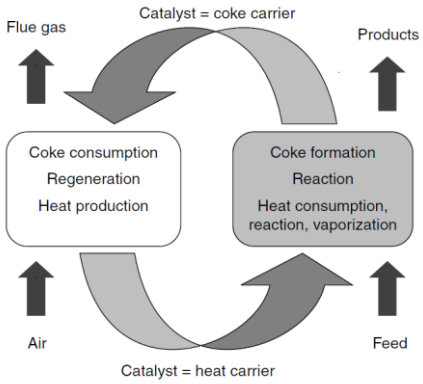

Figure 3 - Reaction-regeneration integration (Gauthier, et al., 2000)

Although the FCC is a mature technology, the replacement of gasoline for diesel fuels is driving the FCC technology to reduce its production in favor of lighter products (Concawe, 2013). Therefore, the evolution and research continues today to change the FCC process concerning the market needs.

2.2. Second riser configuration

In order to achieve the market needs in terms of propylene demand, the dual riser configuration in FCC process has been researched and suggested by different licensors. Axens, an IFPEN group company, proposes several technologies which can use this type of configuration. PetroRiser™ is one of them, which is generally associated with a FCC that treats heavy feeds (R2R unit[2]). In this case part of the catalytic gasoline produced in the main riser is recycled to the second riser. Besides PetroRiser™, the second riser configuration can be adopted for other technologies. One case is the integration of the dual riser FCC unit with an oligomerization unit that produces an oligomer feed which is fed to the second riser.

[2] Residue FCC unit with two regeneration stages.

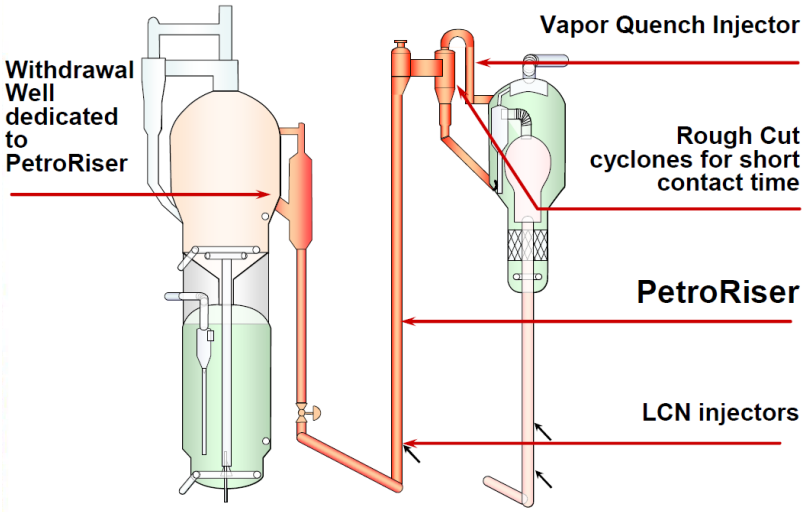

Figure 4 – Dual riser configuration scheme (Do, 2009)

The dual riser FCC configuration is similar to the conventional FCC process. As suggested by its name, this technology considers two risers: one riser orientated towards conversion of the main feed (the conventional) and another one which is dedicated to the production of propylene by cracking a naphtha boiling type of feed (approximately 30-220°C).

The catalyst cycle is the same for both risers, i.e. the second riser uses the same catalyst and regeneration section. Like for the main riser, in the second riser the catalyst and products are separated by a cyclone. The separated catalyst and products are sent to the stripping and fraction zone respectively (the same than for the main riser).

2.2.1. Feedstocks

As referred above, the second riser can have different types of feeds.

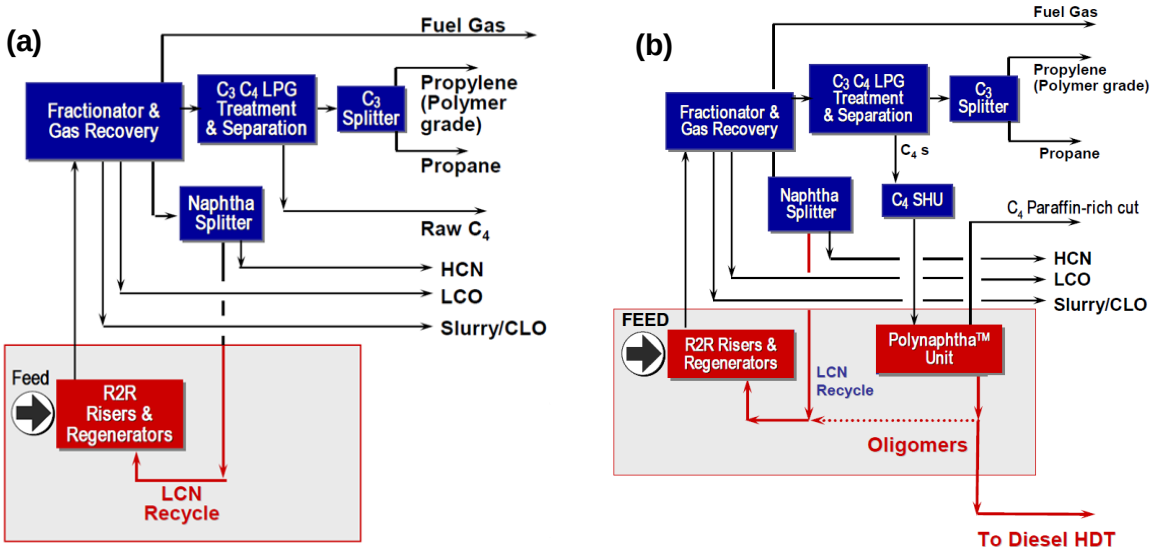

Figure 5 – Possible sources of second riser feedstock: naphtha stream recycled from main riser (a) and oligomers from a oligomerization unit (b) (Do, 2009)

Recycling the fractions produced in the first riser is normally the first option to improve the propylene production. It is the case of light cracked naphtha (LCN), which is produced in the first riser and separated in the main fractionator and naphtha splitter (Figure 5 (a)). After these separations, LCN is recycled to the second riser. Besides catalytic cracked naphtha from FCC, the naphtha sent to the second riser can also have other sources, such as cokers and hydrocrackers units.

In addition to the cracked naphthas, it is also possible to use other feed types, such as an oligomer (feed with very high content of olefins). The association of an oligomerization unit (that Axens commercial name is Polynaphtha™) to the second riser increases significantly the propylene yields. The integration of the oligomerization unit with the FCC consists in sending the C_4 cut obtained in the FCC main riser to this unit, upgrading this it into a high olefinic stream (Figure 5 (b)). Besides the C4 cut, the C_3/C_4 cut can also be fed to this alkylation process.

2.2.1. Products

The FCC converts heavy feeds in lighter and more valuable products. These products are then separated in cuts by their boiling point. Table 1 shows the FCC products divided by typical cuts.

Table 1 – FCC products, their boiling point and characteristics (Fahim, et al., 2010)

Products	Boiling point / Species	Characteristics
Dry gas	P_1+P_2+ H_2 + H_2S	H2S must be removed
Liquefied petroleum gas, LPG	P_3 , O_3, P_4, O_4	Petrochemical feedstock
Gasoline (LCN+HCN)	C_5-220°C LCN: C_5-160°C HCN: 160°C-220°C	Main product, good octane number
Light cycle oil (LCO)	220°C-360°C	Rich in aromatics, diluent for fuel
Heavy cycle oil (HCO)	360°C-440°C	Very rich in aromatics
Slurry	>440°C	Slurry of solids (mainly catalyst coke)
Coke		Consumed in regenerator by combustion

Since the feed to the second riser is in the gasoline boiling range the products coming out from the second riser are mainly light gases (dry gas and LPG) and gasoline. However, small quantities of heavier products (LCO) and coke are also produced.

2.2.2. Operating conditions

The operating conditions for the first riser are typically the same that in the conventional FCC process. On the other hand, the operating conditions for the second riser are more severe than in the first riser. The follow conditions are preferably (Feugnet & Roux, 2011):

First riser

- Cat to Oil ratio (C/O)[3]: 4 to 15, preferably in the range 5 to 10
- Outlet temperature: 510°C to 580°C, preferably in the range 520°C to 570°C

[3] Ratio between the catalyst and the feedstock flow that are introduced in the riser bottom

Second riser

- Cat to oil ratio: 8 to 35, preferably in the range 10 to 25
- Outlet temperature: 550°C to 650°C, preferably in the range 580°C to 610°C
- Contact time[4]: 20 ms to 500 ms, preferably in the range 50 ms to 200 ms
- Solid flow rate: 150 to 600 $kg/(s.m^2)$

For the regeneration section operating conditions are similar to the ones in typical FCC operation (temperature of 660ºC-740ºC).

2.2.3. Catalyst

The conventional FCC catalyst consists of a fine powder where particles have an average diameter of 60-70 µm (Leprince, 2001). It is composed mainly of oxide of silicon and aluminum and other elements but in very small amounts (Grace Davison, 1996). The catalyst complex (Figure 6) is composed by a zeolite, a matrix, a clay (or filler), a binder, and additives.

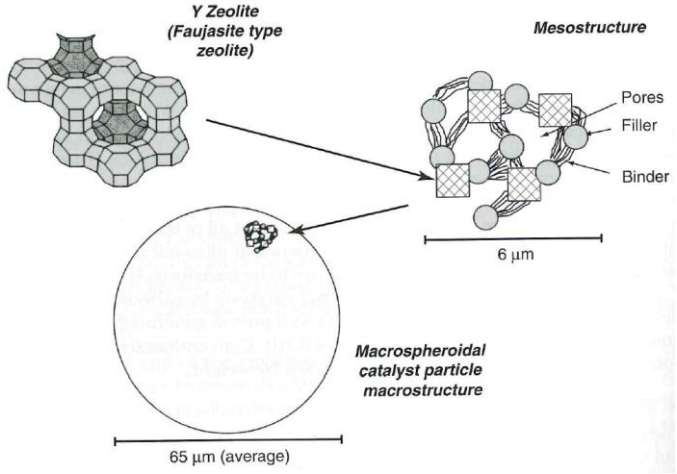

Figure 6 – FCC catalyst scheme (Sadeghbeigi, 2012)

Zeolite

The main zeolitic component in a cracking catalyst is the Y zeolite. The performance of faujasite depends of its manufacture and treatment. There are two main zeolites: Standard Y (HY, REY) and Ultra-stable Y (USY, REUSY). The USY is more resistant to deactivation in the FCC unit and for this reason is the most used in refineries.

USY can be treated with other cations, typically rare-earth mixtures, to remove sodium to form REUSY. Rare-earth raises the activity of the zeolite and delays crystal destruction and dealumination in the steam-calcening environment of the regenerator, i.e. thermal and hydrothermal stability of the catalyst (Grace Davison, 1996). The introduction of rare-earth in the catalyst influences the cracking reaction, promoting the gasoline yield and decreasing the light olefins yields (Guisnet & Ribeiro, 2004). Figure 7 shows the decreasing of octane number with the increase of rare-earth percentage. The

[4] The contact time is defined as the ratio of the volume of catalyst present in the reactor to the volumetric flowrate of fluid passing through the reactor

octane loss is due to promotion of hydrogen transfer reactions that lead to lower olefins yields in gasoline (Sadeghbeigi, 2012).

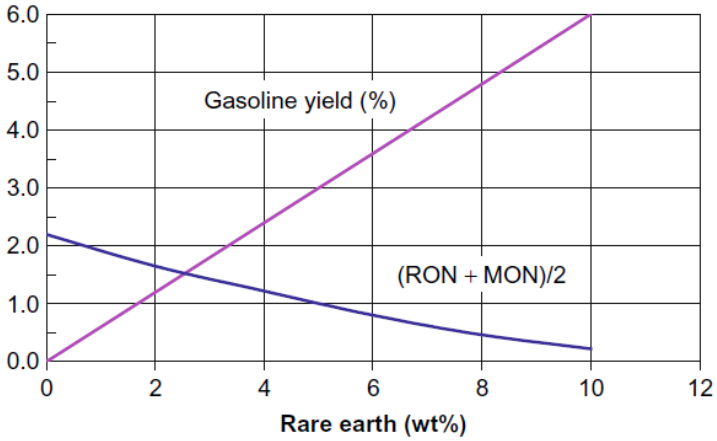

Figure 7 – Effects of rare-earth on gasoline octane and yield, where RON is research octane number and MON is motor octane number (Sadeghbeigi, 2012)

Matrix

The active matrix is the only component in the catalyst that has catalytic activity, excluding the zeolite. Its functionality is to reduce FCC bottoms products and increase the LCO and the light products formation. It has poorer coke and gas selectivity than the zeolite (Grace Davison, 1996). An active matrix can also work as a trap to entrap some of the catalyst poisons such as vanadium and basic nitrogen (Sadeghbeigi, 2012).

Clay and binder

The clay or filler provides a mechanical strength and density for optimum fluidization properties. This component also acts as a heater transfer medium (Grace Davison, 1996).

The binder acts like a "glue" to hold the other parts together providing a good retention and mechanical strength. It can have catalytic activity or not.

Additives

The additives are used to reduce a specific pollutant or to boost some of the product yields. The principal additives of FCC catalyst are:

- Combustion promoters – developed to improve the catalyst regeneration. This additive is also important to satisfy the requirement of CO emissions elimination. The operative COpromoter uses a noble metal base such as platinum and palladium (Leprince, 2001).
- SO_x transfer agents – the coke introduced into the regenerator can have up to 50% of the sulfur present in the feed. However, the SO_x emissions are restricted by law for environmental protect. Several metal oxides are introduced to reduce the SO_x emissions by H_2S production (Guisnet & Gilson, 2002).
- NO_x additive – Part of the nitrogen's feed is deposited on the catalyst. In the regenerator, the coke combustion converts the incoming organic nitrogen to NO_x. Several components have

been tested to reduce NO_x emission such as copper, zinc and/or rare-earth (Sadeghbeigi, 2012).

- Metal traps – some metals such as nickel and vanadium from heavy feeds can be poisons for the catalyst. Nickel catalyzes hydrogenation reactions and consequently increases the coke and gas yield. Vanadium allows the degradation of zeolite structure and subsequently decreases its catalytic activity. The passivation method for these metals is usually based on the introduction of specific components in the feed to control the content of these molecules. Antimony and bismuth are examples of these components for nickel case, where bismuth is less toxic than antimony. The vanadium passivation is achieved with the same method but with tin components (Guisnet & Ribeiro, 2004).
- Bottoms-cracking additive – this additive reduces bottoms products (slurry oil) by converting it to lighter more valuable products such as LCO and naphtha.

The ZSM-5 is also an important additive that acts as co-catalyst. It is used to improve the octane number of gasoline, the primary product target in conventional FCC process. It is used also to improve the production of light olefins, especially propylene. These improvements are obtained mainly by decreasing the average molecular weight of the gasoline, in particular by cracking most of the long paraffins and olefins (C_7+) to produce short paraffins and olefins and by increasing the iso/normal ratio of the paraffins and olefins from C_4 to C_7 (Rahimi & Karimzadeh, 2011).

Nevertheless, the propylene yield does not increase proportionally to the ZSM-5 increase. As presented in Figure 8, this yield is moderately constant with ZSM-5 content higher than 8%. It is important to refer that both of this percentage of ZSM-5 and the maximum propylene yield, achieved for a ZSM-5 content, depend of zeolite characteristics, feedstocks and operation conditions. As expected butylene yield also increases with the ZSM-5 percentage in the catalyst.

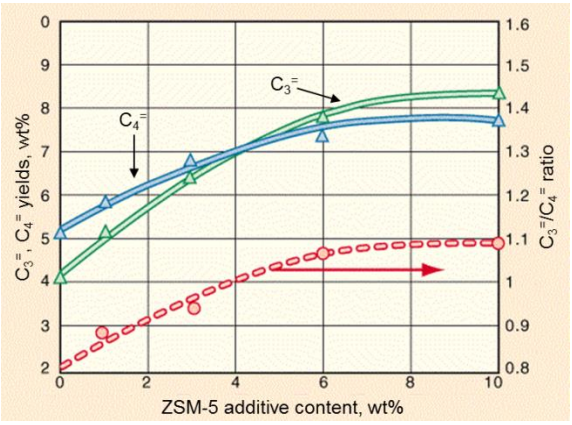

Figure 8 – ZSM-5 effect in propylene and butylene yields (Fu, et al., 1998)

The selectivity cracking of paraffins and olefins is conferred by shape-selectivity of ZSM-5. Its smaller pores have approximately 5.1Å to 5.6Å which size limits the access to only linear or near linear molecules in the gas oil.

The pores sizes enable the access for linear and mono-branched paraffins and olefins. As represented in Table 2, the cycle molecules (which have a critical diameter higher than 5.6Å) cannot have access

to ZSM-5 pore. According with the data from Sigma Aldrich, mono-branched paraffins can access to the pores of ZSM-5. It is expected that mono-branched olefins can also enter in the pores.

Table 2 – Critical diameter for some paraffins and olefins (Sigma Aldrich)

Molecule	Critical diameter (Å)
Methane	4.0
Ethylene	4.2
Ethane	4.4
Propane	4.9
n-Butane to *n*-docosane	4.9
Propylene	5.0
Isobutane to isodocosane	5.6
Cyclohexane	6.1
Benzene	6.7
Toluene	6.7
p-Xylene	6.7
m-Xylene	7.1
o-Xylene	7.4

On the other hand, Jiménez-Cruz and Laredo studied the critical diameter of linear branched paraffins by DFT quantum chemical calculations. As showed in Figure 9, just linear paraffins are sized to access the ZSM-5 pores. The same study referred that ZSM-5 is a good molecular sieve material for selective retention of isoparaffins.

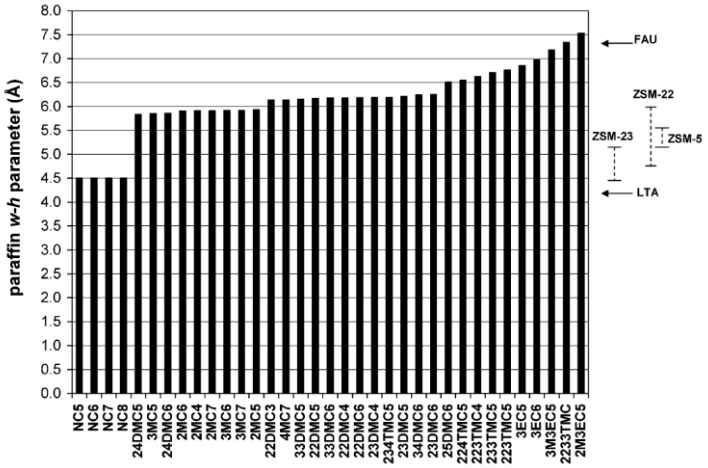

Figure 9 – Comparison of critical molecular parameters for the paraffins. $w - h$ is the average between the width and height for each paraffins that determine if the molecule can enter into the pore. iNCx is a linear alkane, iMCx is a methyl alkane, iECx is a ethyl alkane, ijDMCx is a dimethyl alkane, iMjECx is a methyl-ethyl alkane, ijyzTMCx is a trimethyl or tetramethyl alkane; where x is the carbon atoms number in principal chain and i, j, y, z the carbon number of the principal chain where the branched is located (Jiménez-Cruz & Laredo, 2004)

However, it is not completely correct once ZSM-5 is industrially used in xylene's isomerization.

Equilibrium catalyst

As explained above, one of the characteristics of FCC is the continuous circulation of the catalyst. The catalyst that circulates between the riser and the regenerated is called Equilibrium catalyst (E-cat). As

catalyst equilibrates, it is regenerated several times and feedstock contaminants (such as vanadium and nickel) are deposited on it. Therefore, E-cat changes same properties comparing to the fresh catalyst: loses activity, becomes less selective and undergoes physical changes. To control the quality of the circulating catalyst inventory, refiners take out the E-cat from regenerators and replace it with fresh catalyst (Grace Davison, 1996).

2.2.4. Catalytic Cracking Mechanism

The main reaction in FCC is the cracking as suggested by its name. However, due to the presence of catalyst and high temperatures others reactions take place in the riser. Same examples of these reactions are presented in Table 3.

Table 3 – Main reactions in FCC process (Grace Davison, 1996)

Reagents	Reactions	Products	Reactions	Products
Paraffins	Cracking (protolytic scission) →	Olefins + Paraffins		
	Isomerization →	Branched paraffins		
Olefins	Cracking (β scission) →	Olefins		
	Cyclization →	Napthenes		
	Isomerization →	Branched olefins	Hydrogen transfer →	Branched paraffins
	Hydrogen transfer →	Paraffins		
	Oligomerization →	Longer olefins	Cracking →	Light olefins
	Cyclization Condensation Dehydrogenation →	Coke		
Naphthenes	Cracking →	Alkenes		
	Hydrogen transfer →	Cyclo-olefins	Hydrogen transfer →	Aromatics
	Isomerization →	Naphthenes		
Aromatics	Desalkylation →	Aromatics + olefins		
	Alkilation →	Alkylaromatics		
	Transalkilation →	Other aromatics		
	Condensation →	Polyaromatics+H_2	Condensation →	Coke

The reactions in the second riser will be similar with the conventional riser. The principal reaction is described below and some secondary reactions as well.

Catalytic cracking reactions

The cracking reaction of a hydrocarbon is a scission of a C-C bond to form two molecules lighter than the initial one. This type of reaction is endothermic and for that reason, according to the thermodynamic laws, it is favored at high temperature and low pressure. To describe this reaction, two mechanisms are proposed for acid-catalyzed cracking of hydrocarbons: β-scission and protolytic cracking.

β-scission reaction is defined as a classical bimolecular cracking where the mechanism is divided in three stages:

- Initiation: formation of first carbocation, which depends of the chemical nature of the reactant. The alkenes reactants (with basic character) are absorbed by the Brönsted acid sites in the zeolite. The carbocation is formed by direct protonation. On the other hand, the protonation of saturated hydrocarbons (no basic) is more complicated, and several possibilities are proposed in particular the absorption in Lewis and Brönsted[5] acid sites. However, the alkanes protonation is not very important in FCC, since that alkanes are generally activated on hydride transfer reactions (Figueiredo & Ribeiro, 2007). The carbenium formation depends of its stability that increases with the degree of substitution of the carbon with positive charges. This fact can explain the low extent reaction concerning primary carbenium ions (CRH_2^+) and the inexistence of reactions involving CH_3^+. Once a carbocation is formed it can undergo different reactions, such as isomerization[6] (for a more stable specie), β-scission (and oligomerization which is the reverse reaction) and deprotonation (Caeiro, et al., 2006).
- Propagation: occurs by hydride transfer from a reactant molecule to the adsorbed carbenium ion (bimolecular reaction). The reactant molecule adsorbed is able to isomerize and/or crack (Guisnet & Gilson, 2002).
- Termination – the last step is the occurrence of the carbocation desorption as an olefin. The acid site is regenerated and ready to be used again.

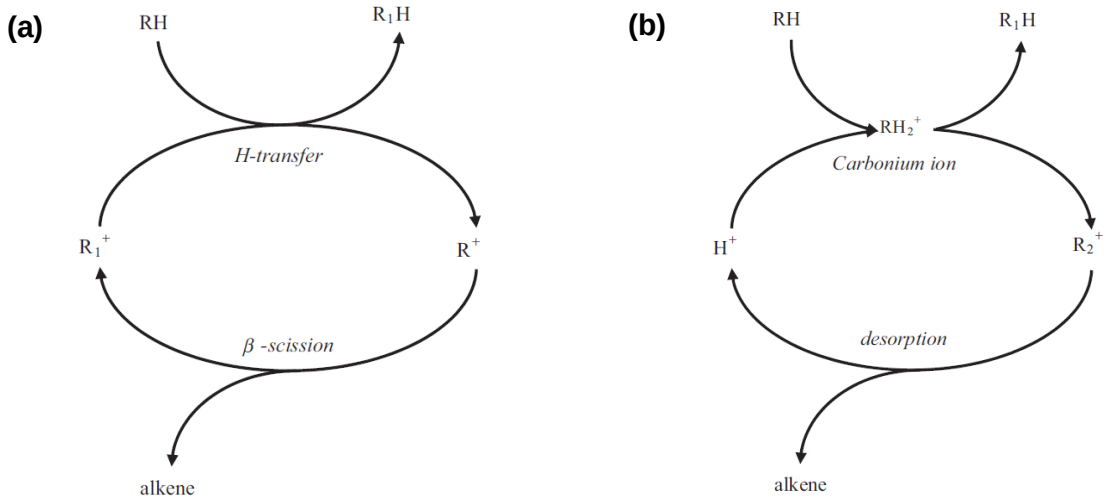

Figure 10 - β-scission (a) and protolytic cracking (b) mechanism for an alkane molecule (Rahimi & Karimzadeh, 2011)

In protolytic cracking, also known as Haag-Dessau cracking or monomolecular cracking, alkanes are protonated to form carbonium ion transition that can undergo C-C bond rupture yielding light alkanes, including methane and ethane (Figure 11 step (a) and (b) respectively). It is also possible the C-H bond cleavage yielding hydrogen and carbocations as show in Figure 11 step (c) (Rahimi & Karimzadeh, 2011). The formation of these light products cannot be accounted by the classical catalytic cracking, for which the smallest alkane cracking product is propane (Kotre, et al., 2000).

[5] The absorption by Brönsted acid site will promote the protolytic cracking
[6] The branched carbocation can desorb giving a branched olefin or undergo a hydride transfer reaction and desorb as a branched paraffins or may crack to give other product (Guisnet & Gilson, 2002)

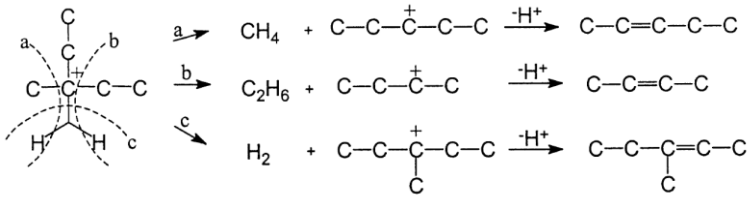

Figure 11 – Preferential protonation and cracking of a 3-methylpentane molecule (Kotre, et al., 2000)

The carbenium ions formed through this mechanism can act as starting molecules to the β-scission mechanism or be desorbed as olefins.

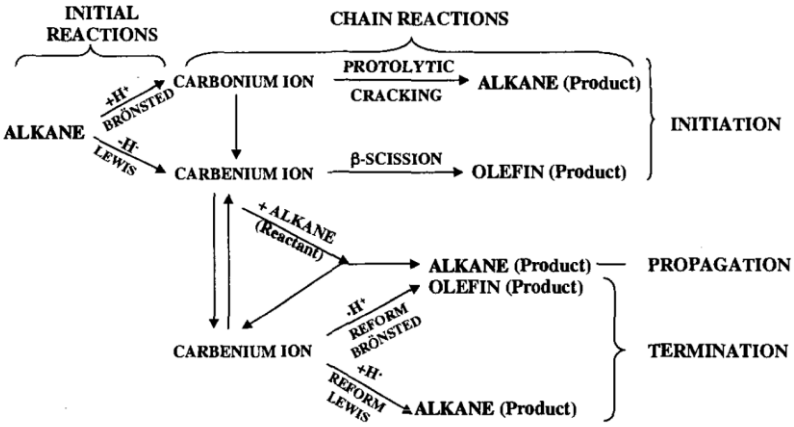

Figure 12 – Simplified reaction network for alkane cracking on zeolite catalysts (Guisnet & Gilson, 2002)

The ratio of protolytic and β-scission cracking depends on reaction conditions, such as temperature and hydrocarbon partial pressure, and the zeolite characteristics. Haag and Dessau found that the activation energy for protolytic cracking is higher than the required for β-scission cracking (Corma & Orchillés, 2000). Therefore, it can be expected that the protolytic mechanism will prevail at high temperature.

Oligomerization

This type of reaction is the opposite of cracking reactions since the molecules get bigger by chain growth with promotion of C-C bond formation. The oligomerization is an endothermic reaction that leads to a molecular reduction. For that reason, it is thermodynamically favored at low temperature and high pressure.

The oligomerization reactions are normally followed by the cracking reaction at high temperatures. However, if the adsorption of the high molecular weight carbenium ions produced occurs before the cracking reaction, the oligomerization will be responsible for the production of long carbon chain (Williams, et al., 1999). Furthermore, Williams et al. (1999) and Carabineiro et al. (2003) assume the association of this reaction to coke production.

Hydrogen transfer

The hydrogen transfer reactions are crucial to achieve the yields and products objectives on FCC. It is a bimolecular reaction where hydrogen from a hydrocarbon donor is transferred to an acceptor. Generally this case appears in FCC as a reaction between an olefin and a naphthene to produce a

paraffin and an aromatic. Moreover, this reaction can have other mechanisms as the reaction between two olefins to give the same products (Sadeghbeigi, 2012).

However, the classic approach is not suitable for light feedstock such as naphtha. This topic will be discussed in model description in sub-chapter 4.2.

Furthermore, this reaction is very important for coke formation since it produces coke precursors.

The hydrogen transfer is highly dependent of the catalyst type and composition. This reaction is bimolecular and for that reason it is promoted by adjacent sites. Therefore, the content of rare-earth will increase hydrogen transfer by the formation of bridges between two to three acid sites in the catalyst framework (Sadeghbeigi, 2012). On the other hand, this reaction is also controlled by the micropore size of the zeolites (steric constrains). Consequently, the small pores of ZSM-5 are not suitable for this type of reaction (Dwyer & Degnan, 1993). The extent of hydrogen transfer is then relatively low in this zeolite.

Coke formation

Coke formation involves several consecutive reactions. Coke is usually formed from alkenes, dienes and aromatics, due to their high reactivity. A strong retention on the zeolite active sites also contributes for the direct formation of coke.

As showed in Figure 13, the reaction between an alkene or a diene and an aromatic will form (soluble) coke. Aromatics can also react with themselves to produce coke. The same type of reactions transforms the soluble coke, which is confined in the zeolites cages, into insoluble coke that grows and overflows onto the external surface of the zeolite (Cerqueira, et al., 2008).

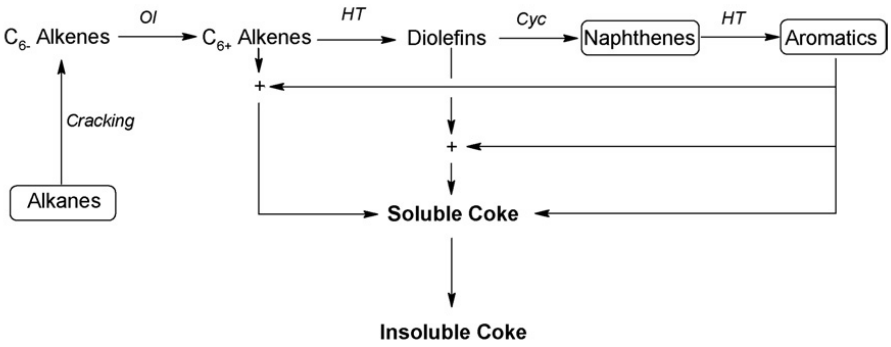

Figure 13 –Mechanism of coke formation, where Ol is oligomerization reaction, HT is hydrogen transfer and Cyc is cyclization (Cerqueira, et al., 2008)

The two possible mechanisms to coke formation proposed by Cerqueria are resumed in Figure 14. The mechanism a) is based on the aromatics alkylation by alkenes. The mechanism b) involves the alkylation of two aromatics. In both mechanisms several reactions take place such as alkylation, hydrogen transfer, cyclization, and isomerization.

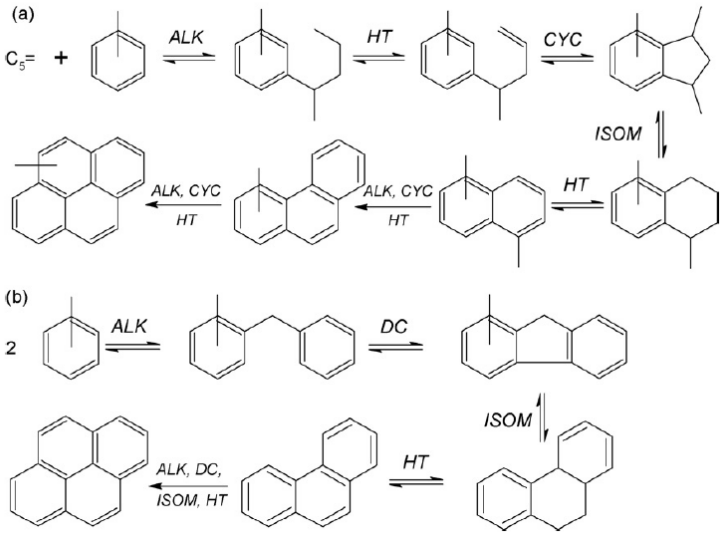

Figure 14 – Coke formation from a) alkenes and aromatics and b) only aromatics, where Alk is alkylation reaction, HT is hydrogen transfer, Cyc is cyclization, ISOM is isomerization and DC is dehydrogenative coupling (Cerqueira, et al., 2008)

Cerqueira et al. assume also that only olefins can react to produce coke. Hence, the reaction mechanism in these conditions must involve the formation of a cycle by oligomerization, followed by hydrogen transfer or dehydrogenation in order to produce an aromatic.

Others authors suggested different pathways and reactions for coke formation. According to Carabineiro et al. the coke formation is suitable by chain-growth reaction with olefins. In 2005, Wang et al. considered two reactions: one between two olefins to produce a coke precursor and hydrogen and another one between the coke precursor formed and a naphthene to yield coke and a paraffin. Longstaff (2012) suggested the reaction of aromatic with ten carbon atoms to form coke and naphthene composed by ten carbon atoms.

2.3. Kinetic models overview

The catalytic cracking mechanism is very complex and it is composed by many species and reactions. Several experimental works studied the catalytic cracking of a pure component, and demonstrated that the number of products is very high.

The modeling of this type of reaction has been studied since the 1980s. Several authors created different approaches which will be described briefly below. Due to the high number of species involved in cracking reactions an usual approach in kinetic modeling is to group/lump the species by their boiling point or chemical nature in order to reduce the number of parameters need to be estimated.

According to the FCC review of Pinheiro et al. (2012), the first approach for catalytic cracking kinetic modelling grouped the species in lumps according to their boiling point. In 1968, Weekman proposed a three-lump model which is focused on feedstock conversion and gasoline selectivity. The lumps comprise the feedstock, the gasoline (C_5-221ºC), the dry gas plus the coke. Several other authors have further cover this lumping approach on the basis of the FCC cuts (Table 1, page 6). However,

this type of approach requires a lot of experimental data because the parameters strongly depend of feeds and products. Furthermore, it does not reflect the fundamental chemistry (Feugnet, 2008).

Some authors have proposed different approaches to establish a relation between the composition and the chemical nature of the feed and the products. Concerning the lumping strategy based on molecules chemical nature, Pinheiro (1999) developed a paraffins cracking model that concern two groups: the adsorbed species and gas phase hydrocarbon. The model, applied to n-heptane, is described for three sets of elementary reactions between all species: cracking reactions, chain growth reactions and hydride transfer reaction. The model was improved by Carabineiro (2003), who distinguished between olefins and paraffins allowing the reactivities distinction of these species.

Recently, Lee et al. (2011) developed a similar approach for kinetic modeling of paraffinic naphtha cracking. In this study, the activation energy is not the same for all cracking reactions. This approach assumes a linear variation of activation energy proportional to the carbon number of the molecule that will crack. Other characteristic corresponds to the pre-exponential factor in Arrhenius law. This factor is subdivided into three modules:

- The first term represents the low frequency vibrational mode at the transition state;
- The second is the entropy change between activated complex and reactants;
- The third term means the number of mole changes in the reaction.

Nevertheless, this method has many assumptions and it depends on the availability of data in the literature to take into account all the proposals effects. The kinetic model of the reactions system includes many parameters that need to be estimated, and for that it is also necessary to have experimental data (Dasila, et al., 2012).

Longstaff (2012) developed a comprehensive naphtha cracking model to predict the cracking of FCC olefinic and saturated naphtha. The model accounted for 13 reaction classes comprising 360 reactions. The kinetic model takes into consideration different pre-exponential factors and activation energies for each reaction. Therefore, the model complexity is too high to solve as a nonlinear regression problem. The study applies a linearization of kinetic parameters into a kinetic map. To reduce the number of parameters a compensation effect was considered.

When modeling a reaction system the methodology adopted will influence the number of parameters that is necessary to determinate as well as the experimental data needed. In this study a molecular lumping strategy has been adopted to describe the catalytic cracking of a naphtha cut. Information on the experimental data used as well as the kinetic model description are given in the next chapters.

3. Experimental data

The data used in this work was obtained with different naphtha feedstocks and conditions. As referred above, the feed sent to the second riser can have different origins. Concerning the different possibilities, four feeds were tested:

- Catalytic gasoline obtained in a main riser;
- Coker gasoline from a coker process unit;
- Oligomeric feed from an oligomerization unit which is fed by C_3 and C_4 cuts. This feed is referred in this work as PolyC3C4[7];
- Oligomeric feed from an oligomerization unit fed with a C_4 cut. This feed will be referred as PolyC4.

The detailed composition of the feedstocks was previously obtained by gas chromatography (GC) analysis, using a dedicated software developed by IFPEN based on automatic peak identification using a retention indices database. This software allows chromatographic processing data to deliver exhaustive analysis of compounds from several types of petroleum samples as light saturate and aromatic compounds of crude oil in the range from C_3 to C_{20} (Darouich, et al., 2005). This type of analysis allows to have the composition by families: parafins, isoparaffins, olefins, naphthenes and aromatics (PIONA composition) as shown in Figure 15. Nevertheless, it is important to refer the software limitations in analysis of C_{6+} compounds, normally in branched alkanes and alkenes. The software increases its error in the categorization by types of this species, i.e. the software can make the difference between a normal and a branched molecule but it cannot distinguish if the molecule ismono-, di-branched, etc.

As expected, the oligomeric feeds (PolyC3C4 and PolyC4) are composed mainly by olefins. The gasolines' composition has a pattern of all the families where the isoparaffins characterizes more than 10% of the feeds. It is also important to refer the aromatic content of catalytic gasoline which is much higher than in the others feeds (namely in the oligomers).

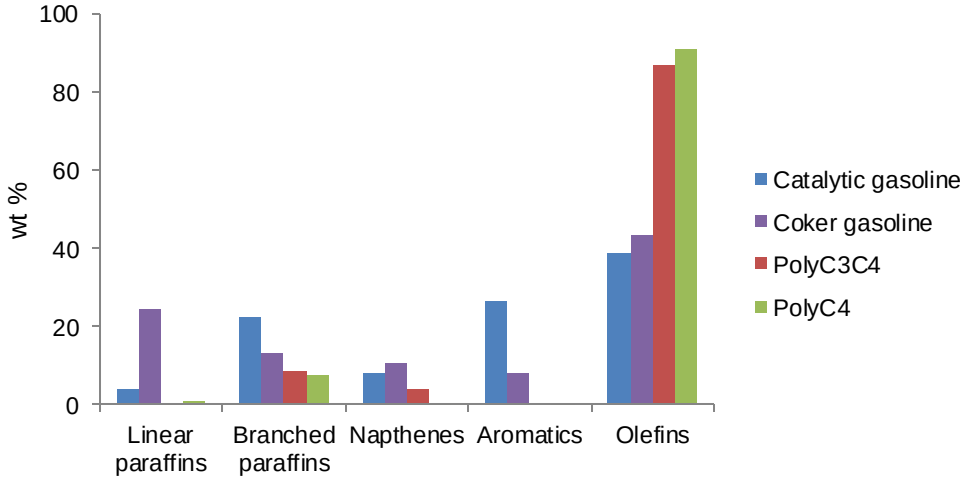

Figure 15 – Feedstocks PIONA composition in mass percentage

[7] The name "Poly-" is from Polynaphtha™, the Axens' commercial name of oligomerization process

The distribution by number of carbon atoms is also possible to analyze. As shown in Figure 16, the analysis was made for the species with less than sixteen carbon atoms. Therefore, it is possible to conclude that in the range of C_{13} to C_{16} the composition is not significant. Generally, most of the components in the feeds have carbon number between C_4 and C_{11}. On the other hand, PolyC4 is mainly composed of olefins species with eight and twelve carbon atoms.

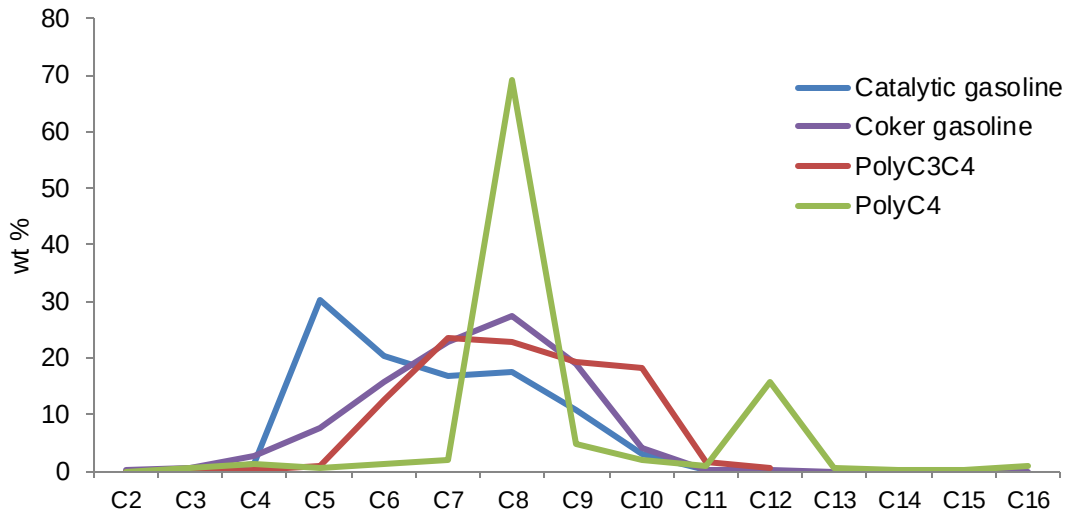

Figure 16 – Carbon atoms distribution for each feedstock

The feedstocks presented above were tested in the riser of the R2R[8] pilot unit at IFPEN. This pilot unit is representative of industrial FCC units operation.

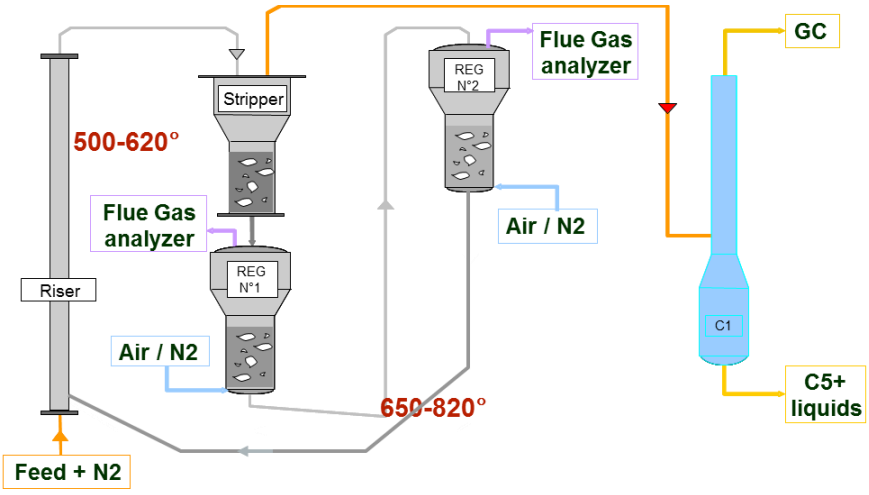

Figure 17 – R2R pilot unit scheme, where REG is the regenerator and C1 the fractionator column

Figure 17 shows the pilot unit scheme where it is possible to observe the riser, the stripper and the two stages regenerator. The feed to be analyzed and the catalyst are introduced in the riser bottom. The products formed and the catalyst are separated in the stripper, where the catalyst is sent to the regenerator composed by two stages. After the coke combustion, the catalyst is again active and able to return to the riser. On the other hand, the products are separated in a fractionator column (C1) into lighter products, such as dry gas, and LPG and C_{5}+ liquid products i.e. gasoline, LCO and slurry.

[8] Type of FCC unit with two stages of regeneration able to process residue feeds.

Products characterization is made after this separation (column C1). The lighter products are analyzed by online GC. The liquid product is characterized using several analyses. First, a simulated distillation curve of the total liquid product is done, that allows to observe the mass yields distribution with the boiling point. After that, the liquid products are separated by a physical distillation in order to obtain the typical cuts: GLN, LCO, HCO and slurry. Each cut is then analyzed separately to identify its composition, sulfur and nitrogen content as well as some physical properties such as density. For GLN, it is possible to have a detailed PIONA composition obtained by GC. Finally, the coke yield is obtained by measuring a sample of catalyst before and after the coke combustion.

The tests were performed according to the second riser operating conditions. Several conditions were done in the operating ranges which are summarized in Table 4.

Table 4 – Operating conditions summary

Feed	Catalytic gasoline	Coker gasoline	PolyC3C4	PolyC4
Temperature, °C	566-597	570-600	567-613	545-625
Cat to Oil (C/O)	9-41	8-49	7-34	10-49
Inert, Nm^3/h	0.35-0.95	0.3-0.45	0.35-0.93	0.18-0.9
Feed flowrate, kg/h	2-6	2-3.15	1.95-6	2-4
Contact time, ms	32-226	33-171	31-187	37-162
Catalyst	A	A	A	B
ZSM-5 %	10%	0%[9],5%[10] and 10%	10%	18%
Number of tests	11	12	9	11

As presented in Table 4, two E-cat are used: A and B. Besides, the ZSM-5 content used is different for each feed. Further comparative characterization of the two catalysts is given in Table 5. The ratio between the values for a given property of the A and B catalyst are presented below.

Table 5 – Properties values ratio between E-cat A and B

Property	A/B catalysts ratio
Z/M ratio	4.1
REO content	2
Ni content	111.3
V content	17.7

Generally, a catalyst with a high content of matrix is well adapted to large molecule cracking of heavy feeds. That is the case of catalyst B that has a higher content of matrix than E-cat A. It is important to refer that the choice of the catalyst is not linked to the feed of the second riser but to the main riser. As already referred above in the dual riser configuration, both risers have the same catalyst system.

With the conditions summarized above (Table 4), it was possible to obtain the experimental yields for each cut. Table 6 shows the obtained cut yields corresponding to the tests with the highest contact time at the temperature of 590°C for each tested feedstock.

[9] Two tests are executed without ZSM-5 additive in catalyst system
[10] Two tests are executed with 5% of ZSM-5 additive in catalyst system

Table 6 – Experimental yields obtained at the highest contact time and 590°C

Yields (wt%)	Catalytic gasoline	Coker gasoline	PolyC3C4	PolyC4
Dry gas (H_2+C1+C2+H_2S)	2.6	5.4	5	5.1
LPG (C3+C4)	14.6	30.3	53.9	65.3
$C3^=$	6.1	11.9	20.7	24.2
LCN (C5-160°C)	67.5	53.3	30.7	23.2
HCN (160-220°C)	9.2	5.6	3.6	2.7
LCO (220-360°C)	3.4	2.4	2.9	1.3
Coke	2.8	3	4	2.6

The propylene yield is lower for the gasoline feeds and its highest value was obtained with PolyC4 feed. This can be easily explained by the composition of the PolyC4 feed, which is mainly C_8 olefins (>80 %wt). The C_8 along with the C_7 olefins are the species with higher reactivity towards propylene production.

Moreover, it was observed that all the four feeds produce similar quantities of dry gas and coke yields.

4. Second riser model and simulator

The second riser model, which name is Petroriser[11], has been developed in IPFEN and is implemented in *Fortran* language. For the development of Petroriser simulator two reactor model codes are available: one exclusively for the kinetic parameters estimation that represents the pilot unit riser and another one used to simulate an industrial riser that takes into account the industrial riser hydrodynamics and uses the kinetic parameters obtained with the first code. The parameters estimation uses data from R2R pilot, which hydrodynamics is different from an industrial riser. Hence, the hydrodynamic models have to be described separately.

This study only considers the kinetics model and for that reason just this part will be described below.

Sub-chapters 4.1 to 4.4 describe the state of the art where are presented the reactive species, the reactions and main assumptions. Then in sub-chapter 4.5 the proposed modifications to the code are presented. Finally, in sub-chapter 4.6 the optimization procedure is explained.

In order to simplify the reaction network description and the results discussion, the following nomenclature is used: P_n as paraffins, iP_n as isoparaffins, O_n as olefins, N_n as naphthenes and A_n as aromatics, where the index n represents the number of carbon atoms in each molecule.

4.1. Reactive Species

As referred in introduction chapter, the reactive species were lumped according to their chemical nature: paraffins, olefins, naphthenes and aromatics. The lumps considered in the model are the following ones:

- Paraffins lump (P): concerns the paraffins (linear and branched) with one to twelve carbon atoms,
- Olefins lump (O): includes the olefins (linear and branched) with two to twelve carbons,
- Naphthenes lump (N): distinguishes the more reactive naphthenes such as N_6, N_7 and N_8 from the N_{comp} (which groups N_5 and N_{9+})[12],
- Aromatics lump (A): includes A_6 to A_{12},
- Coke,
- LCO,
- H_2,
- Hydrogen hydride, H_2^*.

Sulfur and nitrogen compounds are not considered in the model.

The kinetic model for the second riser considers then a total of 45 molecular lumps.

[11] The simulator has the same name than Petroriser™ technology licensed by Axens, but it is not exclusively to be used in this process. The Petroriser simulator is able for the second riser simulation independent of its feed.
[12] This differentiation was established according the experimental data

4.2. Reaction network

Firstly, the reaction network was established based on the experimental data described in chapter 3. Then, the first model version of 2008 implemented by Feugnet was upgraded in 2010 and 2012 by adding new reactions and by improving the description of the reaction scheme and catalyst effects.

At present, the reaction network is composed by the following reactions:

- Catalytic cracking (β-scission and protolytic cracking),
- Hydrogen transfer,
- Oligomerization,
- LCO formation,
- Coke formation,
- Thermal cracking,
- Olefins cyclisation.

Each reaction has different assumptions which are briefly described in the next paragraphs.

Catalytic cracking (β-scission and protolytic cracking)

The catalytic cracking concerns the paraffins and olefins.

The paraffins' cracking mechanism depends of the acid site type where the molecule is absorbed: if it is a Brönsted or a Lewis site. In a Brönsted site, the cracking occurs through protolytic cracking. If absorbed on a Lewis acid site, the cracking will go through a β-scission mechanism. Nevertheless, in both cracking mechanisms the paraffin absorbed produces a lighter paraffin and an olefin (Feugnet, 2008).

In this reaction type, it was assumed that just paraffins with more than 5 carbon atoms (P_{5+}) will crack, and the reaction is given by the equation below:

$$P_i \rightarrow P_j + O_{i-j} \qquad \text{Eq. 1}$$

Where i varies between 5 and 12 and j between 3 and i-3.

On the other hand, the olefins are absorbed by Brönsted acid site and consequently the cracking occurs by β-scission mechanism (Feugnet, 2008). In this reaction, the products are only olefins and not an olefin and a paraffin as in the case of paraffins' cracking reaction. For the olefins species cracking is only available for molecules with more than 6 carbon atoms (O_{6+}).

$$O_i \rightarrow O_j + O_{i-j} \qquad \text{Eq. 2}$$

i ranges from 6 to 12 and j from 3 to i-3.

Hydrogen transfer

In the FCC process hydrogen transfer reactions are usually represented between olefins and naphthenes to produce aromatics and paraffins. However, this reaction is commonly referred in the literature for conventional feeds, i.e. heavy feedstocks. For lighter feeds this assumption does not make sense. Experimental data of pure olefins and paraffins cracking shows the occurrence of this

reaction without the presence of naphthenes (Feugnet, 2008). For this reason, another mechanism is proposed to take into account the olefin cyclisation to produce aromatics. This mechanism is divided in three steps and is described below:

Step 1: Reaction of two olefins to produce an aromatic and three hydrides:

$$O_i + O_j \rightarrow A_{i+j} + 3H_2^* \quad \text{Eq. 3}$$

Where i ranges from 2 to 5 and j from 3 to 5, and $i + j$ is higher than 6. It is possible to consider the auto-cyclization of long olefins (O_{9+}). Nevertheless, the experimental data proposes that the cracking of longer olefins is faster than cyclization. For that reason, the long olefins cyclisation is not consider.

Step 2: Naphthenes dehydrogenation to produce an aromatic and three hydrides

$$N_i \rightarrow A_i + 3H_2^* \quad \text{Eq. 4}$$

This reaction is considered for naphthenes N_6 to N_8. The experimental data suggests that reaction does not occur for naphthenes N_{9+}.

Step 3: Reaction of an olefin and the hydrides from Step 1 and 2 to form a paraffin

$$O_i + H_2^* \rightarrow P_i \quad \text{Eq. 5}$$

This reaction takes place with O_2 to O_{12}.

Oligomerization

This reaction was introduced in 2012 to improve the olefins O_3-O_5 fit (Fernandes, 2010). The oligomerization reaction promotes C-C bonds formation and occurs with reduction in the number of molecules, so it is thermodynamically favored at low temperature and high pressure. This reaction is described in the equation below:

$$O_n + O_i \rightarrow O_{n+i} \quad \text{Eq. 6}$$

With $3 \leq n \leq 5$ and $4 \leq i \leq 5$.

LCO formation

As assumption, LCO was considered as a di-aromatic molecule which molecular representation is C_xH_y. The LCO is produced from aromatic condensation (Eq. 7).

$$\frac{x_{LCO}}{n} A_n \rightarrow LCO + \frac{1}{2} \times \frac{x_{LCO}(2n-6) - y_{LCO}\, n}{n} H_2 \quad \text{Eq. 7}$$

Coke formation

As for the LCO cut, an assumption has to be made for the coke molecular structure. Typically, the coke has 5% in hydrogen (Feugnet, 2008). The coke molecular structure will be represented as C_xH_y. Coke is produced from aromatic condensation as described in the equation below:

$$\frac{x_{Coke}}{n} A_n \rightarrow Coke + \frac{1}{2} \times \frac{x_{Coke}(2n-6) - y_{Coke}\, n}{n} H_2 \quad \text{Eq. 8}$$

Thermal cracking

Thermal cracking can be divided in two main reactions:

- C-C boundary break:

$$C_{m+n}H_{2(m+n)+2} \rightarrow C_mH_{2m} + C_nH_{2n+2}$$ Eq. 9

In this reaction, one paraffin and one olefin are produced. This reaction is a radical reaction which involves a β-scission.

- Dehydrogenation:

$$C_mH_{2m+2} \rightarrow C_mH_{2m} + H_2$$ Eq. 10

Dehydrogenation leads to the formation of H_2. This specie is not, however, observed in experimental data.

Besides the dehydrogenation reaction only happens at 700°C, while the C-C boundary break reaction occurs at temperatures above 300°C. Therefore, the C-C boundary break was considered as the main thermal cracking reaction since in the second riser the temperature[13] does not achieve a such high temperature in order that dehydrogenation reactions can take place (Feugnet, 2008).

It was also assumed that the aromatics and naphthenes do not undergo thermal cracking, and only olefins and paraffins are concerned by this type of reaction. Based on experimental data it was concluded that sensitivity of olefins and paraffins for thermal cracking is different. Therefore, it was considered two sets of reaction to considered separately the olefin (Eq. 11) and paraffin (Eq. 12 and Eq. 13) thermal cracking.

$$O_i \rightarrow O_2 + O_{i-2}$$ Eq. 11

Where i ranges from 4 to 12.

$$P_j \rightarrow P_1 + O_{j-1}$$ Eq. 12

$$P_j \rightarrow O_2 + P_{j-2}$$ Eq. 13

Where j can have values from 3 to 12.

Olefin cyclisation

Olefins cyclisation reactions have been included in the model reaction network in its last version dating from 2012. The objective was to reduce the deviation on aromatics lump. The hydrogen transfer reaction, that produced aromatics, takes places after the cyclisation. Therefore, it was considered the formation of naphthenes from olefin cyclisation. With this assumption the naphthenes formed in this reaction will be considered in hydrogen transfer reaction to form aromatics (Palma, 2012). This reaction just occurs in the range O_6 to O_8 and according with the follow equation:

$$O_i \rightarrow N_i$$ Eq. 14

Where i can be 6, 7 or 8.

4.3. Kinetic model

The present reaction network includes 125 reactions of seven different types:

- 52 catalytic cracking reactions
  - 16 olefins β-scission cracking reactions
  - 36 paraffins protolytic cracking reactions

[13] The temperature is preferably in the range 580°C to 610°C (sub-chapter 2.2.2)

- 22 hydrogen transfer reactions
    - 8 Step 1 reactions
    - 3 Step 2 reactions
    - 11 Step 3 reactions
- 5 olefins oligomerization reactions
- 7 LCO formation reactions
- 8 Coke formation reactions
- 28 thermal cracking reactions
    - 9 reactions for olefins
    - 19 reactions for paraffins
- 3 olefins cyclisation reactions

To model the reaction network the kinetic rates for each one of the reactions are given by an Arrhenius law type equation. To simplify the model and due to the lack of experimental data several assumptions were made.

One of the assumptions of this model is that the catalyst deactivation is not taken into account. The coke concentration on catalyst produced from light feeds is normally less than 0.2% even when the reaction finishes, the catalyst decay is, therefore, neglected (Wang, et al., 2005).

Furthermore, the mechanisms of adsorption/desorption are also neglected since it would be difficult to estimate adsorption/desorption rates with the experimental data available.

Finally, in order to reduce the number of parameters to estimate, simple expressions relating the rate constant with the nature of the reacting species, their chain length and symmetry have been implemented.

The next topics present the correlations for each reaction type. In the following expressions, the reference temperature considered, T_{ref} is 550°C.

Catalytic cracking

The kinetic rate for catalytic cracking reactions is based in Arrhenius law and the kinetic constants are correlated to reactive species chain length like in the model proposed by Carabineiro, et. al (2003) and Pinheiro, et al. (1999). Catalytic cracking constants are also impacted by the ZSM-5 content which has an effect on light fractions production. The rate constant is obtained from Eq. 15 and Eq. 16, for paraffins and olefins cracking respectively.

$$K_{pcr} = K_{pcr}^{0} \cdot \exp\left(-\frac{Ea_{pcr}}{R} \cdot \left(\frac{1}{T} - \frac{1}{T_{ref}}\right)\right) \cdot \exp\left(-\left(\frac{\alpha_{cr}}{i} + \beta_{cr} \cdot \left(j - \frac{i}{2}\right)^{2}\right)\right)\left(1 + f_{ZSM-5,pcr}(i,j)\right) \quad \text{Eq. 15}$$

$$K_{ocr} = K_{ocr}^{0} \cdot \exp\left(-\frac{Ea_{ocr}}{R} \cdot \left(\frac{1}{T} - \frac{1}{T_{ref}}\right)\right) \cdot \exp\left(-\left(\frac{\alpha_{cr}}{i} + \beta_{cr} \cdot \left(j - \frac{i}{2}\right)^{2}\right)\right)\left(1 + f_{ZSM-5,ocr}(i,j)\right) \quad \text{Eq. 16}$$

Where K_{pcr}^{0} and K_{ocr}^{0} are the parameters for the cracking rate magnitude of paraffin and olefins cracking, respectively. These parameters are related to the overall rate of cracking for all the possible reactants of each reaction set. i and j are number of carbon atoms of the reactant and the product, respectively according to the chemical reaction (Eq. 1 and Eq. 2, page 22).

By taking into account the reactant chain length and the symmetrical scission in kinetic constant rate calculation, it is possible to use one single rate expression for all reactants (Pinheiro, et al., 1999). For this, two structure parameters are needed:

- α_{cr} is the chain-length parameter which is related to the way that cracking rate increases with the number of carbon atoms in the reactant;
- β_{cr} is the symmetry parameter that defines the variation of the rate constant, with the type of products (Carabineiro, et al., 2003).

The structure parameters have the same values for paraffins and olefins.

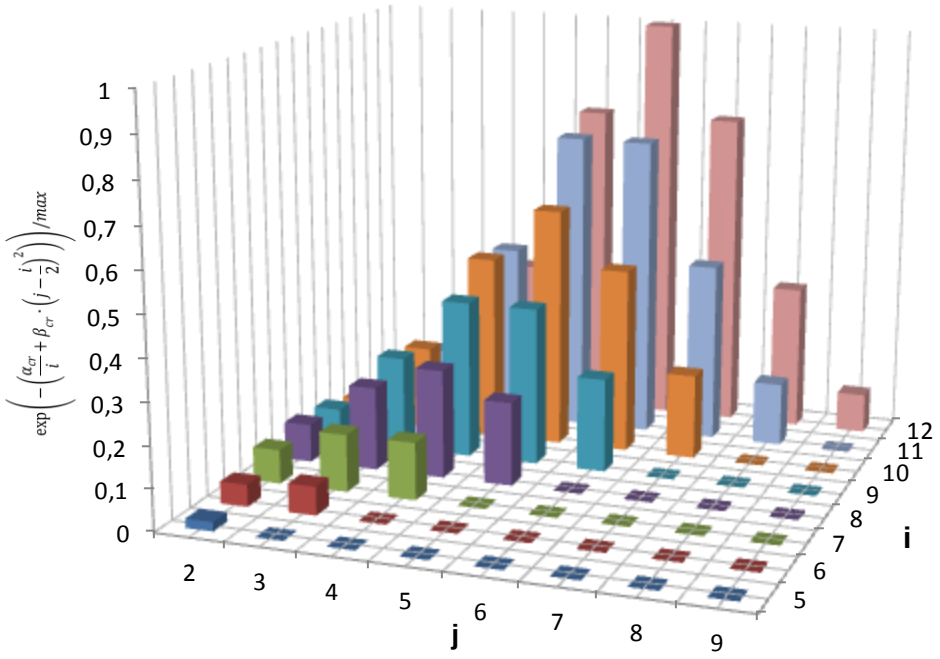

Figure 18 – Representation of molecule structure function for catalytic cracking normalized with its maximum value

Concerning this molecule structure function, the cracking rate follows a normal distribution where the maximum is verified for the symmetrical scission. This can be observed in Figure 18 for each i. For example, for $i = 12$, a reactant molecule with 12 carbon atoms, a normal distribution is observed during j, where the maximum is established for cracking in two molecules with 6 carbon atoms each.

As discussed in sub-chapter 2.2.4, the presence of ZSM-5 promotes the cracking for long paraffins and olefins. This effect was not considered until 2012. At the time, it was introduced a function in order to modulate the kinetic rate increasing in catalytic cracking reactions due to the presence of this

zeolite. The influence of ZSM-5 is only considered in the cracking of paraffins from P_7 to P_9 and olefins from O_6 to O_{10} (Palma, 2012).

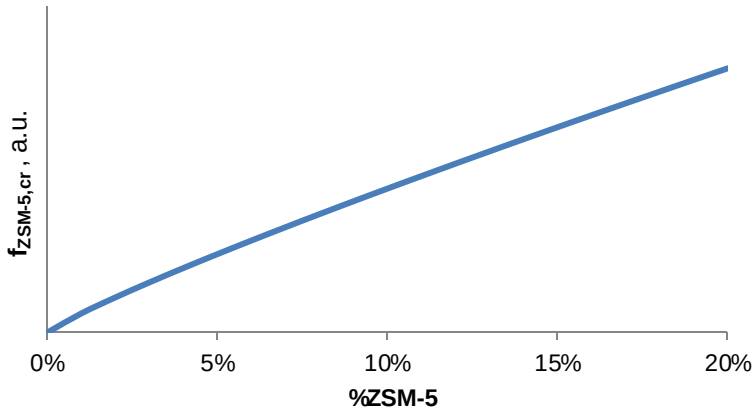

Figure 19 - ZSM-5 influence for kinetic rate of paraffins and olefins catalytic cracking in function of ZSM-5 content percentage

Figure 19 describes the function $f_{ZSM-5,cr}$ which has the same behavior for paraffins and olefins cracking. As expected, the function depends of ZSM-5 percentage in the catalyst and its value without ZSM-5 is zero. This function also depends of the number of carbon atoms of the reactant, i. However the variation with carbon number is very limited, i.e. the function is quite similar for all reactions in the same set (olefins or paraffins).

Hydrogen transfer

As described in the previous chapter, the hydrogen transfer reaction is subdivided in three steps. Therefore, the kinetic rate is defined separately for each step. For all of them, it is not considered the activation energy because it was assumed that hydrogen transfer are very fast reactions and therefore independent of temperature level (Feugnet, 2008).

Step 1: Reaction of two olefins to produce aromatic and three hydrides

$$K_{ht1} = K^0_{ht1} \cdot f_{ht1}(i,j) \cdot (1 + f_{ZSM-5,ht1}) \qquad \text{Eq. 17}$$

The function f_{ht1} depends of i and j which are respectively the number of carbon atoms of reactants concerning the reaction represented by Eq. 3 (page 23). This function takes into account the cracking dependence factor on the reactant carbon chain length similarly to what has been done in Carabineiro's (2003) study. f_{ht1} is graphically represented in Figure 20.

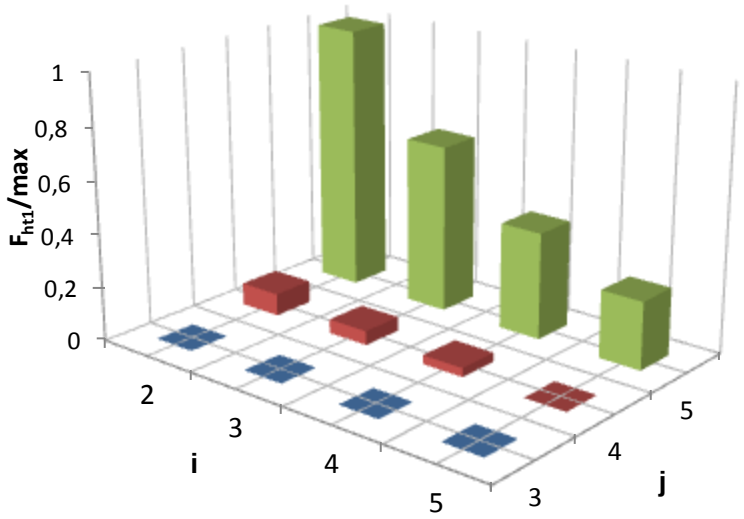

Figure 20 – Representation of f_{ht1} normalized with its maximum value in function of i and j, the reactant carbon numbers

Regarding the f_{ht1} representation, it is possible to conclude that kinetic constant will be favored by the reaction of a small olefin with a longer one. For example, considering an olefin O_3, if it reacts with another O_3 the effect of this function will be almost neglected. Nevertheless, if this molecule reacts with an O_4 the effect will be higher and with an O_5 much higher.

Although the ZSM-5 does not impacts directly hydrogen transfer reactions, it has been considered that the presence of ZSM-5 in the catalyst has a dilution effect in hydrogen transfer reactions. As presented in sub-chapter 2.2.4, zeolites as ZSM-5 show relatively low hydrogen transfer values. The function represented in Figure 21 introduces the effect of dilution considered for the ZSM-5 content (Palma, 2012).

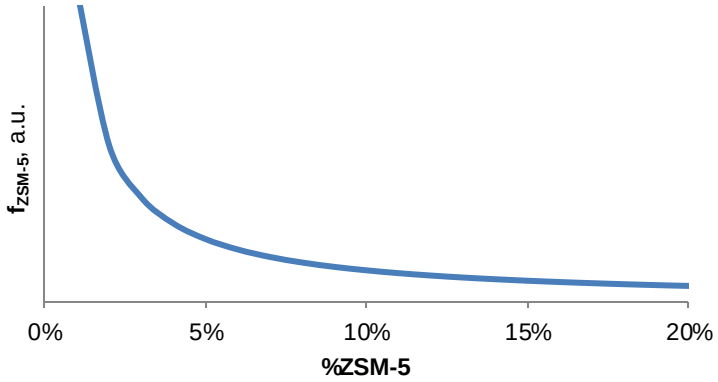

Figure 21 - ZSM-5 influence for kinetic rate of hydrogen transfer reaction (step 1) in function of ZSM-5 content percentage

This function was implemented for the interval between 10% and 18% of ZSM-5 additive in the E-cat, since the experimental data at the time (2012) included only percentages of ZSM-5 content in this range. However, below 10% of ZSM-5, this function should not be applied, since the function increases very significantly when the content of ZSM-5 is lower than 5%.

Step 2: Naphthenes dehydrogenation to produce an aromatics and three hydrides

$$K_{ht2} = K_{ht2}^{0} \cdot f_{ht2}(i) \quad \text{Eq. 18}$$

Step 3: Reaction of a olefin and the hydrides from Step 1 and 2 to form a paraffin

$$K_{ht3} = K_{ht3}^{0} \cdot f_{ht3}(i) \quad \text{Eq. 19}$$

In the same way that Step 1, the kinetic constant of Step 2 and 3 are conditioned by f_{ht2} and f_{ht3}. Furthermore, these functions depend of i which is the number of carbon atoms of the reactant concerning the reaction in analysis (Eq. 4 or Eq. 5, page 23). These functions introduce the cracking dependence of the reactant carbon chain length.

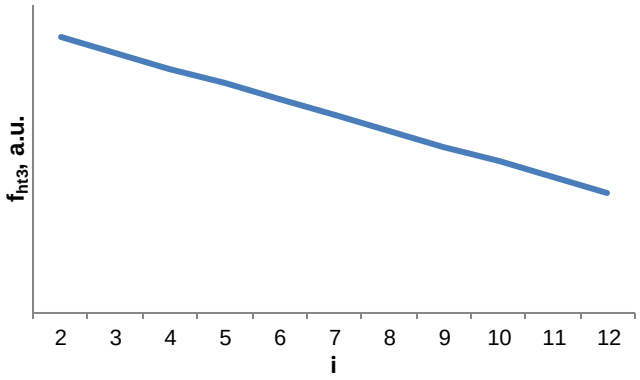

Figure 22 – Representation of f_{ht3} in function of i, the reactant carbon number

Figure 22 represents f_{ht3}, which has the same behavior that f_{ht2}. According to the representation above, the kinetic rate for these reactions is promoted for small molecules.

Oligomerization

The kinetic rate for the oligomerization reaction is obtained by the Arrhenius law. However, it was considered a different K_{Oligom}^{0} for each reaction (Fernandes, 2010). Therefore, this reaction type contributes with 5 pre-exponential constants ($i \leq 5$) that need to be estimated.

$$K_{Oligom,i} = K_{Oligom,i}^{0} \cdot \exp\left(-\frac{Ea_{Oligom}}{R} \cdot \left(\frac{1}{T} - \frac{1}{T_{ref}}\right)\right) \quad \text{Eq. 20}$$

LCO and coke formation

For LCO and coke formation reactions, it is used the Arrhenius law without specific modifications. The Eq. 21 and Eq. 22 represent the kinetic rate for LCO and coke formation respectively.

$$K_{LCO} = K_{LCO}^{0} \cdot \exp\left(-\frac{Ea_{LCO}}{R} \cdot \left(\frac{1}{T} - \frac{1}{T_{ref}}\right)\right) \quad \text{Eq. 21}$$

$$K_{Coke} = K_{Coke}^{0} \cdot \exp\left(-\frac{Ea_{Coke}}{R} \cdot \left(\frac{1}{T} - \frac{1}{T_{ref}}\right)\right) \quad \text{Eq. 22}$$

Thermal cracking

As explained in sub-chapter 2.2.4, thermal cracking is considered only for paraffins and olefins. Nonetheless, the paraffins and olefins cracking are described separately in two sets of reactions.

The olefins thermal cracking (*th1*) is defined by Eq. 11 and its kinetic rate is given by Eq. 23. The paraffin thermal cracking (*th2*) is resumed in Eq. 12 and Eq. 13, and its kinetic rate is obtained with Eq. 24.

$$K_{th1} = K_{th1}^{0} \cdot \exp\left(-\frac{Ea_{th1}}{R} \cdot \left(\frac{1}{T} - \frac{1}{T_{ref}}\right)\right) \cdot f_{th1}(i) \qquad \text{Eq. 23}$$

$$K_{th2} = K_{th2}^{0} \cdot \exp\left(-\frac{Ea_{th2}}{R} \cdot \left(\frac{1}{T} - \frac{1}{T_{ref}}\right)\right) \cdot f_{th2}(j) \qquad \text{Eq. 24}$$

The above equations are both based on Arrhenius law with two corrective functions (f_{th1} and f_{th2}) to stand for the dependence of the reactant carbon chain length.

f_{th1} and f_{th2} are graphically represented by Figure 23. As it can be observed, thermal reaction is promoted for long carbon chain length. Moreover, if we look at the trend of f_{th1} we see that olefins O_{8+} are extremely reactive for thermal cracking.

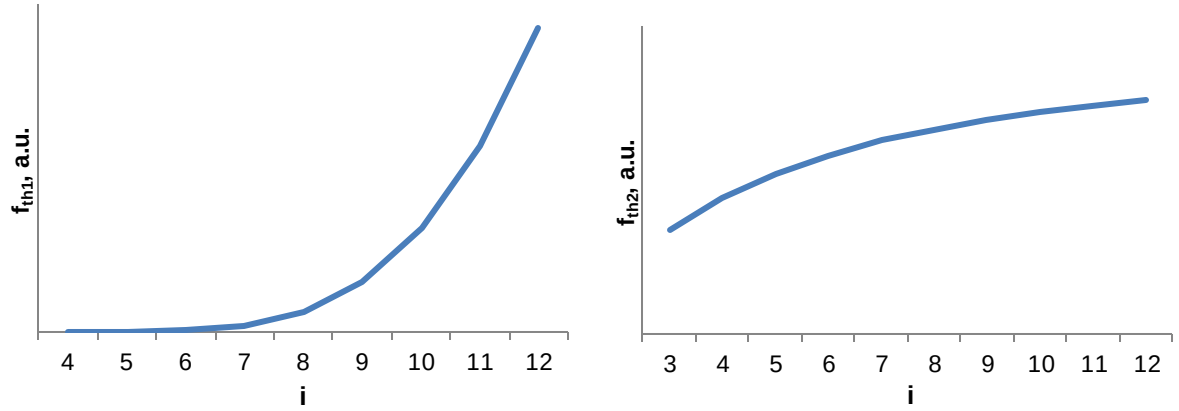

Figure 23 – Representation of f_{th1} and f_{th2} in function of i, the reactant carbon number

Olefin cyclisation

The kinetic rate is given by an Arrhenius law, and the pre-exponential constant and activation energy were considered to be the same for all the reactions of this type..

$$K_{Cycli} = K_{Cycli}^{0} \cdot \exp\left(-\frac{Ea_{Cycli}}{R} \cdot \left(\frac{1}{T} - \frac{1}{T_{ref}}\right)\right) \qquad \text{Eq. 25}$$

4.4. Model implementation

For the model implementation, it is necessary to establish the material and pressure balances. Therefore, it is necessary to make some assumptions:

- R2R pilot is considered as a plug flow
- Small pressure drop and consequently the catalyst concentration is uniform along the riser
- Pressure drop is neglected
- Isothermal operation (light feeds cracking enthalpy is low)

The material and pressure balances are achieved according to dZ slices as showed in Figure 24.

.

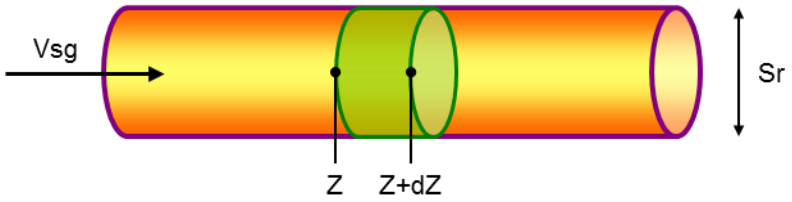

Figure 24 – Control volume scheme

The several reactions occur in different phases (gas and solid) and depend or not of the presence of the catalyst. Besides there is accumulation of product species in both gas and solid phases. Therefore, the material balances for each phase have to be described separately.

First of all, it is essential the distinction between catalytic and thermal reactions. The catalytic reactions take place in the catalyst (solid phase), while the thermal reactions occur in the gas phase. Second, although there are several reactions taking place in the solid phase most of the product species after their formation will desorb from the catalyst and go to the gas phase, except for coke that will remain in the solid phase adsorbed and/or trapped in the catalyst sites leading to catalyst deactivation.

Material balance in gas phase (for catalytic and thermal reactions)

$$(1-\varepsilon_S)\cdot\frac{\partial C_i^g}{\partial t} = -\frac{\partial}{\partial Z}\left(V_{sg}\cdot C_i^g\right) + \rho_S\cdot\varepsilon_S\cdot\sum_{n=1}^{gas\ catalytic\ reactions}\left(\mu_{i,n}\cdot V_n\right) + (1-\varepsilon_S)\cdot\sum_{n=1}^{thermal\ reactions}\left(\mu_{i,n}\cdot V_n'\right) \quad \text{Eq. 26}$$

Where:

- ε_S is the solid void fractions or hold-up;
- V_{sg} is the superficial gas velocity $(m\ s^{-1})$;
- ρ_S is the solid density $(kg\ m^{-3})$;
- C_i^g is the molar concentration of the specie i in the gas phase $(mol\ m^{-3})$;
- n is the reaction number;
- V_n is the reaction n rate $(mol\ s^{-1}\ kg_{catalyst}^{-1})$;
- V_n' is the reaction n rate in $mol\ s^{-1}\ m^{-3}$.
- $\mu_{i,n}$ is the stoichiometric coefficient of the specie i in the reaction n;
- t is time (s).

Material balance in solid phase

$$\varepsilon_S\cdot\frac{\partial C_i^s}{\partial t} = \rho_S\cdot\varepsilon_S\cdot\sum_{n=1}^{solid\ catalytic\ reactions}\left(\mu_{i,n}\cdot V_n\right) - \frac{\partial}{\partial Z}\left(V_{sg}\cdot C_i^s\right) \quad \text{Eq. 27}$$

Finally, it is important to establish the pressure balance in order to describe the volume expansion. The balance is obtained considering the gases mass balances of all the species.

Pressure balance – partial pressure and volume expansion

$$\frac{\partial V_{sg}}{\partial Z} = \frac{RT}{P_t} \cdot (\rho_S \cdot \varepsilon_S) \cdot \left[\sum_{i}^{\textbf{species gas}} \sum_{j=1}^{catalytic\ reactions} (\mu_{i,j} \cdot V_n) + (1 - \varepsilon_S) \cdot \sum_{i}^{\textbf{species gas}} \sum_{j=1}^{thermal\ reactions} (\mu_{i,j} \cdot V'_n) \right] \quad \text{Eq. 28}$$

Rate equations

Concerning the calculation of kinetic rate, it is admitted that reactions are elementary, excluding coke formation which is considered a first order reaction.

Therefore, for the reaction n,

$$\mu_{i,n} \cdot [i] + \mu_{j,n} \cdot [j] \rightarrow product(s) \quad \text{Eq. 29}$$

The components i and j react according to their stoichiometry coefficient $\mu_{i,n}$ and $\mu_{j,n}$ respectively. The kinetic rate is obtained by Eq. 30.

$$V_n = K_X P p_i^{\mu_{i,n}} P p_k^{\mu_{j,n}} \quad \text{Eq. 30}$$

4.5. Model modifications

4.5.1. ZSM-5 effect review

As described above in chapter 4.3, the ZSM-5 influence is taken into account in hydrogen transfer reaction as a dilution factor. Nevertheless, the equation that describes this effect was established based on data with 10 and 18% of ZSM-5 content. The present function predicts incoherent values for the range between 0% and 10% of ZSM-5.

Some experimental tests of coker gasoline were obtained with 0% and 5% of ZSM-5 in the catalyst. For that reason and for coherence purposes the mathematical form of this function had to be reevaluated. The new function is graphically presented in the graph below.

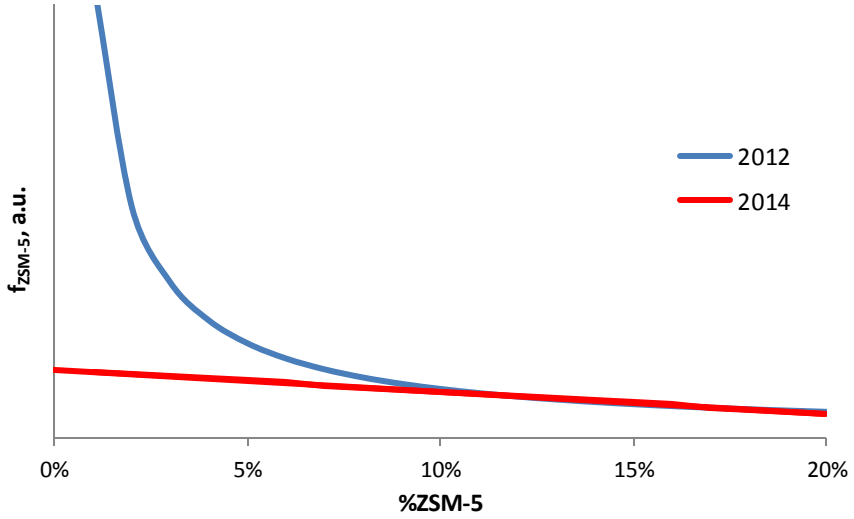

Figure 25 – Comparison of ZSM-5 effect function in 2012 and its improvement in 2014

In the new approach, it was assumed a smooth decreasing from 0% to 10% and the same behavior in range between 10% and 20%. The previous function and the new approach are compared in Figure 25. As it can be seen, both functions give about the same values between 10 and 18% of ZSM-5 content.

Concerning the catalytic cracking, the carbon atoms number does not influence the ZSM-5 function results. For that reason, the function will be simplified without this dependence.

4.5.2. LCO formation as a first order reaction

As referred in the model implementation chapter, the reaction to produce LCO is an elementary reaction, meaning that the reaction order for LCO formation is the same as the reactant stoichiometric index for LCO formation which can be relatively high. Since during the simulation work it was observed that the model did not gave good prediction for LCO production, and for some experimental tests did not even anticipated the formation of this cut[14] a revision to the kinetic rate equation was done.

After reviewing LCO kinetic rate equation, it has been concluded that considering a reaction order dependent on the stoichiometric coefficient was not appropriate for LCO formation. In the new model, LCO formation is therefore considered as a first order reaction. This modification also facilitates the convergence when the reactants leading to LCO formation (Aromatics) are weakly represented, like in the oligomers case.

4.5.3. Isoparaffins implementation

Previous works have taken place at IFPEN with the purpose of improving the second riser model predictions (Palma, 2012). However, no distinction was made between linear and branched hydrocarbons until now. Consequently, it is considered at this point the same set of components and reactions for normal and branched paraffins/olefins. Although with the assumptions made, the structural parameters and reactions are not necessarily the same for the normal and branched

[14] This observation was made after the isoparaffins implementation.

molecules. For that reason, in this work the isoparaffins were implemented as well as a set of reactions for these new species.

Before the isoparaffins implementation in reaction network, it is necessary to make some more assumptions. Starting with the components, the isoparaffins can be mono-branched, di-branched, tri-branched, etc. If it was considered all the types or the majority of possibilities, the number of species and reactions would increase exponentially. Therefore, it was decided to just consider the isoparaffins without the distinction of the number of branches. Consequently, it is necessary to add 9 additional species in the model, representing the isoparaffins with 4 to 12 carbon atoms (iP4 to iP12). The new model will then have a total of 54 molecular lumps.

By splitting paraffins into normal and branched, new reactions need to be implemented in the reaction network. In order to simplify it by reducing the reaction number, it will be assumed:

- The previous reactions or kinetic expressions do not require any changes[15],
- The paraffins and isoparaffins catalytic cracking will only produce linear paraffins,
- The isoparaffins are produced only from isomerization and isoparaffins thermal cracking reactions.

If it had been considered isoparaffins as a product of catalytic cracking, the reaction number would have increased too much for this first approach in implementing isoparaffins in the kinetic model. It was then decided that, for the moment, only the isoparaffins catalytic and thermal cracking and the isomerization reactions would be considered. For the two firsts reactions, the same approach and assumptions for paraffins were made.

Isoparaffins catalytic cracking

The isoparaffins cracking is only present for iP_{5^+}, according to the next equation:

$$iP_i \rightarrow P_j + O_{i-j} \qquad \text{Eq. 31}$$

Where i ranges from 5 to 12 and j from 3 to i-3.

The kinetic rate is defined by Eq. 32 which is similar to the one used for paraffin cracking. Nevertheless, the structure parameters are not necessarily the same for normal and branched paraffins. For that reason, it is assumed a different value for these parameters ($\alpha_{cr,iso}$ and $\beta_{cr,iso}$).

$$K_{pcr,iso} = K^0_{pcr,iso} \cdot \exp\left(-\frac{Ea_{pcr,iso}}{R} \cdot \left(\frac{1}{T} - \frac{1}{T_{ref}}\right)\right) \cdot \exp\left(-\left(\frac{\alpha_{cr,iso}}{i} + \beta_{cr,iso} \cdot \left(j - \frac{i}{2}\right)^2\right)\right) \qquad \text{Eq. 32}$$

As discussed in sub-chapter 2.2.3, some studies refer that the pores sizes of ZSM-5 are not enable the access for branched molecules. For this reason, the ZSM-5 effect was not taken into account.

Isoparaffins thermal cracking

Thermal cracking for isoparaffins was established in the same way that for paraffins. Thermal cracking for branched alkanes is then given according to Eq. 33 and Eq. 34.

[15] The paraffins lump that was presented in chapter 4.2 and 4.3 will describe the normal paraffins.

$$iP_j \rightarrow P_1 + O_{j-1} \quad \text{Eq. 33}$$

$$iP_j \rightarrow O_2 + iP_{j-2} \quad \text{Eq. 34}$$

Where i can have values from 3 to 12.

The kinetic rate constant is defined by Eq. 35 in the same way as for paraffin thermal cracking. Once again, the f_{th2} parameters will be different between the both types of paraffins.

$$K_{th2,iso} = K^0_{th2,iso} \cdot \exp\left(-\frac{Ea_{th2,iso}}{R} \cdot \left(\frac{1}{T} - \frac{1}{T_{ref}}\right)\right) \cdot f_{th2,iso}(j) \quad \text{Eq. 35}$$

Isomerization

Differently from the last reactions, the isomerization reaction is a chemical equilibrium between paraffins and isoparaffins (Eq. 36).

$$P_i \rightleftarrows iP_i \quad \text{Eq. 36}$$

Where i ranges between 4 and 12.

In this case, the kinetic rate is more complex than for the previous irreversible reactions. The reversible reaction defines the equilibrium that has to be taken into account in kinetic rate (Eq. 37).

$$r = K_{i,ISOM}\left(Pp_{nP} - \frac{Pp_{iP}}{K_{eq}}\right) \quad \text{Eq. 37}$$

The equilibrium constant is obtained by thermodynamic data which is available in literature (Joly, et al., 1997). The equilibrium constant, K_{eq} depends of the temperature (Eq. 38).

$$K_{eq}(T) = \exp\left(-\frac{\Delta G_r(T)}{RT}\right) \quad \text{Eq. 38}$$

Where the difference of Gibbs free energy, ΔG_r is given by the equation below.

$$\Delta G_r(T) = \sum_j v_j \Delta H_{f,j}(T) - T\sum_j v_j S_{f,j}(T) \quad \text{Eq. 39}$$

With $v_j = 1$ for the isoparaffins and $v_j = -1$ for the paraffins. ΔH_f and S_f are calculated by Eq. 40 and Eq. 41, respectively.

$$S_f(T) = S°_f + \int_{298}^{T} C_p(T)dT \quad \text{Eq. 40}$$

$$\Delta H_f(T) = \Delta H°_f + \int_{298}^{T} C_p(T)dT \quad \text{Eq. 41}$$

The thermodynamic data used in these calculations is from another IFPEN project, and for this reason this data is confidential and will not be presented herein.

On the other hand, the kinetic rate constant is obtained using Arrhenius law, where the isomerization constant, K^0_{Isom}, was obtained from parameters estimation for each isomerization reaction (Eq. 42). The activation energy was considered to be the same for all isomerization reactions.

$$K_{Isom,i} = K^0_{Isom,i} \cdot \exp\left(-\frac{Ea_{Isom}}{R} \cdot \left(\frac{1}{T} - \frac{1}{T_{ref}}\right)\right) \quad \text{Eq. 42}$$

Moreover, the reactions that were introduced were assumed to be elementary reactions.

4.6. Optimization

In the previous sections several parameters have been identified in the kinetic expressions that need to be estimated and optimized. The optimal values of the various parameters in the model are determined by minimizing an objective function with respect to the parameters. This objective function depends on the selected optimization principle, which is determined by the statistical distribution of the experimental errors. A widely used method is the least squares principle. This method minimizes the sum of the squares of the errors, i.e. of the deviations between the observed values and the values predicted by the model. Hence, the objective function is described by Eq. 43.

$$minimize \left\{ ssq = \sum_{x} \left(y_{experimental,x} - y_{calculated,x} \right)^2 W_x \right\} \quad \text{Eq. 43}$$

Where W_x represents the weight conferred for the observable in analysis. $y_{experimental}$ and $y_{calculated}$ are the experimental and calculated value of each observable, respectively. The weight for the observables is given according to its importance and sensibility to the model.

The minimization of the objective function can be performed with any optimization algorithms. However, special algorithms are available for the minimization of a sum of squares, such as the Gauss method for linear problems and the Newton-Gauss method for nonlinear models. For reducing the possibilities of divergence, it was used the Levenberg-Marquardt algorithm which is more constrained and robust than other methods.

The mass balances obtained experimentally are the basis for the optimization, where the observables are the yields of the components. However, with the isoparaffins introduction it was necessary to consider the ratio between the isoparaffins and the total of paraffins as observable. This upgrade enables a favorable equilibrium establishment between normal and branched paraffins. The total observables number to optimize is 2666.

The activation energies were previously chosen in the literature ranges to achieve better results (Table 7). For the new reactions of isoparaffins, it was assumed the same activation energy of normal paraffins catalytic and thermal cracking. The activation energy of isomerization was obtained by exploratory solution methodology starting with a value from a IFPEN report.

The decision for not try to estimate the activation energies was based in the fact that the experimental data available was obtained in a relative narrow range of temperature. Therefore it would be difficult to obtain well estimated values for activation energies.

Table 7 – Activation energies values used in the model

Reaction	$Ea, J\ mol^{-1}$
n-paraffins catalytic cracking	56234
Olefins catalytic cracking	50119
LCO formation	44668
Coke formation	44668
Olefins thermal cracking (th1)	50003
n-paraffins thermal cracking (th2)	50816
Oligomerization	50119
Cyclisation	50119
Isoparaffins catalytic cracking	56234
Isoparaffins thermal cracking	50816
Isomerization	50000

The others kinetic parameters were obtained by optimization. The 41 parameters are divided between pre-exponential constants, structure parameters and ZSM-5 factors according with the following table:

Table 8 – Kinetic parameters distribution by reaction

Reaction	Pre-exponential constants	Structure parameters	ZSM-5 factors
n-paraffins and olefins catalytic cracking	2	2	3
Hydrogen transfer, step 1	1	2	2
Hydrogen transfer, step 2	1	1	0
Hydrogen transfer, step 3	1	1	0
LCO formation	1	0	0
Coke formation	1	0	0
Olefins thermal cracking (th1)	1	1	0
n-paraffins thermal cracking (th2)	1	1	0
Oligomerization	5	0	0
Cyclisation	1	0	0
Isoparaffins catalytic cracking	1	2	0
Isoparaffins thermal cracking	1	1	0
Isomerization	9	0	0

This page was intentionally left blank.

5. Results

The implementation of isoparaffins in the model introduced more species, reactions and parameters to optimize. The main differences between the previous version of Petroriser and the model obtained in this work are presented in Table 9.

Table 9 – Characteristics and execution time for the models of 2012 and 2014

Model	2012	2014
Composition	PONA	PIONA
Number of components	45	54
Number of reactions	125	187
Number of reversible reactions	0	9
Number of mass balances[16]	31	43
Number of parameters to optimize	27	41
Total execution time for a single mass balance simulation (s)	4,01	20,98
Total execution time for an iteration of one parameter optimization for a single mass balance (s)	11,95	126,20

It is important to refer that the execution times presented in Table 9 were obtained in a Intel® Core™ 2 (CPU Intel 2.66 GHz, 4GB RAM) for a tolerance error less than 10^{-3}. As presented above, the processor time taken by the simulator is much higher with the new model. The time for one mass balance simulation, i.e. the solution of a mass balance with the given parameters, increases five times. Consequently, the execution time to optimize one parameter for a single mass balance also increases. With the new model version, the optimization for a given set of parameters and mass balances can take more than 72 h. The longtime required for parameters optimization has restrained the number of modifications that could be implemented in the model and tested.

The high execution time can be justified by the simulator structure. The mass balances are solved in dynamic state and its convergence is obtained when the steady state is achieved. With the introduction of new species and additional reversible reactions it was already expected that the time to reach the steady state would be even longer.

In the last version of second riser model, the structure parameters and ZSM-5 factors are the same for all the feeds. On the other hand, the pre-exponential constants were estimated separately for each feed to distinguish the difference between their reactivities.

One of the long-term goals in the second riser model development is to obtain a single set of kinetic parameters for all type of feeds. To approach this goal it was first tried to group the feeds. By analyzing their composition (Figure 15) it seems evident that there are two types of feeds and subsequently two sets of pre-exponential factors. The gasolines are composed by a complex PIONA family and must be concerned in one of these sets. The oligomers are composed mainly by olefins and isoparaffins and are able to be represented in the other set.

After optimizing the parameters, it was possible to conclude that gasolines can be represented by one set of pre-exponential constants, without significantly deteriorating the model quality of prediction. The

[16] Mass balance is an experimental test performed in the conditions established in chapter 3

same method was tried for the oligomers, however for this type of feed the results are worst. This is probably justified for the use of different catalysts in the experimental tests (see Table 4 and Table 5). The catalyst A used in PolyC3C4 tests has a higher content of rare-earth than catalyst B used in PolyC4 tests. Rare-earth content in FCC catalyst is known to promote the catalytic activity, but it also promotes the hydrogen transfer reaction. Furthermore, E-cat A has much higher content of metal contaminants such as nickel and vanadium than E-cat B, and it is well accepted that metals contaminants decrease the catalytic cracking performance. Finally, catalyst B (used in PolyC4 tests) has a higher content in matrix that is supposed to favor the cracking of large molecules and it has also a higher content in ZSM-5. However, without a full characterization of catalysts it is difficult to conclude about their effects in the results.

It has then been decided to keep three different sets of pre-exponential constants: one single set for all gasoline type feeds (catalytic and coker gasoline) and two different sets for the two oligomers respectively.

Table 10 – Results for the sets of pre-exponential constants for the different feeds normalized with the correspondent value for gasolines feeds

$K^0_{feed}/K^0_{gasolines}$	Gasolines	PolyC3C4	PolyC4
Olefins catalytic cracking	1	1,01	1,43
n-paraffins catalytic cracking	1	$8{,}14\times10^{1}$	$2{,}49\times10^{-1}$
Hydrogen transfer, step 1	1	$4{,}60\times10^{-1}$	$1{,}31\times10^{-1}$
Hydrogen transfer, step 2	1	1,87	5,26
Hydrogen transfer, step 3	1	5,30	$5{,}28\times10^{2}$
LCO formation	1	6,03	5,31
Coke formation	1	5,08	$1{,}22\times10^{1}$
Olefins thermal cracking (th1)	1	$2{,}00\times10^{-2}$	$9{,}47\times10^{-2}$
n-paraffins thermal cracking (th2)	1	$2{,}90\times10^{1}$	$5{,}57\times10^{1}$
Oligom.: $O_4 + O_4 \rightarrow O_8$	1	$6{,}75\times10^{-1}$	$5{,}34\times10^{-1}$
Oligom.: $O_4 + O_5 \rightarrow O_9$	1	$3{,}09\times10^{-3}$	$4{,}81\times10^{-7}$
Oligom.: $O_5 + O_5 \rightarrow O_{10}$	1	$2{,}45\times10^{1}$	3,48
Oligom.: $O_4 + O_3 \rightarrow O_7$	1	1,22	$5{,}66\times10^{-1}$
Oligom.: $O_5 + O_3 \rightarrow O_8$	1	1,23	$5{,}23\times10^{-7}$
Olefin cyclisation	1	$2{,}36\times10^{-7}$	$6{,}09\times10^{1}$
Isoparaffins catalytic cracking	1	$4{,}47\times10^{4}$	3,51E+05
Isoparaffins thermal cracking	1	2,43	$1{,}21\times10^{-7}$
P_4/iP_4 Isomerization	1	$1{,}28\times10^{-1}$	$2{,}06\times10^{-1}$
P_5/iP_5 Isomerization	1	$3{,}63\times10^{-1}$	7,84
P_6/iP_6 Isomerization	1	$7{,}39\times10^{4}$	$8{,}30\times10^{-4}$
P_7/iP_7 Isomerization	1	$1{,}19\times10^{-5}$	$6{,}40\times10^{-7}$
P_8/iP_8 Isomerization	1	$3{,}92\times10^{-3}$	$4{,}44\times10^{-3}$
P_9/iP_9 Isomerization	1	$5{,}98\times10^{4}$	$1{,}31\times10^{5}$
P_{10}/iP_{10} Isomerization	1	$1{,}24\times10^{3}$	$1{,}25\times10^{-2}$
P_{11}/iP_{11} Isomerization	1	1,02	$2{,}66\times10^{-6}$
P_{12}/iP_{12} Isomerization	1	$4{,}09\times10^{1}$	$3{,}31\times10^{-8}$

The differences between the three sets of pre-exponential factors obtained for the feeds are given in Table 10.

By analyzing the differences between the oligomer feeds, it can be seen that PolyC4 has higher values for olefins and isoparaffins catalytic cracking that can be justified by the decrease of catalytic cracking performance conferred by high vanadium contents. Nonetheless, for the case of normal paraffins catalytic cracking, the trends are not according with that. However, estimating this parameter for these feeds is quite difficult since the representation of normal paraffins in the feeds is very weak.

Looking to the hydrogen transfer reaction, it was expected higher values in PolyC3C4 comparing to the PolyC4 that are conferred by the double content in rare-earth of E-cat A. Nevertheless, this is not observed in the pre-exponential constants results. The reason for that can be explained by the rare-earth location. The rare-earth can be located on the zeolite and on the matrix (Echard & Feugnet, 2007). In the zeolite, it promotes the hydrogen transfer and in the matrix the rare-earth mainly plays the role of a vanadium trap. Unfortunately, the information about the rare-earth location was not provided by the catalyst suppliers and for that reason it is difficult to compare the different results and to quantify the impact of the rare-earth (Echard & Feugnet, 2007). It is important to refer that the analysis above about the different catalysts reactivities is just a proposition to try to explain the results. However, as already referred it is difficult drawing conclusions without complete characterization of catalysts and additional experimental data. More precisely, experimental data on the two catalysts, A and B, using the same feed and same operating conditions would be of great help.

A similar comparison can also be done between gasolines and oligomers results. The main difference in their composition is the aromatics content that is almost inexistent in oligomer feeds (Figure 15). In the kinetic model it is assumed that coke is produced exclusively by aromatics. However, feeds testing have demonstrated that all feeds produce identical amounts of coke (Table 6). It is then expected a lower pre-exponential constant factor for gasolines which is reflected by the results. The same type of observations can be done for LCO formation.

The structure parameters for linear and branched paraffins also need to be analyzed. It was assumed for both cases the same type of function that takes into account the chain-length and the cracking symmetry. However, different parameters for normal and iso paraffins were estimated to define this function. Figure 26 presents its results for C_{12} normal- and iso- paraffins cracking situation.

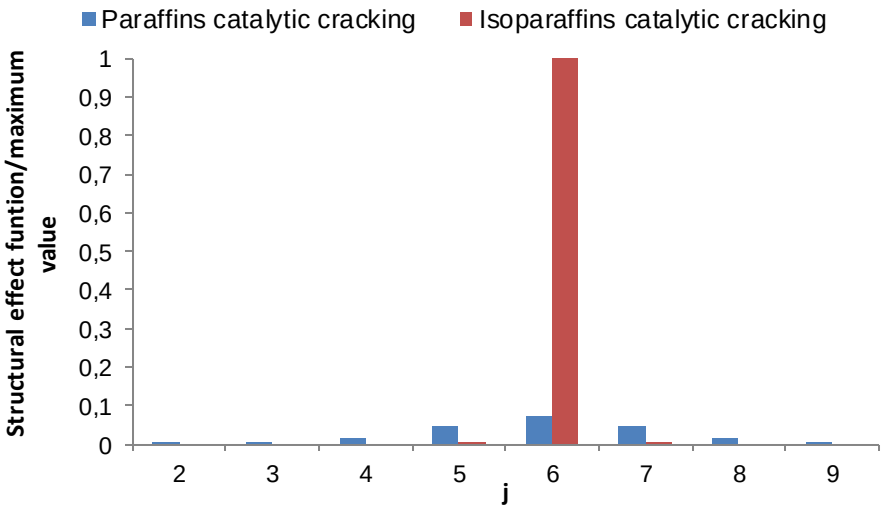

Figure 26 – Molecule structure function in catalytic cracking of normal and branched paraffins with 12 carbon atoms ($i = 12$). The values were normalized with the maximum value of both situations.

If the C_{12} is a normal paraffin the effect of the structure function it will be close to what is expected, i.e. a smooth normal distribution function (Figure 18, page 26). On the other hand, if the C_{12} is an isoparaffin the consequence is a very abrupt response. The function presents a very high value for cracking reactions that produce two molecules with 6 carbon atoms (almost 14 times higher than the analogue for linear paraffins), while for a non-symmetric cracking the function response is nearly zero.

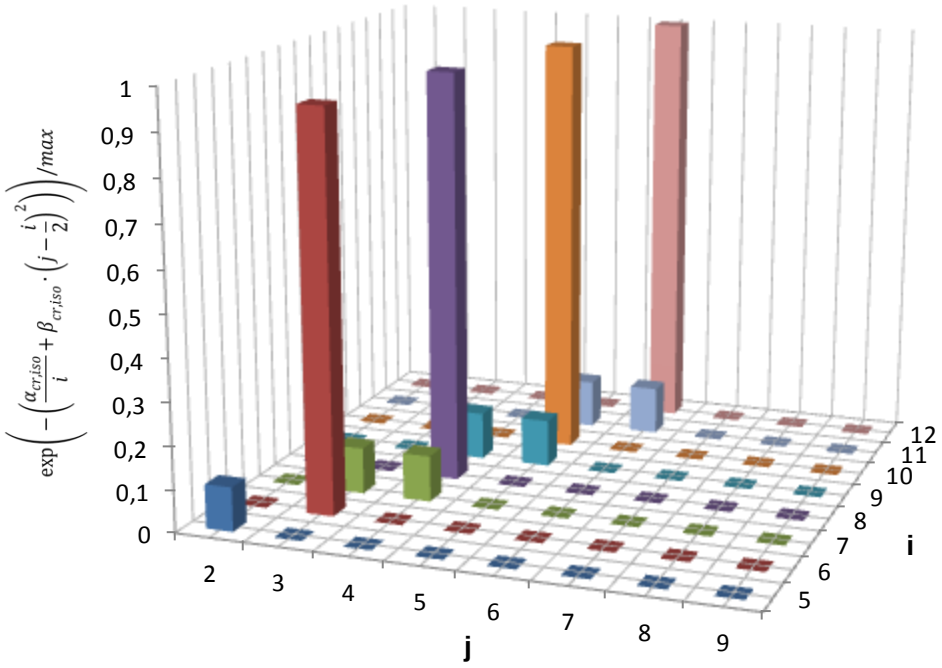

Figure 27 – Result representation of molecule structure function for isoparaffins catalytic cracking normalized with its maximum value

Figure 27 represents the isoparaffins results for this function in the applicability range. As discussed above, the function just predicts the effect for the symmetrical cracking cases since for the other cases its value is nearly zero. Besides, the values for this function are much lower (10 times less) for the molecules with odd carbon atoms number. This behavior for isoparaffins is not expected and will affect

the results for linear and branched paraffins. In conclusion, the molecule structure function for isoparaffins cracking needs to be reevaluated.

In the next sub-chapters, the simulator and experimental results are compared in the form of parity diagrams. Firstly, the FCC main standard cuts will be analyzed and after the species that have more relevance in terms of model improvements and market value. This analysis will be done separately for gasoline, PolyC3C4, and PolyC4 and will be related to the results of the previous version dating from 2012.

5.1. Standard cuts yields prediction for all the feeds

Firstly, it is useful to analyze the yields prediction of the main cuts of all feeds in the same representation to have an overall idea of the model performance.

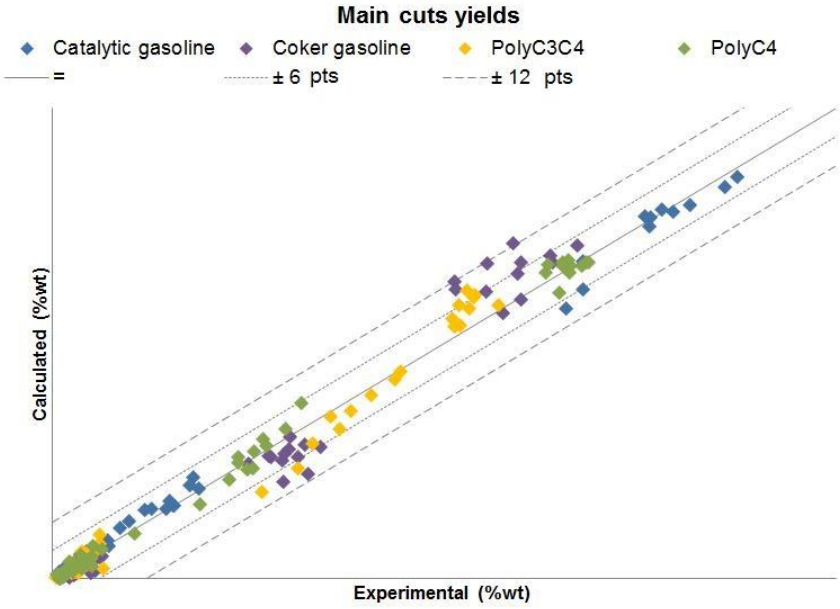

Figure 28 – Main cuts yields parity diagram for all the feeds

Figure 28 represents the parity diagram for this situation. This type of charts will be supported by lines that represent the parity axis (denoted as "=") and two tolerance lines (symbolized as "±X" where X is the value of the absolute error, in points). The tolerance appears as absolute error and is calculated by the difference between the experimental and calculated yield. Table 11 gives detail information about the tolerance of experiments simulated for each cut.

Table 11 – Absolute error tolerance intervals of main cuts

% of yields within tolerance	Tolerance (pts)								
	±0.5	±1	±2	±4	±6	±8	±10	±12	±14
Dry Gas	37%	72%	95%	100%					
LPG	14%	23%	42%	72%	84%	93%	98%	100%	
Gasoline	5%	14%	44%	65%	79%	86%	93%	98%	100%
LCO	33%	58%	95%	100%					
Coke	21%	51%	93%	98%	100%				

For the catalytic and coker gasoline predictions, obtained with the same set of parameters, it is clear the difference between their reactivity. Coker gasoline is the feed presenting more dispersion and less accuracy.

To support the chart analysis in a more objective way, the next results of the model are evaluated also on the basis of mean squared error of prediction (MSEP), which is calculated by the Eq. 44 (Kano, et al., 2000).

$$MSEP = \frac{1}{N}\sum_{n=1}^{N}\left(x(n) - \hat{x}(n)\right)^2 \qquad \text{Eq. 44}$$

Where x is the experimental yield, $\hat{x}$ is its estimate and N is the number of measurements (points). The prediction is much better, how much lower MSEP is. The MSEP values are available each chart subtitle and also in Appendix 4.

5.2. Dry gas (H_2, C_1 and C_2)

The following figures represent the parity diagram for each feed. As shown in Table 6 (page 20), the dry gas has generally low yields and for that reason it is difficult to obtain a good prediction.

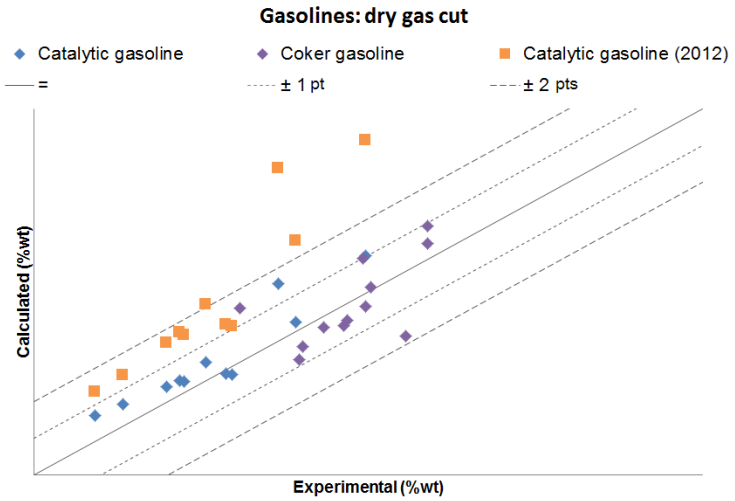

Figure 29 – Parity diagram of dry gas cut for catalytic and coker gasolines ($MSEP_{Catalytic\ gasol.2012} = 6 \times 10^{-4}$; $MSEP_{Catalytic\ gasol.2014} = 5 \times 10^{-5}$; $MSEP_{Coke\ gasol.2014} = 8 \times 10^{-5}$)

By analyzing the catalytic gasoline and comparing to the 2012 model results, it is observed that the data predicted with the new model presents a lower tolerance error. Coker gasoline results are only available for the model present version and as it can be seen they present some dispersion and are generally underestimated. The MSEP of the two feeds are in the same order of magnitude.

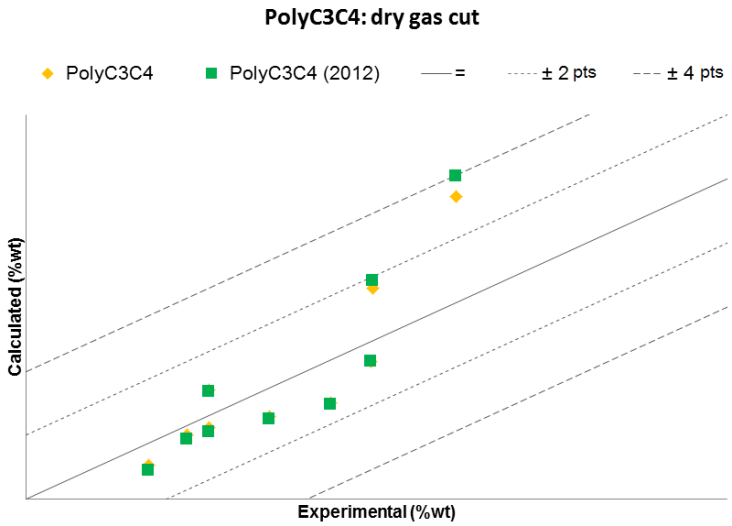

Figure 30 - Parity diagram of dry gas cut for PolyC3C4 ($MSEP_{2012} = 3 \times 10^{-4}$; $MSEP_{2014} = 2 \times 10^{-4}$)

For PolyC3C4, the results are quite similar comparing with the 2012 results. For the highest yield, prediction is slightly improved with the new model.

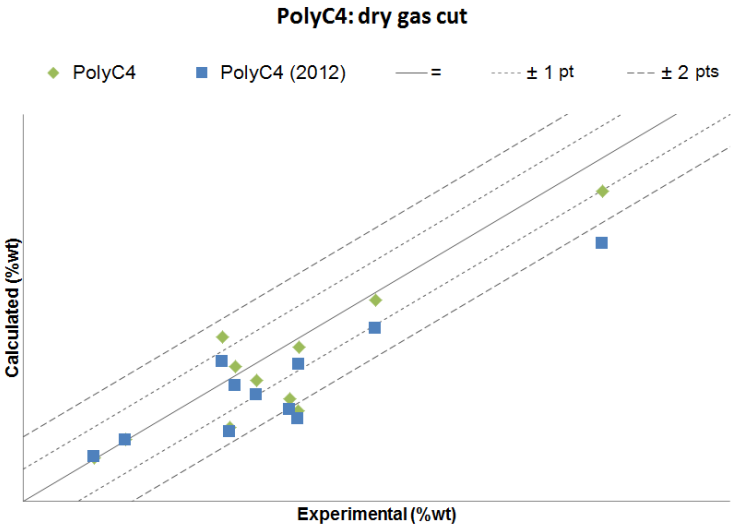

Figure 31 - Parity diagram of dry gas cut for PolyC4 ($MSEP_{2012} = 2 \times 10^{-4}$; $MSEP_{2014} = 1 \times 10^{-4}$)

According to Figure 31, the dry gas yields predictions are slightly improved compared to 2012 results.

Table 12 presents the tolerance intervals obtained for each feed.

Table 12 – Absolute error tolerance intervals of dry gas cut for all feeds

% of yields within tolerance	Tolerance (pts)			
	±0.5	±1	±2	±4
Catalytic gasoline	55%	82%	100%	
Coker gasoline	25%	83%	100%	
PolyC3C4	22%	67%	89%	100%
PolyC4	45%	55%	91%	100%

In summary, 95% of the mass balances are predicted within ±2 points of margin. Globally the values obtained for dry gas cut prediction were improved.

As the dry gas has a very low yield it is important to analyze the relative error. Table 13 presents the percentage of experimental points in the intervals considered. It is possible to conclude that the predicted values can be twice the experimental ones.

Table 13 – Relative error precision intervals of dry gas cut for all feeds

% of yields within precision	Precision					
	20%	30%	40%	50%	75%	100%
Catalytic gasoline	55%	73%	73%	91%	91%	100%
Coker gasoline	67%	92%	100%			
PolyC3C4	33%	44%	89%	89%	100%	
PolyC4	64%	64%	91%	100%		

5.2.1. Species distribution

The dry gas cut is mainly composed by methane and ethane that will be discussed in this sub-chapter. The hydrogen is also a component that appears in this cut but in very low concentrations and therefore less relevance will be given to this specie.

The methane results are described in Figure 32 to Figure 34.

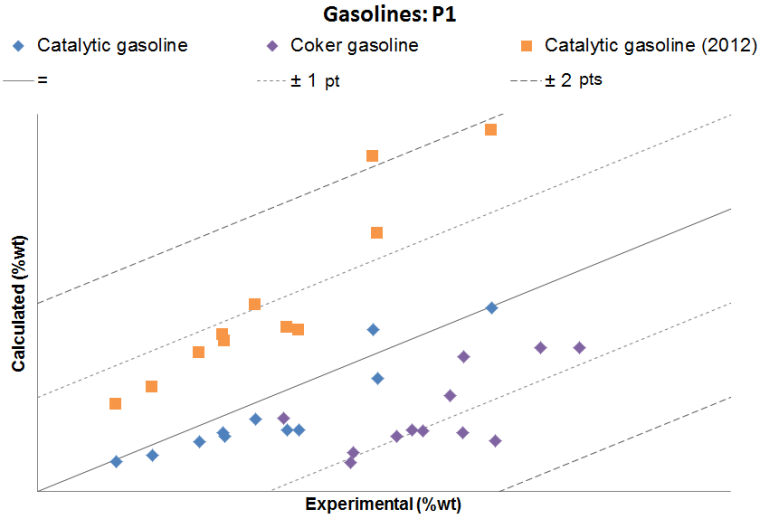

Figure 32 – P_1 parity diagram for catalytic and coker gasoline ($MSE\,P_{Catalytic\ gasol.2012} = 1 \times 10^{-4}$; $MSE\,P_{Catalytic\ gasol.2014} = 6 \times 10^{-6}$; $MSE\,P_{Coke\ gasol.2014} = 9 \times 10^{-5}$)

For catalytic gasoline, the prediction of methane yield is better with the new approach. As observed, the 2012 results are overestimated within a tolerance of ±2 points approximately, while with the new model, the dispersion decreased and the results can now be described within ±0.5 points interval. For the coker gasoline methane yields prediction is underestimated within a ±1.5 points interval, presenting a higher deviation to the parity axe.

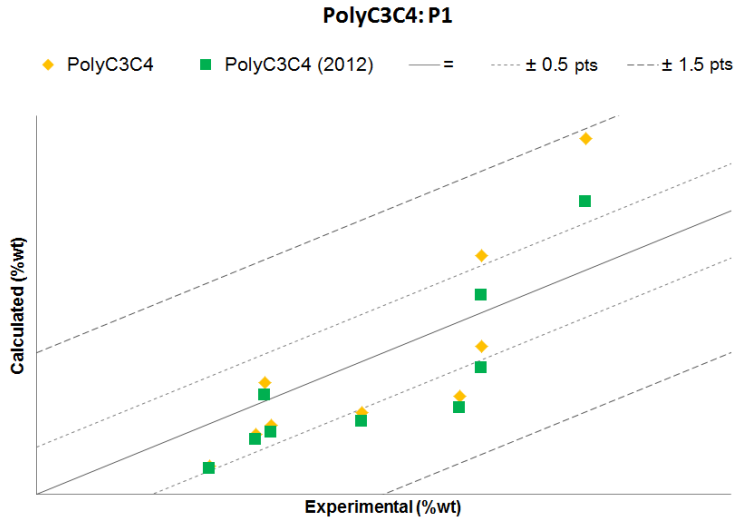

Figure 33 - P_1 parity diagram for PolyC3C4 ($MSEP_{2012} = 3 \times 10^{-5}$; $MSEP_{2014} = 4 \times 10^{-5}$)

Both oligomer feeds results have the same behavior with the new improvements (Figure 33 and Figure 34). The 2014 model predicts higher yields values, and this increase is greater for higher experimental yields. Concerning PolyC3C4, this increase leads to slightly worsts results, with a decrease in accuracy.

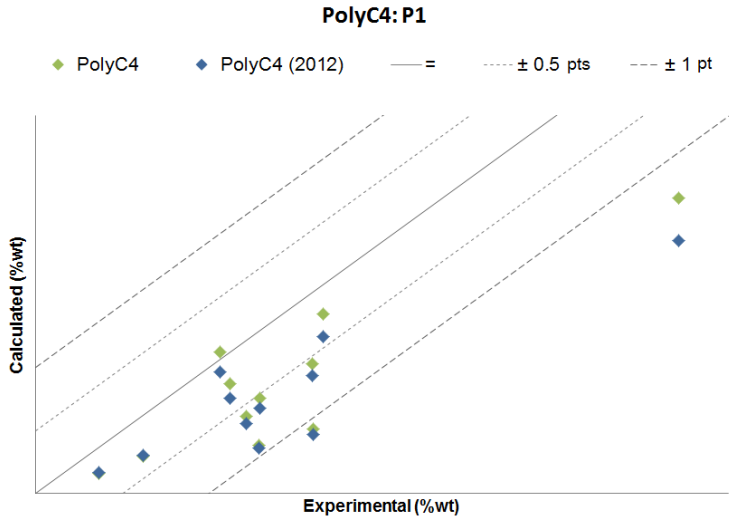

Figure 34 - P_1 parity diagram for PolyC4 ($MSEP_{2012} = 6 \times 10^{-5}$; $MSEP_{2014} = 5 \times 10^{-5}$)

On the other hand, for the PolyC4 feed results were improved and the accuracy increased. This conclusion is supported also by the MSEP value.

Table 14 presents the details of the tolerance margins.

Table 14 – Absolute error tolerance intervals of P_1 for all feeds

% of yields within tolerance	Tolerance (pts)			
	±0.25	±0.5	±1	±1.5
Catalytic gasoline	64%	100%		
Coker gasoline	8%	17%	58%	100%
PolyC3C4	11%	56%	89%	100%
PolyC4	36%	45%	82%	100%

Altogether the results for P_1 were improved. This specie is produced only by thermal cracking. The differentiation between linear and branched isoparaffins implied the creation of a new set of thermal cracking reaction and its kinetic parameters distinction. With that, it was possible to take into account the different contribution of paraffins to produce methane and improve its results.

Methane yields are generally underestimated which can suggest the production of methane by other additional reactions. In the literature review it has been shown that protolytic cracking can produce light paraffins such as methane (Haag-Dessau mechanism). This reaction is not taken into account since the methyl carbonium ions are very instable species. Furthermore, the molecule structure function is not favorable for this type of reaction. For this reason, the reaction network of the model should be remaining constant in terms of methane production.

The results obtained for ethane are given in Figure 35 to Figure 37.

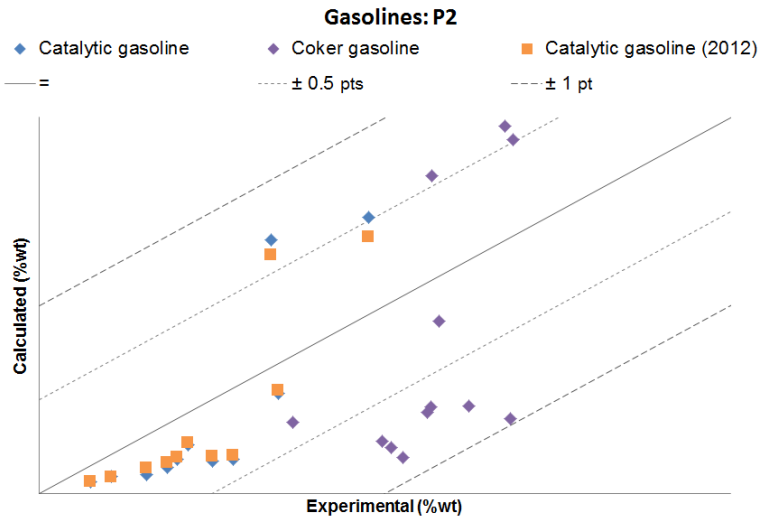

Figure 35 – P_2 parity diagram for catalytic and coker gasoline ($MSE\,P_{Catalytic\ gasol.2012} = 8 \times 10^{-6}$; $MSE\,P_{Catalytic\ gasol.2014} = 1 \times 10^{-5}$; $MSE\,P_{Coke\ gasol.2014} = 5 \times 10^{-5}$)

For catalytic gasoline, ethane yields prediction is worst in comparison to 2012 predictions. high yields. For the coker gasoline, ethane yields prediction is more dispersed and less accurate than for catalytic gasoline.

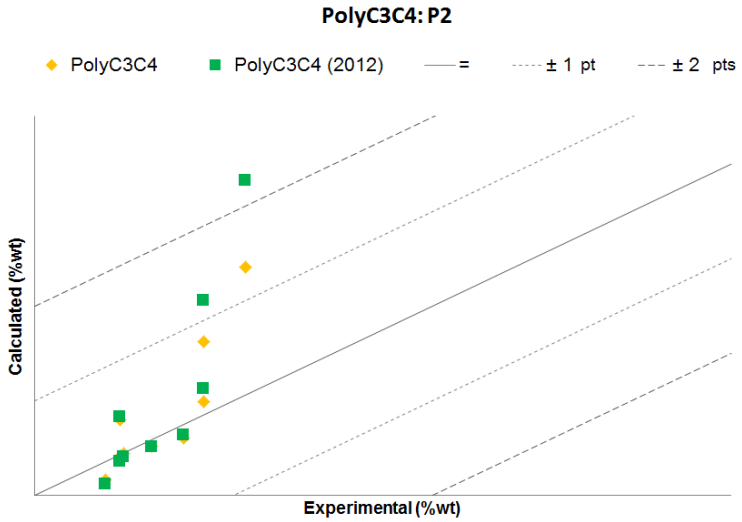

Figure 36 – P_2 parity diagram for PolyC3C4 ($MSE\,P_{2012} = 8 \times 10^{-5}$; $MSE\,P_{2014} = 3 \times 10^{-5}$)

For PolyC3C4, the model improvements achieved better results in the prediction of ethane yields that are within an interval of ±1.5 points.

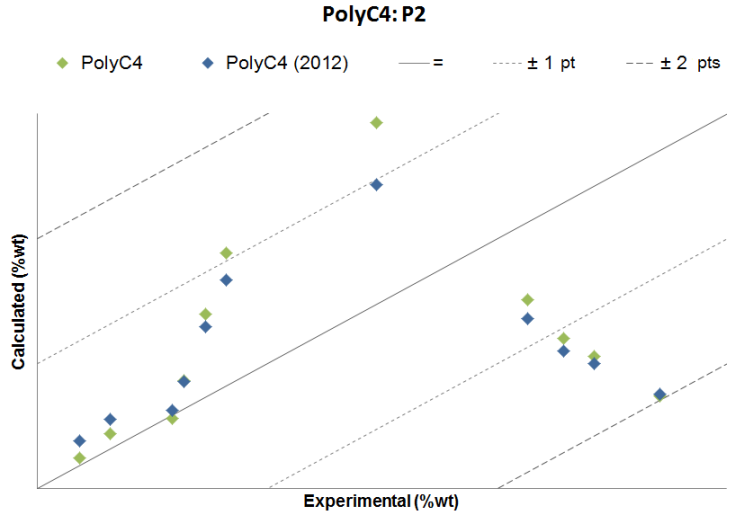

Figure 37 – P_2 parity diagram for PolyC4 ($MSEP_{2012} = 9 \times 10^{-5}$; $MSEP_{2014} = 1 \times 10^{-4}$)

The estimation of ethane yield for PolyC4 is still quite dispersed. Nevertheless, the estimation is well produced for the lower yields.

The tolerance intervals are presented in Table 15.

Table 15 – Absolute error tolerance intervals of P_2 for all feeds

% of yields within tolerance	Tolerance (pts)				
	±0.25	±0.5	±1	±1.5	±2
Catalytic gasoline	67%	82%	100%		
Coker gasoline	8%	17%	100%		
PolyC3C4	67%	78%	89%	100%	
PolyC4	36%	36%	55%	91%	100%

The results for ethane are quite similar to the older version; only in PolyC3C4 were observed improvements. With the changes of the reaction network, the ethane can be produced also by isoparaffins catalytic cracking. However, the production of ethane by isoparaffins cracking is almost null with the kinetic parameters obtained and the present structure function. The improvements are probably provided by the differentiation between paraffins and/or the optimization work.

5.3. LPG (C_3 and C_4)

The results of LPG cut are presented in Figure 38 to Figure 40.

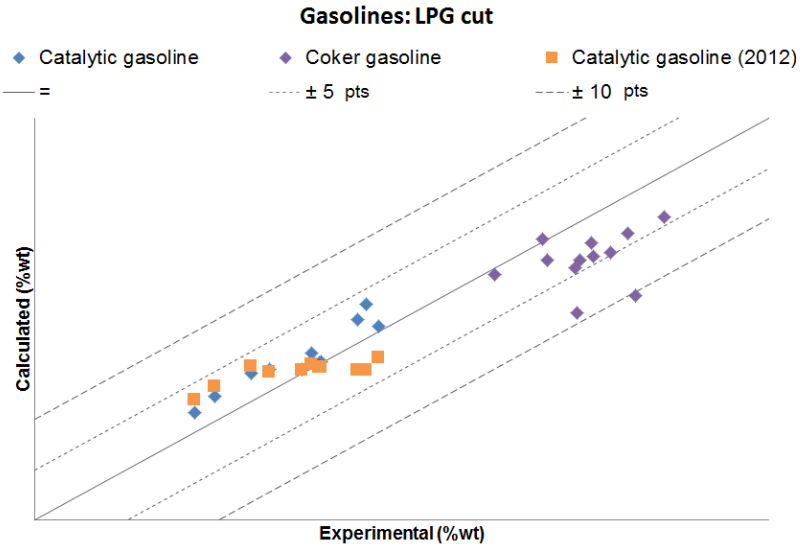

Figure 38 - Parity diagram of LPG cut for catalytic and coker gasoline ($MSE\,P_{Catalytic\ gasol.2012} = 6 \times 10^{-4}$; $MSE\,P_{Catalytic\ gasol.2014} = 4 \times 10^{-4}$; $MSE\,P_{Coke\ gasol.2014} = 3 \times 10^{-3}$)

First, for catalytic gasoline the LPG yields given by the older model version (2012) were slightly dispersed, being overestimated for low yields and underestimated for high yields. The new model reduced the dispersion observed, however all the yields are now slightly overestimated. On the contrary, for the coker gasoline LPG yields are underestimated with 75% of the experiments predicted within a tolerance of ±5% points.

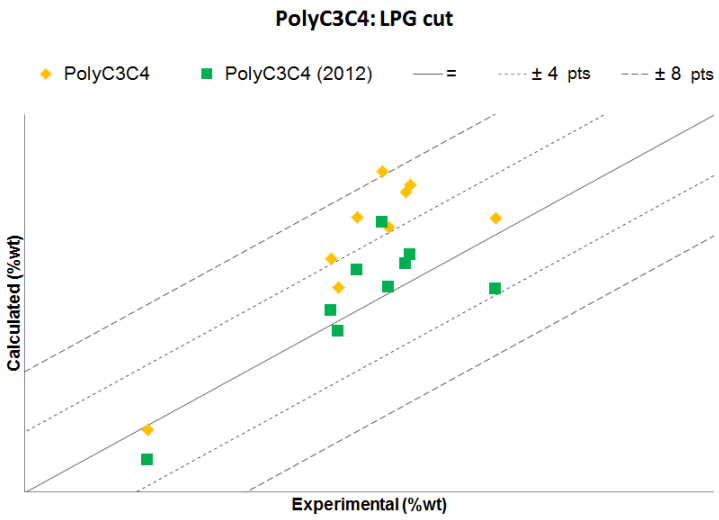

Figure 39 - Parity diagram of LPG cut for PolyC3C4 ($MSEP_{2012} = 6 \times 10^{-4}$; $MSEP_{2014} = 3 \times 10^{-3}$)

Concerning PolyC3C4, the new approach decreases the accuracy. The tolerance margin increases from ±5 points to approximately ±8 points.

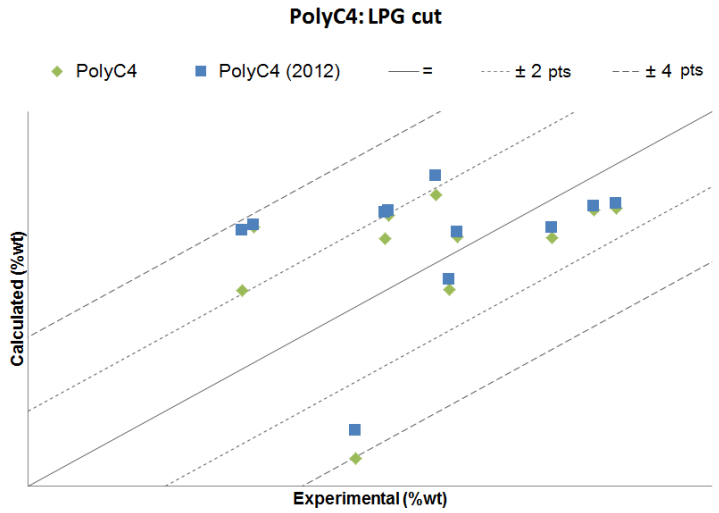

Figure 40 - Parity diagram of LPG cut for PolyC4 ($MSEP_{2012} = 5 \times 10^{-4}$; $MSEP_{2014} = 4 \times 10^{-4}$)

Finally, the results on LPG yields prediction obtained for the cracking of the PolyC4 feed are quite similar to the results obtained with the older model version.

Table 16 shows the tolerance margins.

Table 16 – Absolute error tolerance intervals of LPG cut for the different feeds

% of yields within tolerance	Tolerance (pts)						
	±1	±2	±4	±6	±8	±10	±12
Catalytic gasoline	36%	45%	100%				
Coker gasoline	17%	25%	58%	75%	83%	92%	100%
PolyC3C4	11%	22%	33%	56%	89%	100%	
PolyC4	27%	73%	91%	100%			

5.3.1. Species distribution

The LPG is composed by paraffins and olefins with three and four carbon atoms, i.e. P_3, P_4, iP_4, O_3 and O_4. Only the olefins will be analyzed in more detail in this sub-chapter, since the propylene and the butenes are important bricks in the petrochemistry industry[17].

Maximizing propylene is the goal of the second riser configuration. Therefore, predicting propylene yields is extremely important in the model. The results are presented in Figure 41 to Figure 43.

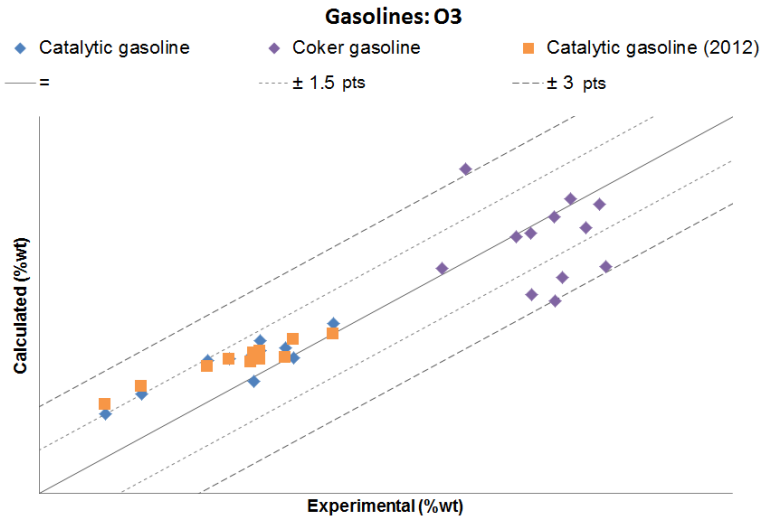

Figure 41 – O_3 parity diagram for catalytic and coker gasoline ($MSEP_{Catalytic\ gasol.2012} = 1 \times 10^{-4}$; $MSEP_{Catalytic\ gasol.2014} = 9{,}7 \times 10^{-5}$; $MSEP_{Coke\ gasol.2014} = 3 \times 10^{-4}$)

Regarding catalytic gasoline, the propylene yield is now predicted with a similar accuracy than the older model version. However, it is observed a high dispersion in the coker gasoline results. For this feed, almost half the experimental tests have tolerance greater than ±2 points.

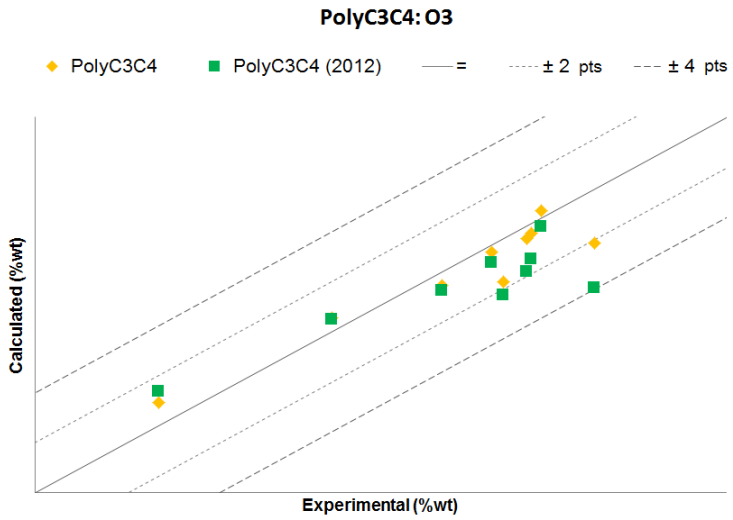

Figure 42 - O_3 parity diagram for PolyC3C4 ($MSEP_{2012} = 3 \times 10^{-4}$; $MSEP_{2014} = 1 \times 10^{-4}$)

The PolyC3C4 results with the new model version present the same behavior than the old model. However, it is observed a slight improvement reducing the margin.

[17] iP_4 will be analyzed with the rest of isoparaffins

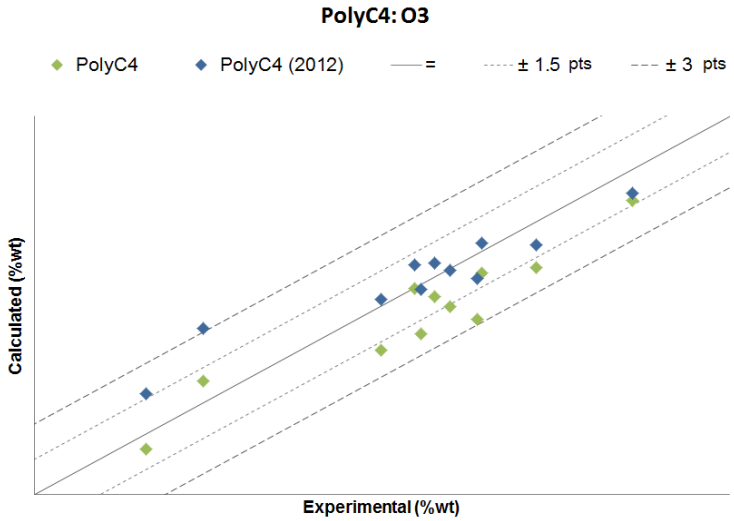

Figure 43 - O_3 parity diagram for PolyC4 ($MSEP_{2012} = 1.6 \times 10^{-4}$; $MSEP_{2014} = 2.4 \times 10^{-4}$)

As shown in Figure 43, the predicted propylene yields for PolyC4 are underestimated. For high yields, the accuracy with the new simulator is lower than with the previous version.

Table 17 details the values of tolerance for all feeds.

Table 17 – Absolute error tolerance intervals of O_3 for all feeds

% of yields within tolerance	Tolerance (pts)					
	±0.5	±1	±2	±2.5	±3	±3.5
Catalytic gasoline	37%	55%	100%			
Coker gasoline	42%	58%	67%	92%	92%	100%
PolyC3C4	33%	78%	89%	100%		
PolyC4	9%	45%	82%	91%	100%	

The butenes are also an important species. The results obtained for these species are given in Figure 44 to Figure 46.

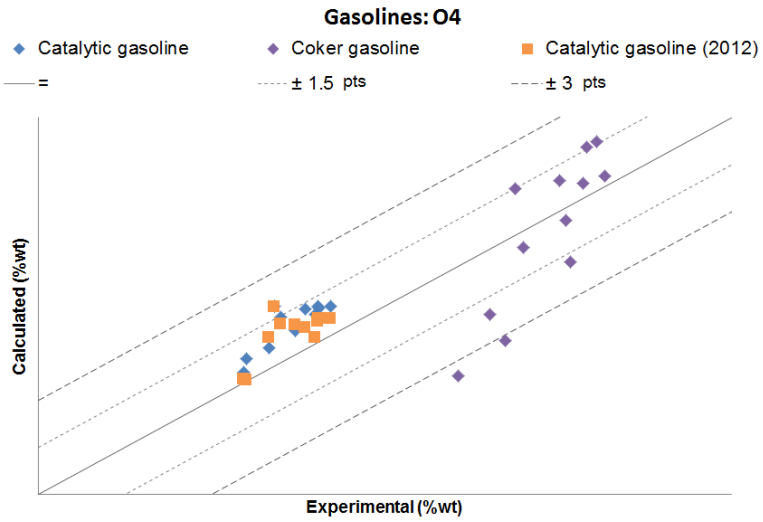

Figure 44 – O_4 parity diagram for catalytic and coker gasoline ($MSEP_{Catalytic\ gasol.2012} = 8 \times 10^{-5}$; $MSEP_{Catalytic\ gasol.2014} = 1 \times 10^{-4}$; $MSEP_{Coke\ gasol.2014} = 3 \times 10^{-4}$)

In catalytic gasoline, the quality of prediction of O_4 yield with the new model is quite similar to the older one. Results for coker gasoline are only available with the new model and as it can be seen there is more dispersion and higher deviations to the parity axe than for the catalytic gasoline. 92% of the coker gasoline experimental tests are predicted within ±3 points margin.

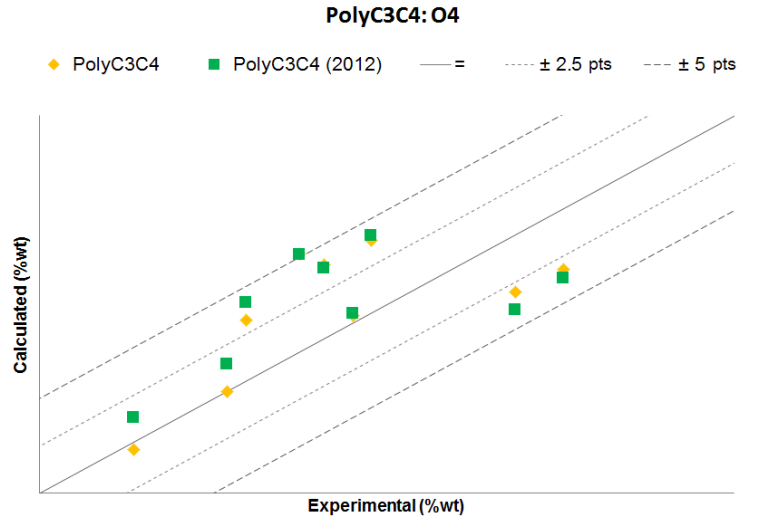

Figure 45 - O_4 parity diagram for PolyC3C4 ($MSEP_{2012} = 1.2 \times 10^{-3}$; $MSEP_{2014} = 9.7 \times 10^{-4}$)

Small improvements are observed in the results for PolyC3C4 as well as for PolyC4, where the maximum tolerance is approximately ±8 points.

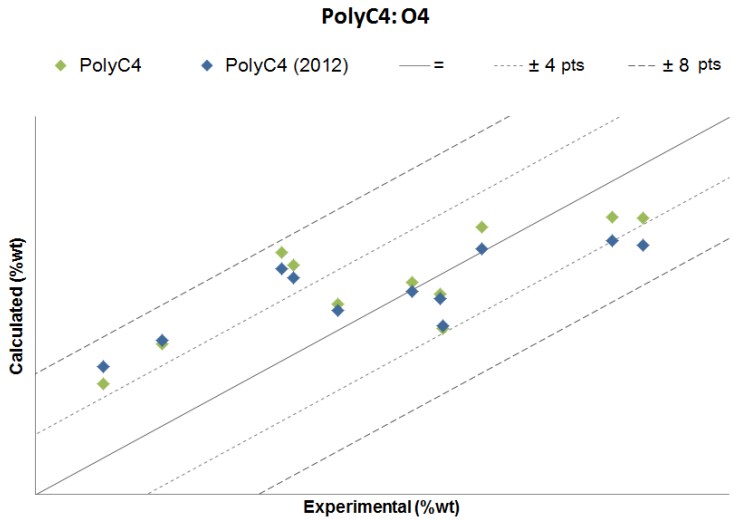

Figure 46 - O_4 parity diagram for PolyC4 ($MSE\,P_{2012} = 1.7 \times 10^{-3}$; $MSE\,P_{2014} = 1.6 \times 10^{-3}$)

The details of the tolerance intervals for butene prediction are presented in Table 18.

Table 18 – Absolute error tolerance intervals of O_4 for all feeds

% of yields within tolerance	Tolerance (pts)						
	±1	±1.5	±2	±3	±5	±6	±7.5
Catalytic gasoline	55%	91%	100%				
Coker gasoline	25%	25%	67%	75%	100%		
PolyC3C4	33%	33%	33%	33%	89%	100%	
PolyC4	9%	18%	36%	45%	73%	91%	100%

5.4. Gasoline cut ($C_5 - C_{12}$)

The gasolines have a more complex composition than the previous cuts since they include many more species (C5 to C12). Therefore results analysis will not be done for all gasoline species separately but instead species will be grouped by type of molecular family (PIONA). The results for this global cut yield are presented in Figure 47 to Figure 49.

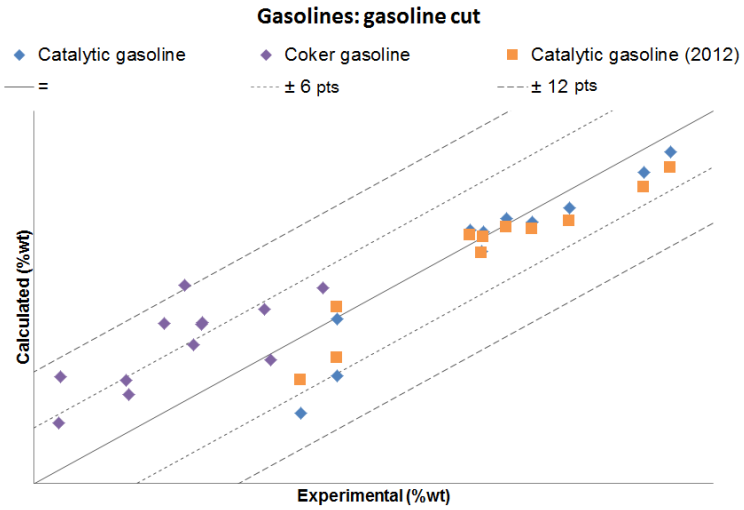

Figure 47 - Parity diagram of gasoline cut for catalytic and coker gasolines ($MSEP_{Catalytic\ gasol.2012} = 8 \times 10^{-4}$; $MSEP_{Catalytic\ gasol.2014} = 1 \times 10^{-3}$; $MSEP_{Coke\ gasol.2014} = 5 \times 10^{-3}$)

Starting with the catalytic gasolines, the results presented above show that for the low gasoline yields tolerance increases from ±5 points to ±7 points. On the other hand, the prediction for high gasoline yields is improved. Like before, the coker gasoline results present significant dispersion and a higher tolerance error than catalytic gasoline.

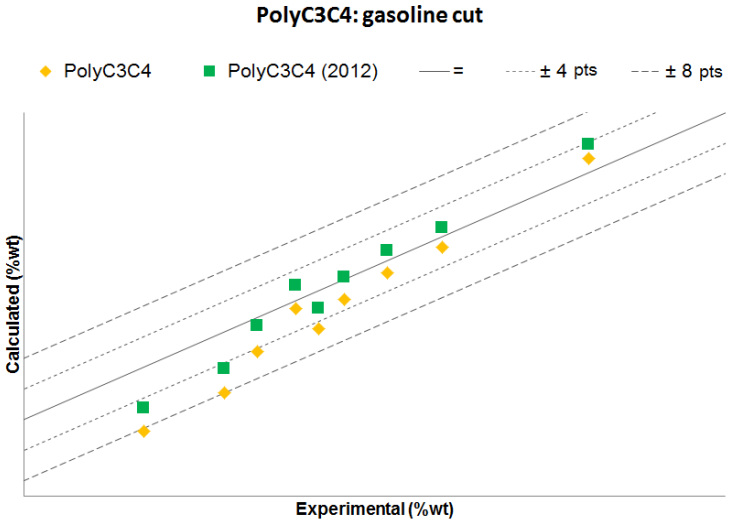

Figure 48 - Parity diagram of gasoline cut for PolyC3C4 ($MSEP_{2012} = 9 \times 10^{-4}$; $MSEP_{2014} = 2 \times 10^{-3}$)

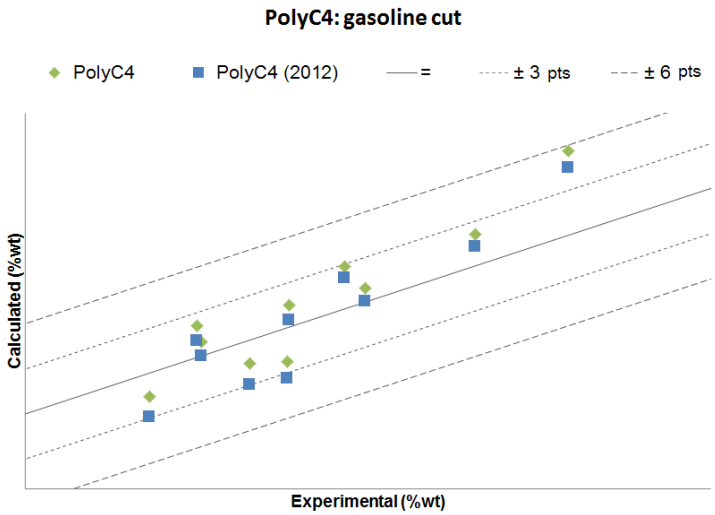

Figure 49 - Parity diagram of gasoline cut for PolyC4 ($MSE\,P_{2012} = 6.3 \times 10^{-4}$; $MSE\,P_{2014} = 6.4 \times 10^{-4}$)

The predictions given by the two model versions are quite similar for oligomer feeds. Nonetheless, it is observed a slight increasing of the tolerance error with the new version.

In general, the new model version did not improve quality of prediction for the gasoline cut. Table 19 presents the tolerance intervals obtained with the new model for the gasoline cut.

Table 19 – Absolute error tolerance intervals of gasoline cut for the different feeds

% of yields within tolerance	Tolerance (pts)					
	±2	±6	±8	±10	±12	±14
Catalytic gasoline	73%	82%	91%	100%		
Coker gasoline	17%	58%	67%	75%	92%	100%
PolyC3C4	44%	78%	89%	100%		
PolyC4	45%	100%				

As explained, the gasoline has a PIONA composition which components have from five to twelve carbon atoms[18]. Olefins, aromatics, naphthenes and isoparaffins families' results will be discussed in the next sub-chapters. The total paraffins (sum between linear and branched) will be presented and compared with the 2012 results. Further, the ratio between the isoparaffins and the total paraffins will also be presented and some comments about their implementation will be given.

5.4.1. Olefin lump

The results for olefin family are represented in Figure 50 to Figure 52.

[18] Concerning the model

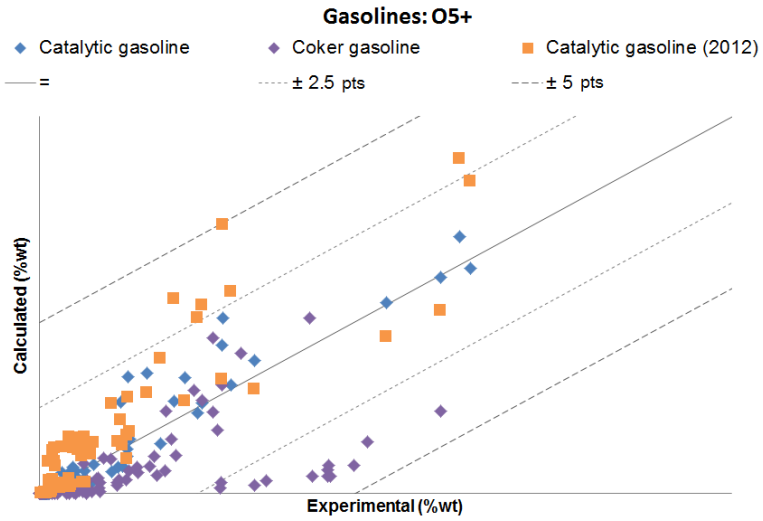

Figure 50 - Parity diagram of olefin lump in gasoline cut for catalytic and coker gasolines ($MSE\,P_{Catalytic\,gasol.2012} = 1 \times 10^{-4}$; $MSE P_{Catalytic\,gasol.2014} = 2 \times 10^{-5}$; $MSE\,P_{Coke\,gasol.2014} = 2 \times 10^{-4}$)

For the catalytic gasoline feed, gasoline olefins prediction given by the new model is more accurate than olefins predicted with the 2012 model. It is observed a reduction of the tolerance error from ±4.5 points to ±2 points approximately. For the coker gasoline the model presents significant dispersion, with the simulator predicting overestimated values as well as underestimated values for the same group of experimental yield. Amongst the olefins species in the gasoline cut, for the coker feed, the one presenting the highest underestimation is O_5.

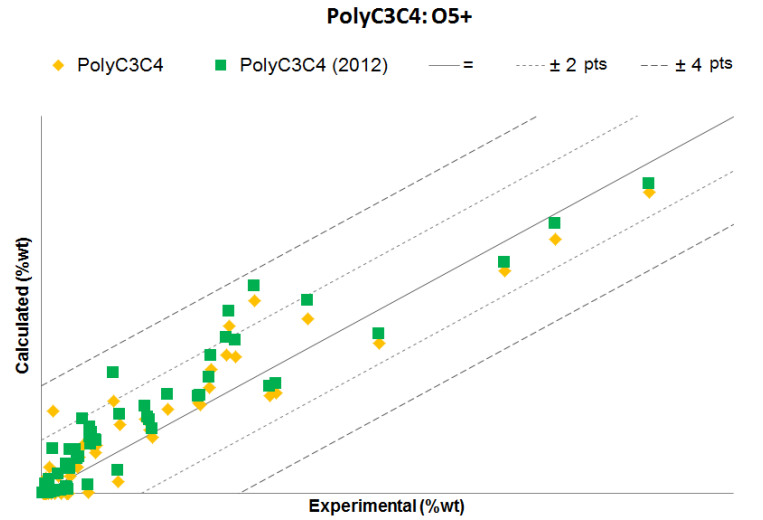

Figure 51 - Parity diagram of olefin lump in gasoline cut for PolyC3C4 ($MSEP_{2012} = 1 \times 10^{-4}$; $MSEP_{2014} = 7 \times 10^{-5}$)

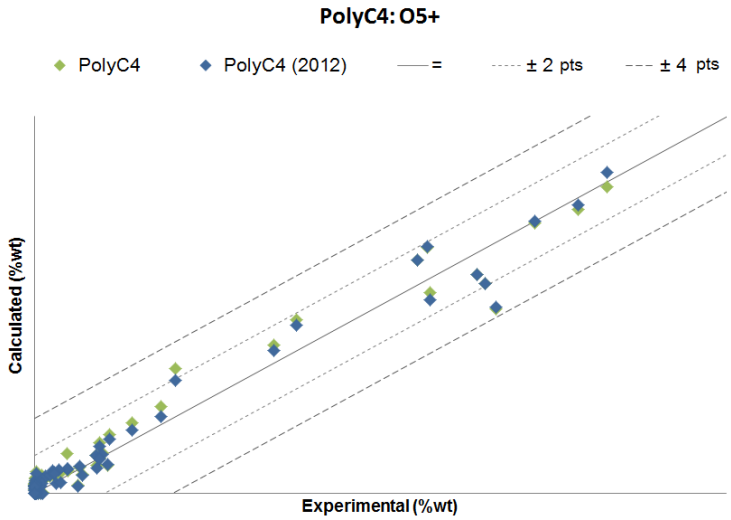

Figure 52 - Parity diagram of olefin lump in gasoline cut for PolyC4 ($MSEP_{2012} = 4 \times 10^{-5}$; $MSEP_{2014} = 6 \times 10^{-5}$)

For oligomer feeds, the new model presents almost the same yield predictions for O_{5^+} than the last version.

The prediction of olefins in gasoline was done with more accuracy that can be justified for the new parameters. However, it is visible a high underestimation for O_5 with the coker gasoline that can be indicate the difference of reactivities between gasolines once this specie is well estimated in catalytic gasoline. O_5 undergoes in three oligomerization reactions.

5.4.2. Aromatic lump

The aromatic lump is mainly composed of species with six to eight carbon atoms. These products represent the benzene, toluene and xylene, also known as BTX products in petrochemistry. The BTX products are important in the economical point of view, and can be sent to an aromatic complex (Do, 2009). For these reasons, they will be analyzed separately.

Starting with benzene, its results are showed in Figure 53 to Figure 55.

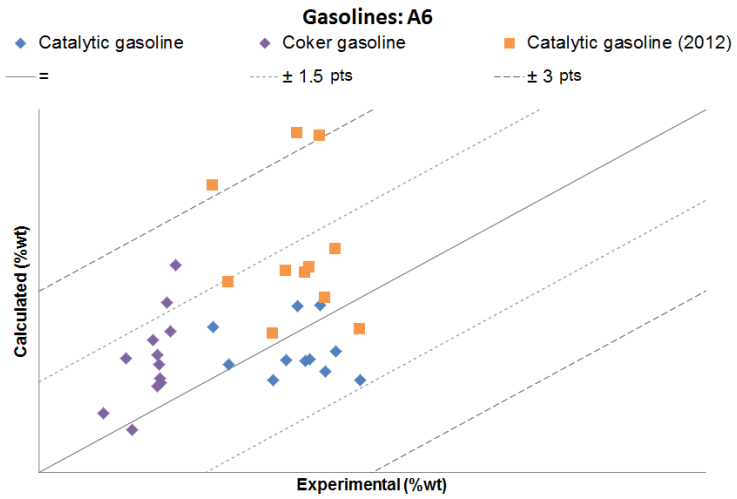

Figure 53 - Parity diagram of A_6 for catalytic and coker gasoline ($MSEP_{Catalytic\ gasol.2012} = 3 \times 10^{-4}$; $MSEP_{Catalytic\ gasol.2014} = 5 \times 10^{-5}$; $MSEP_{Coke\ gasol.2014} = 1 \times 10^{-4}$)

The results for catalytic gasoline are improved and the tolerance to described then was reduced to ±1.5 points. For coker gasoline, 84% of the experimental tests are estimated a within a tolerance of ±1.3 points.

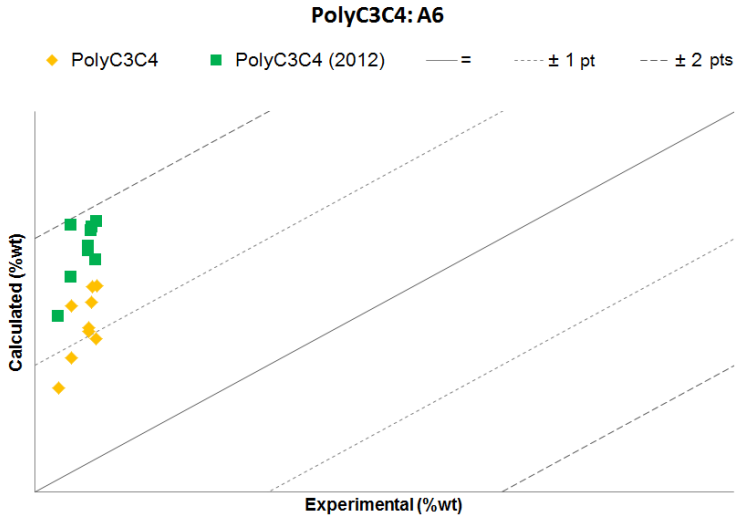

Figure 54 - Parity diagram of A_6 for PolyC3C4 ($MSEP_{2012} = 3 \times 10^{-4}$; $MSEP_{2014} = 1 \times 10^{-4}$)

The results improvements are also observed in PolyC3C4. The new model predicts that all experimental tests with this charge can be estimated with a tolerance of +1.5 points.

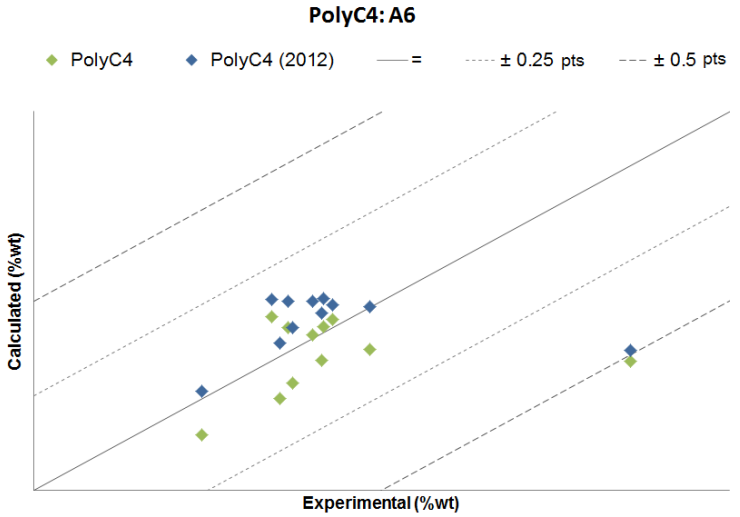

Figure 55 - Parity diagram of A_6 for PolyC4 ($MSEP_{2012} = 2.8 \times 10^{-6}$; $MSEP_{2014} = 3 \times 10^{-6}$)

Regarding PolyC4, the accuracy of results remains almost constant. 91% of the experimental tests are described within a tolerance of ±0.125 points. The tolerance intervals are accessible in Table 20.

Table 20 – Absolute error tolerance intervals of A_6 for all feeds

% of yields within tolerance	Tolerance (pts)					
	±0.5	±0.75	±1	±1.5	±2	±2.5
Catalytic gasoline	36%	73%	91%	100%		
Coker gasoline	33%	58%	67%	83%	92%	100%
PolyC3C4	0%	11%	33%	100%		
PolyC4	91%	100%				

The results for toluene, A_7, are showed in Figure 56 to Figure 58.

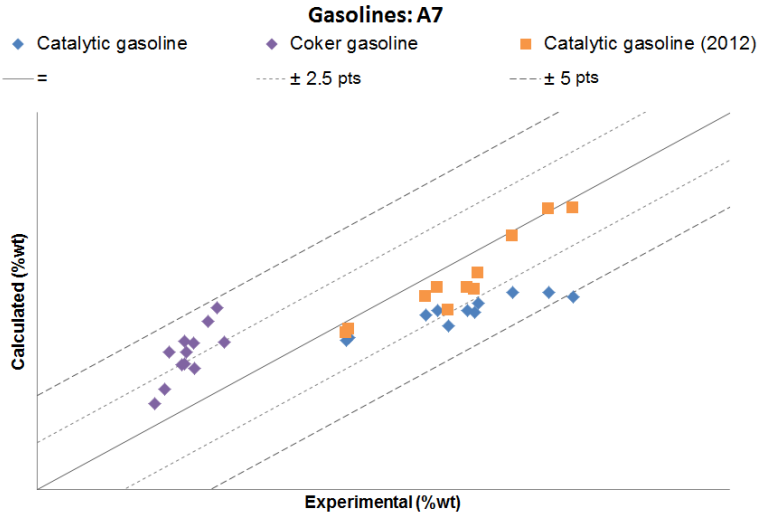

Figure 56 - Parity diagram of A_7 for catalytic and coker gasoline ($MSEP_{Catalytic\ gasol.2012} = 2 \times 10^{-4}$; $MSEP_{Catalytic\ gasol.2014} = 9 \times 10^{-4}$; $MSEP_{Coke\ gasol.2014} = 9 \times 10^{-4}$)

A_7 results for catalytic gasoline are greatly deteriorated comparing to the 2012 results. The percentage of experimental tests that are estimated within a tolerance of ±2.5 points decreases from 100% to 36%. On the other hand, the prediction of coker gasoline is done within a margin of ±2.5 points for 50% of its experimental tests.

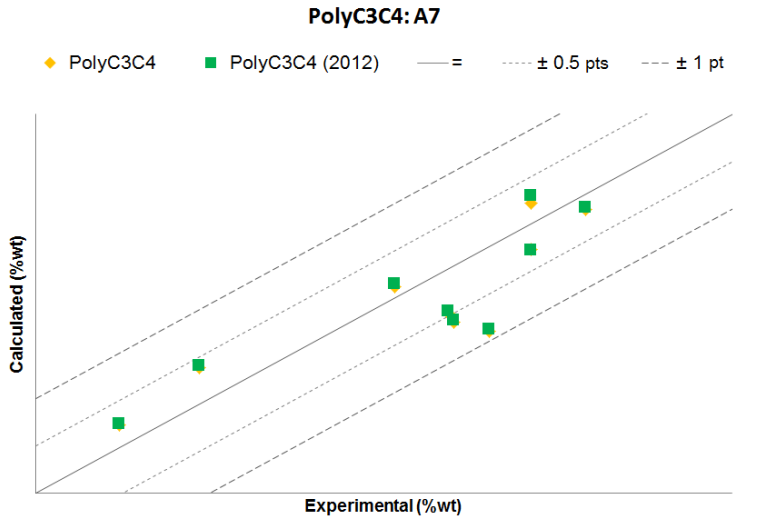

Figure 57 - Parity diagram of A_7 for PolyC3C4 ($MSEP_{2012} = 2 \times 10^{-5}$; $MSEP_{2014} = 2 \times 10^{5}$)

For PolyC3C4, the results are quite similar to the 2012, where the accuracy remains constant.

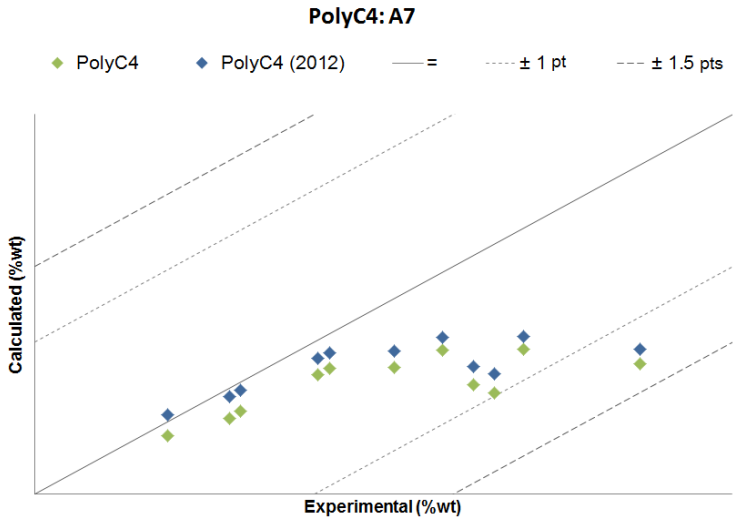

Figure 58 - Parity diagram of A_7 for PolyC4 ($MSEP_{2012} = 3 \times 10^{-5}$; $MSEP_{2014} = 4 \times 10^{-5}$)

As PolyC3C4, the results for PolyC4 are similar. Nevertheless, a decrease in the accuracy of all experiences is noticeable. Table 21 presents the accuracy intervals for each feedstock.

Table 21 - Absolute error tolerance intervals of A_7 for all feeds

% of yields within tolerance	Tolerance (pts)					
	±0.5	±1	±1.5	±4	±5	±5.5
Catalytic gasoline	0%	9%	18%	82%	91%	100%
Coker gasoline	0%	0%	8%	83%	100%	
PolyC3C4	78%	100%				
PolyC4	55%	91%	100%			

The results for A_8 are represented by Figure 59 to Figure 61.

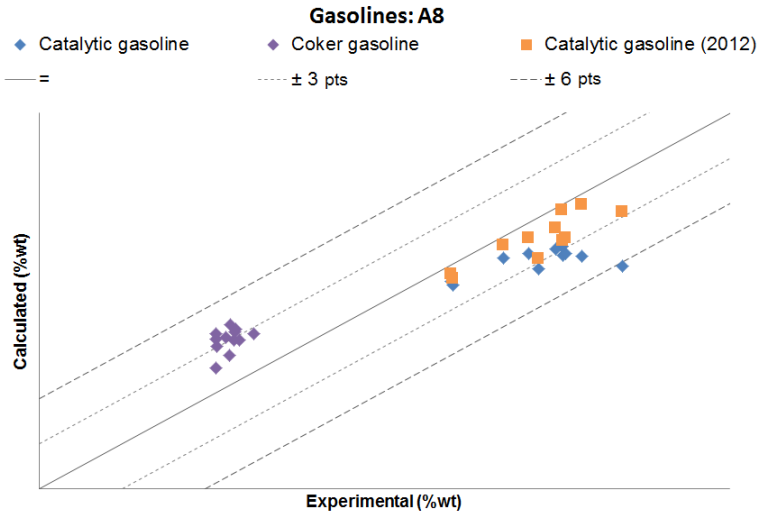

Figure 59 - Parity diagram of A_8 for catalytic and coker gasoline ($MSEP_{Catalytic\ gasol.2012} = 3 \times 10^{-4}$; $MSEP_{Catalytic\ gasol.2014} = 1 \times 10^{-3}$; $MSEP_{Coke\ gasol.2014} = 1 \times 10^{-3}$)

Beginning with catalytic gasoline, it is possible to observe in Figure 59 a higher underestimation of A_8 results as well as a decrease of the accuracy. 55% of its experimental tests are estimated within a

tolerance of ±3 points. The prediction of coker gasoline is overestimated, where 33% of the mass balances are predicted with a margin of ±3 points.

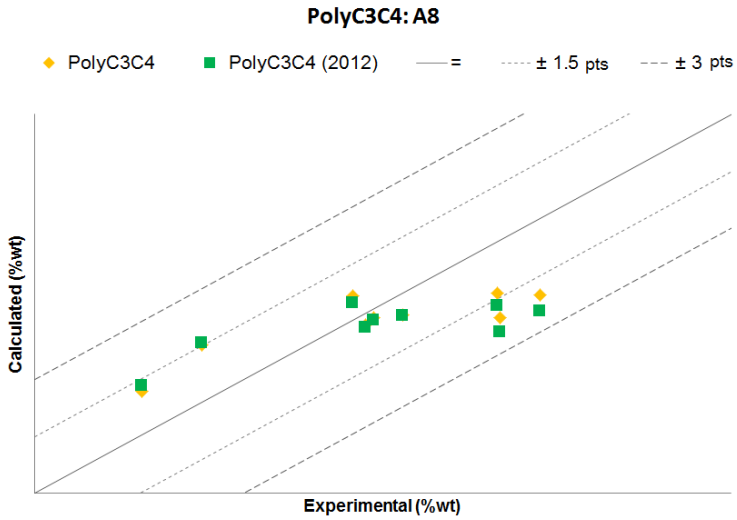

Figure 60 - Parity diagram of A_8 for PolyC3C4 ($MSEP_{2012} = 2.2 \times 10^{-4}$; $MSEP_{2014} = 1.6 \times 10^{-4}$)

The results for PolyC3C4 are very similar in comparison with the older values. However it is verify a slight decreasing of the accuracy.

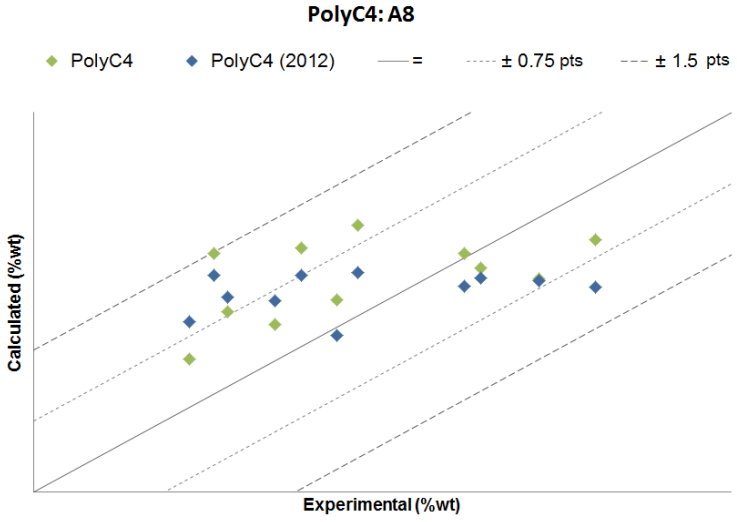

Figure 61 - Parity diagram of A_8 for PolyC4 ($MSEP_{2012} = 6 \times 10^{-5}$; $MSEP_{2014} = 5 \times 10^{-5}$)

For PolyC4, the more recent values present more dispersion than the older ones, even with the improvements of some points (Figure 61).

Table 22 - Absolute error tolerance intervals of A_8 for all feeds

% of yields within tolerance	Tolerance (pts)					
	±1	±1.5	±2	±3	±4	±6.5
Catalytic gasoline	0%	27%	27%	55%	82%	100%
Coker gasoline	0%	0%	17%	42%	100%	
PolyC3C4	44%	67%	78%	100%		
PolyC4	82%	100%				

Looking at the gasolines' results, it can be noticed that catalytic gasoline results are generally underestimated and the opposite happens with coker gasoline. The different reactivities can be responsible for it.

The results for the A_{9^+} are not very significant. For that reason their parity diagrams are available in Appendix 1. However, it is important to refer that the simulator cannot predict the yields for A_{11} and A_{12}. The calculated yields for these species remain nulls as the 2012 results. It can propose that aromatics can have different probability to produce LCO and coke, like paraffins/olefins for catalytic cracking.

5.4.3. Naphthene lump

The naphthenes are the family with less representation in terms of composition. Their results are showed in Figure 62 to Figure 64.

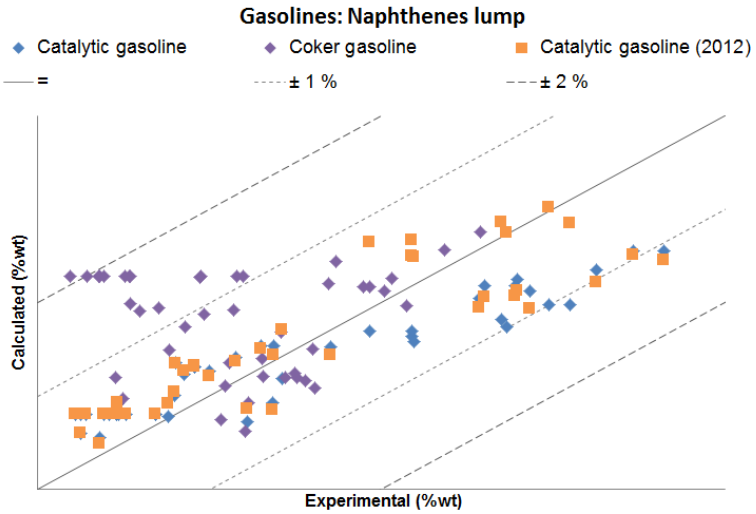

Figure 62 - Parity diagram of naphthenes lump in gasoline cut for catalytic and coker gasolines ($MSE\,P_{Catalytic\ gasol.2012} = 2 \times 10^{-5}$; $MSE\,P_{Catalytic\ gasol.2014} = 3 \times 10^{-5}$; $MSE\,P_{Coke\ gasol.2014} = 1 \times 10^{-4}$)

The simulator can predict the yields for catalytic gasoline with approximately ±1 point of margin. On the other hand, the prediction for coker gasoline just can be done with approximately ±2 point of tolerance. It is important to refer that, 2% in absolute error for a specie/lump with a weak representation is can be a huge difference as exemplified for dry gas.

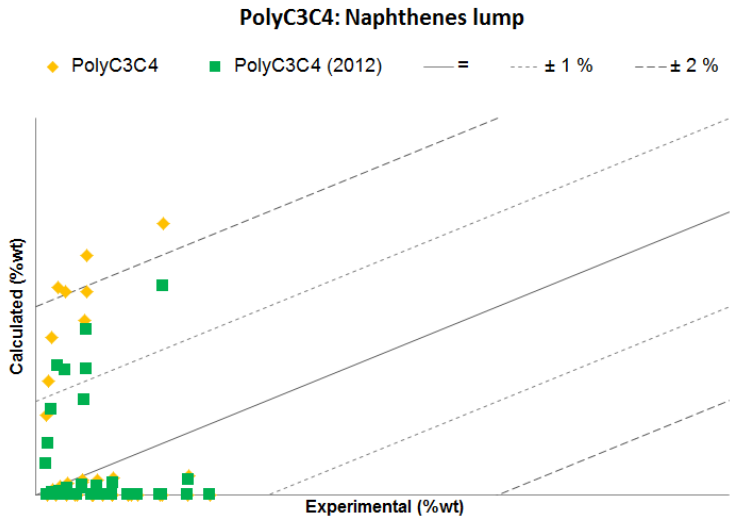

Figure 63 - Parity diagram of naphthenes lump in gasoline cut for PolyC3C4 ($MSEP_{2012} = 4 \times 10^{-5}$; $MSEP_{2014} = 9 \times 10^{-5}$)

For PolyC3C4, the prediction of naphthenes yields is worst with the new approach. With the new model, the simulator predicts higher yields than the 2012 results. Additionally, it cannot estimate the yields for the majority of the experimental tests, where give a value almost null.

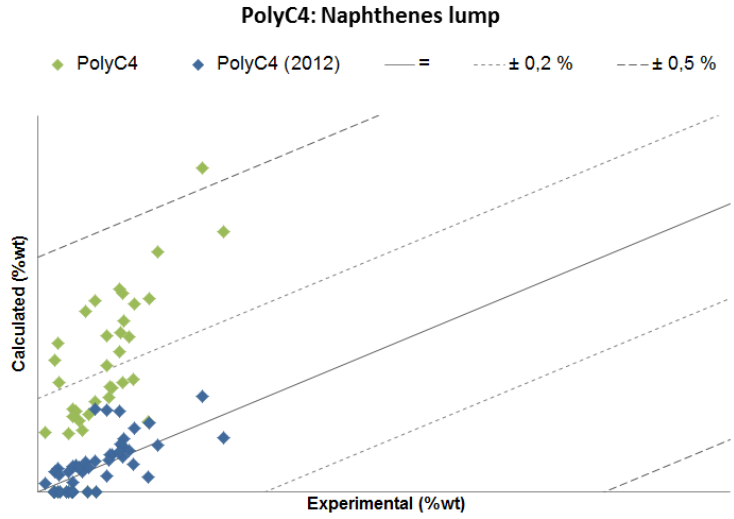

Figure 64 - Parity diagram of naphthenes lump in gasoline cut for PolyC4 ($MSEP_{2012} = 2 \times 10^{-7}$; $MSEP_{2014} = 5 \times 10^{-6}$)

Analyzing the PolyC4 feed results, it is possible to observe in Figure 64 that simulation is less accurate than the previous model. The naphthenes are now overestimated against to a good prediction of 2012.

It is important to notice that results for oligomer feeds are not very significant because the yields are very low and may be considered as traces.

5.4.4. Total paraffin lump

As explained above, it will be analyzed the total paraffins (the sum between normal and branched) composition in order to compare the results obtained in 2014 and 2012.

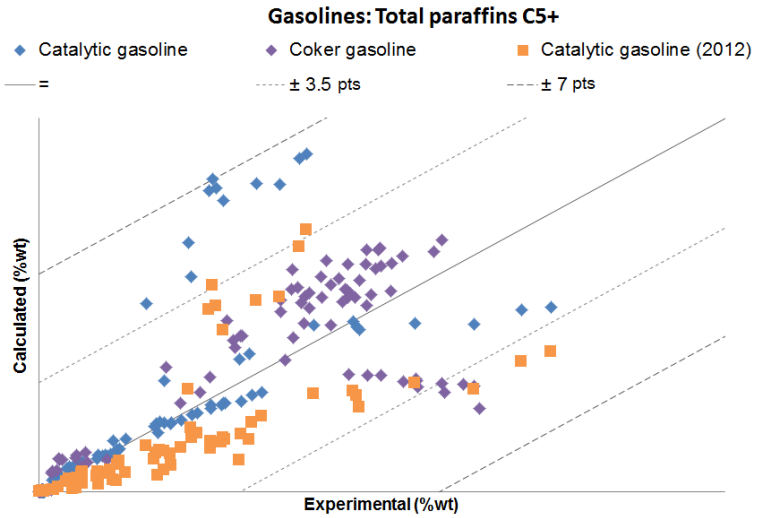

Figure 65 - Parity diagram of total paraffins lump in gasoline cut for catalytic and coker gasolines ($MSE\,P_{Catalytic\ gasol.2012} = 2 \times 10^{-4}$; $MSE\,P_{Catalytic\ gasol.2014} = 4 \times 10^{-4}$; $MSE\,P_{Coke\ gasol.2014} = 3 \times 10^{-4}$)

The results for catalytic gasoline are more dispersed with the new model where the margin of tolerance increases from ±3.5 points to ±6.5 points (Figure 65). The specie that is more overestimated is C_5.

The results of coker gasoline are also dispersed. However, it has an inferior tolerance than catalytic gasoline. In this case, C_5 is the specie that is more underestimated.

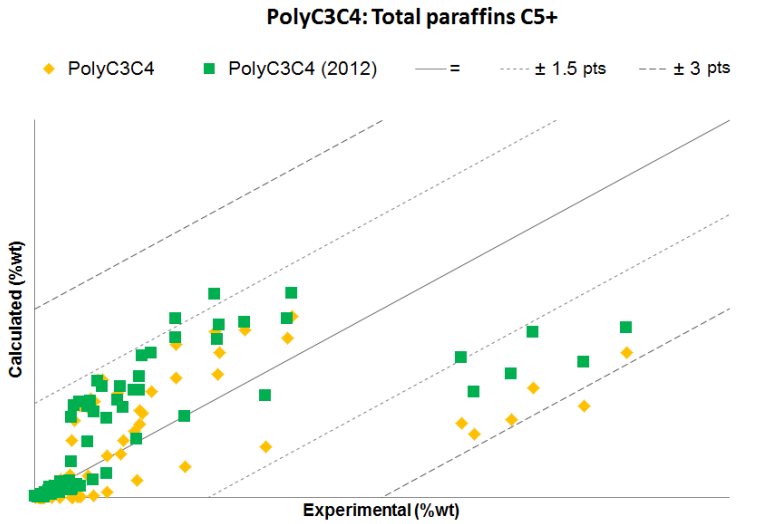

Figure 66 - Parity diagram of total paraffins lump in gasoline cut for PolyC3C4 ($MSE\,P_{2012} = 1.8 \times 10^{-4}$; $MSE\,P_{2014} = 2.3 \times 10^{-4}$)

According with Figure 66, PolyC3C4 results are underestimated comparing with the older ones. C_7 is the specie that is more underestimated. Globally, the accuracy decreases for its results.

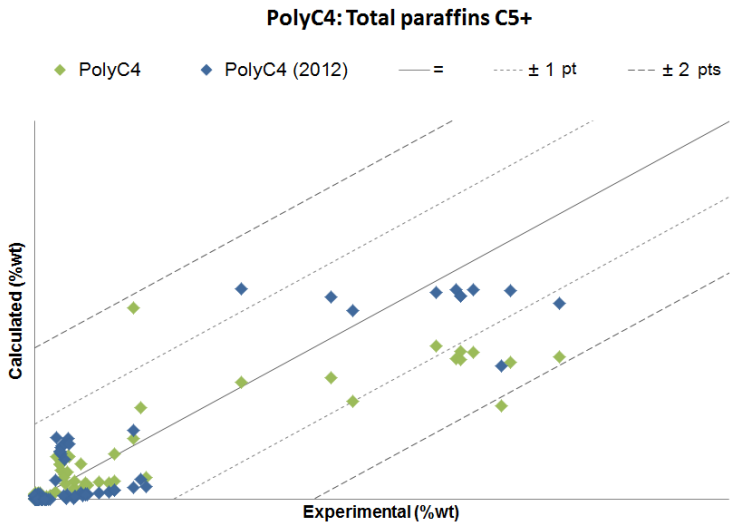

Figure 67 - Parity diagram of total paraffins lump in gasoline cut for PolyC4 ($MSEP_{2012} = 2 \times 10^{-4}$; $MSEP_{2014} = 6 \times 10^{-5}$)

The yields for PolyC4 were obtained with more accuracy for low yields than the previous one, as showed in Figure 67. However, the results for high yields, that correspond to C_5, decrease the accuracy.

5.4.5. Isoparaffin lump

The isoparaffins family was introduced in the present work, and for that reason the comparison with the 2012 results is not possible. In this sub-chapter it will be presented the general results of the family. To understand the quality of the implementation in the next sub-chapter the ratio between the branched and total paraffins will be discussed. The isoparaffins in gasoline are composed of species with more than five carbon atoms. However, it will present here the iP_4 in order to simplify the discussion of isoparaffins implementation (and only for this reason).

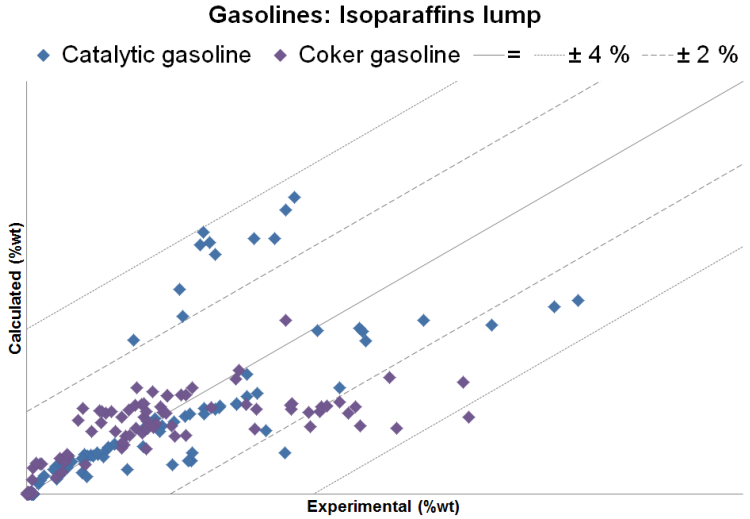

Figure 68 - Parity diagram of isoparaffins lump (C_4-C_{12}) for catalytic and coker gasoline ($MSEP_{Catalytic\ gasol.} = 2 \times 10^{-4}$; $MSEP_{Coke\ gasol.} = 1 \times 10^{-4}$)

Starting with the catalytic gasoline, it is possible to observe that some tests are underestimated and others are overestimated. The results overestimated correspond to iP_5 results and the underestimation

to iP_4 and iP_6 results. On the other hand, the results of coker gasoline which are underestimated correspond to iP_4 and iP_5 results.

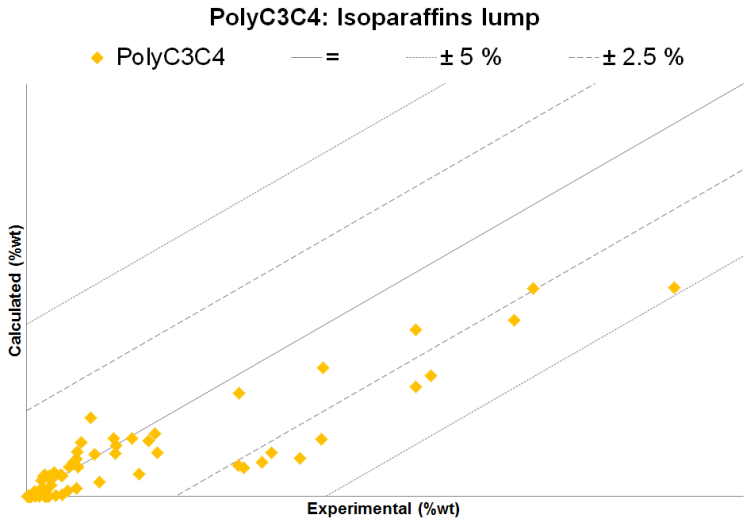

Figure 69 - Parity diagram of isoparaffins lump (C_4-C_{12}) for PolyC3C4 ($MSEP_{2014} = 2 \times 10^{-4}$)

In the results of PolyC3C4 it is notorious also an underestimation of some points. These points represent the results of iP_4 and iP_7 that are the species with high yields.

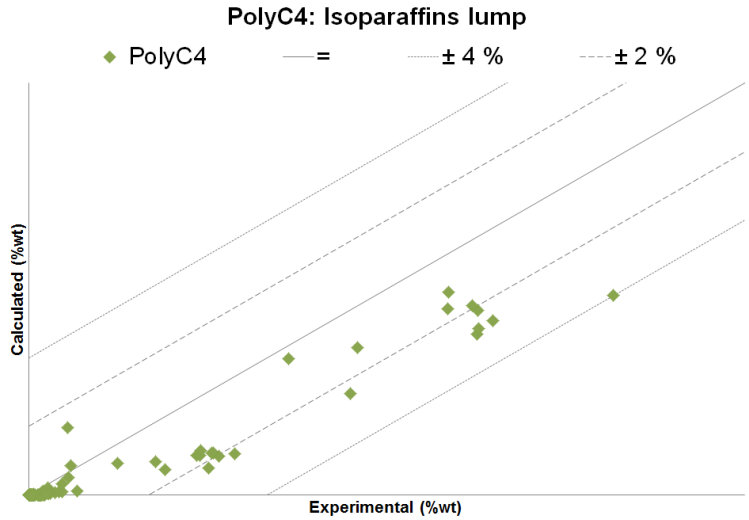

Figure 70 - Parity diagram of isoparaffins lump (C_4-C_{12}) for PolyC4 ($MSEP_{2014} = 1 \times 10^{-4}$)

A similar deviation is detected for PolyC4, where the underestimation described the iP_4 and iP_5 results.

5.4.6. Isoparaffin and total paraffins ratio

The suitable results of the ratio between isoparaffins and paraffins are achieved with the alteration of objective function[19]. Before this modification, the calculated ratio has normally a value of 1, i.e. the simulator predicts that paraffins equilibrium is directed to produce branched paraffins. The result

[19] Introduction of the ratio between the isoparaffins and the total of paraffins as observable (described in chapter 4.6)

analysis will be done component by component, where it will expose the four feeds in the same representation.

Figure 71 represents the parity diagram for the ratio of iP_4.

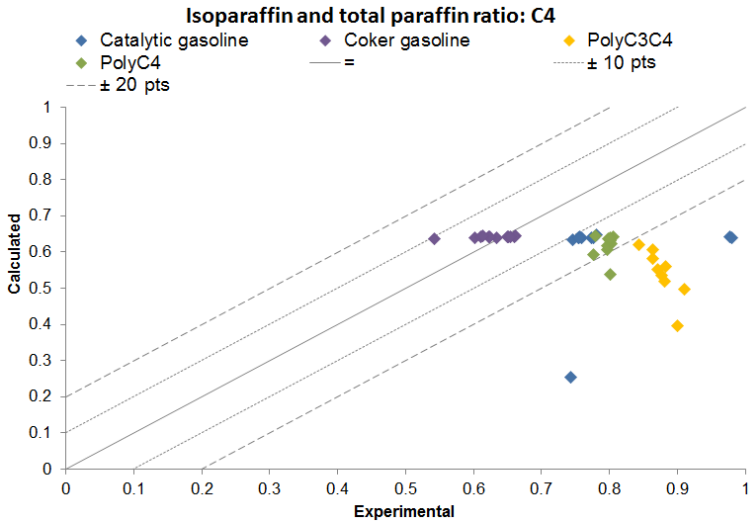

Figure 71 – Isoparaffin and total paraffin ratio for C_4

Figure 71 shows that coker gasoline feed is a higher accuracy than the other in the ratio between isoparaffins and normal paraffins. The majority of experimental tests of catalytic gasoline are predicted within a tolerance lesser than -15 points. Nevertheless, three of the catalytic gasoline tests are estimated with a much higher deviation (two with a tolerance of -35 points and the other with -50 points). Analyzing these three experimental tests, it was concluded that they were tested with extreme operation condition (higher/lesser temperature) than the others. The oligomer feeds results are obtained with a greater tolerance than gasolines (excluding the three points of catalytic gasoline). This result is quite expected, once the oligomers have a weak composition in normal and branched paraffins.

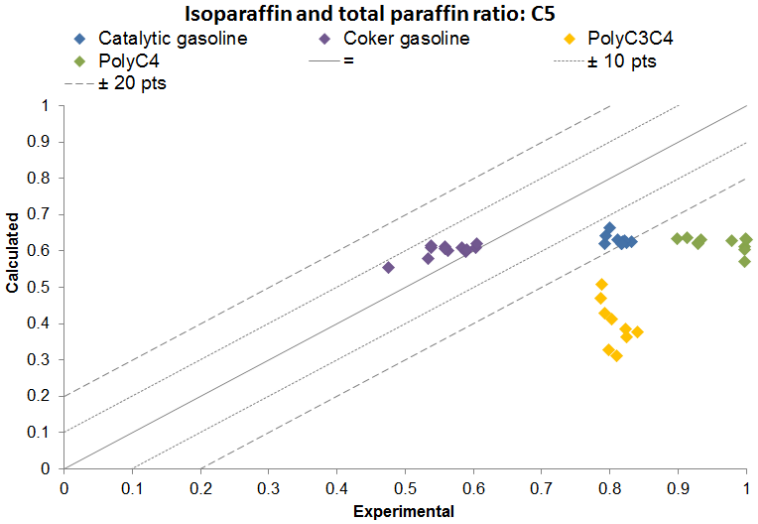

Figure 72 - Isoparaffin and total paraffin ratio for C_5

The results of ratio between iP_5 and the total paraffins C_5 are presented in Figure 72. Once again, the ratio is predicted with more exactitude for the gasolines. However, all the tests of catalytic gasoline are predicted with a similar accuracy.

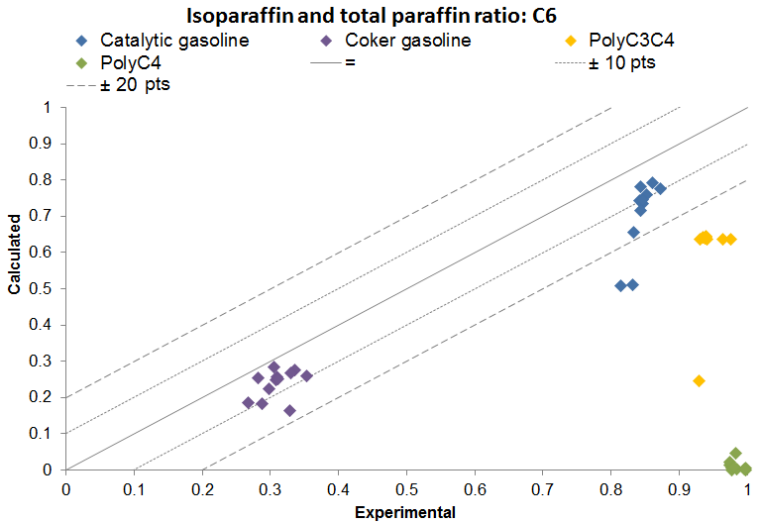

Figure 73 - Isoparaffin and total paraffin ratio for C_6

The results for C_6, presented in Figure 73, have the same behavior than C_4: the catalytic gasoline has two points that have a much greater tolerance than the others. These experimental essays were tested with a lower and a higher temperature and higher C/O. The same behavior is observed with PolyC3C4, where the point that has less accuracy it was tested with a higher C/O. Concerning PolyC4, the simulator cannot predict the formation of isoparaffins, where the experimental data indicates the opposite, i.e. the paraffins in output are just branched.

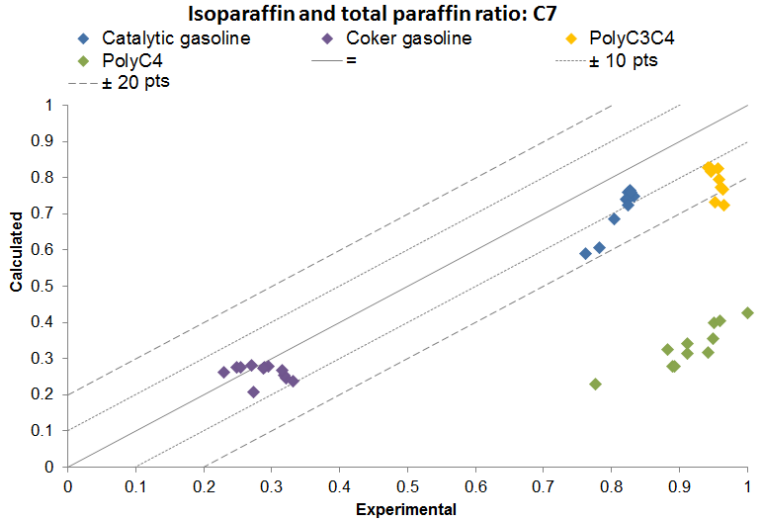

Figure 74 - Isoparaffin and total paraffin ratio for C_7

The C_7 ratio results are displayed in Figure 74. By observation of this parity diagram it is perceived that the estimation of equilibrium between normal and branched is not well predicted for PolyC4. An equivalent performance happens with C_8 species (Figure 75).

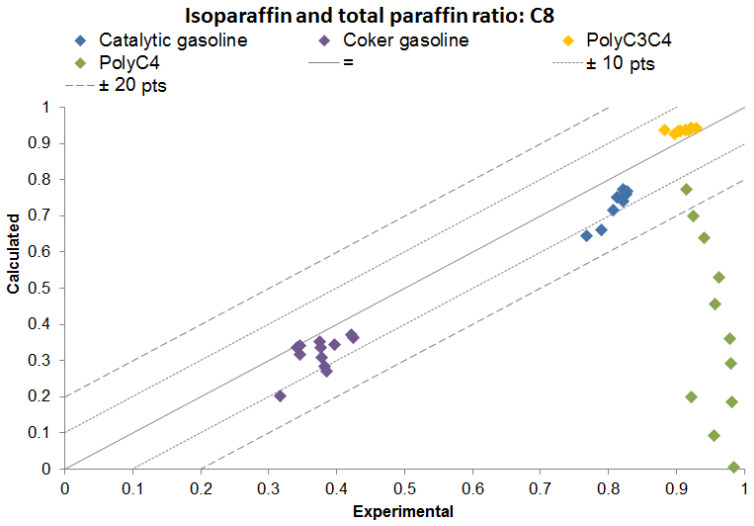

Figure 75 - Isoparaffin and total paraffin ratio for C_8

The C_8 results for PolyC4 are much dispersed. Reminding the feeds compositions, the isoparaffins content in this charge is mainly C_8. With that, good results were expected concerning this species. But it is not verified in Figure 75, where the results appear to have a stochastic behavior.

Regarding C_9 ratio (Figure 76), the simulator predicts a better equilibrium between paraffins for PolyC4. In PolyC3C4, it is observed that one point has a lower accuracy than the others. This experimental test was obtained for with a temperature lesser than the normal (590ºC).

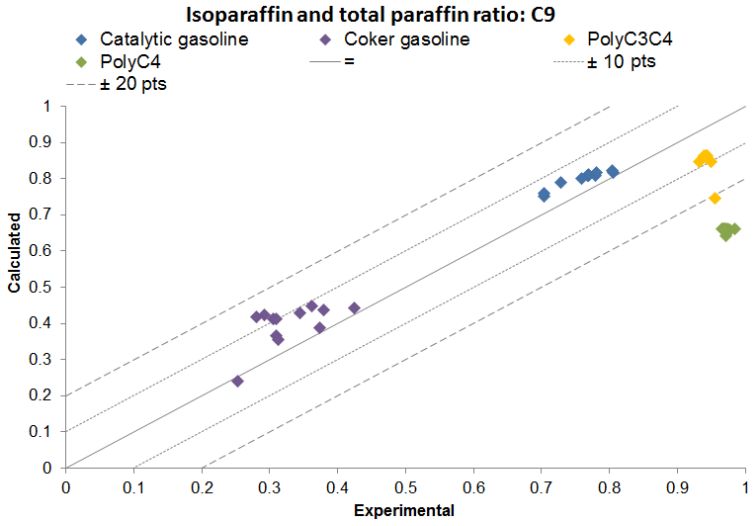

Figure 76 - Isoparaffin and total paraffin ratio for C_9

The $iP_{10}+$ species are not very relevant for this analysis once that are weak representation in composition of the feedstocks. Its parity diagrams are accessible in Appendix 1. In these diagrams is possible to observe that simulator cannot predict the formation of isoparaffins on PolyC4 (as showed in C_6 analysis, Figure 73).

5.5. LCO

As explained in sub-chapter 4.5.2, the kinetic expression of LCO formation was changed to consider it as a first order reaction. The upgrade was to achieve a better performance for this cut after the

isoparaffins implementation. For that reason, the alteration cannot predict a better result comparing with the 2012 results.

The results for this cut are showed for each charge in Figure 77 to Figure 79.

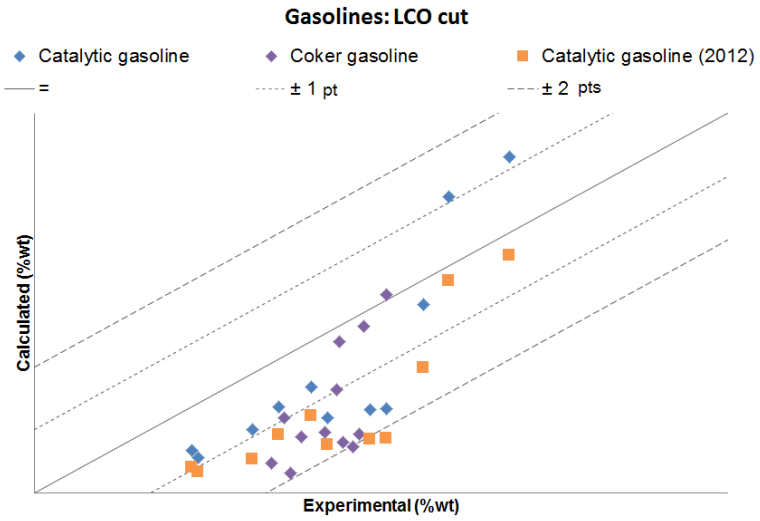

Figure 77 - Parity diagram of LCO cut for catalytic and coker gasolines ($MSEP_{Catalytic\ gasol.2012} = 2 \times 10^{-4}$; $MSEP_{Catalytic\ gasol.2014} = 1 \times 10^{-4}$; $MSEP_{Coke\ gasol.2014} = 2 \times 10^{-4}$)

Starting with catalytic gasoline, the results have generally a better accuracy. 55% of the experimental tests are predicted within a tolerance of ±1 point. Coker gasoline was a suitable prediction as well, where 42% of its experimental tests are estimated within a tolerance of ±1 point.

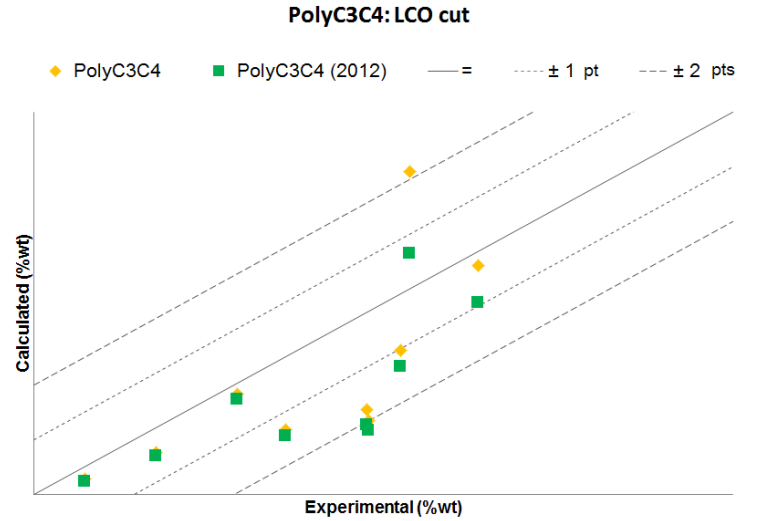

Figure 78 - Parity diagram of LCO cut for PolyC3C4 ($MSEP_{2012} = 1.6 \times 10^{-4}$; $MSEP_{2014} = 1.7 \times 10^{-4}$)

Concerning PolyC3C4, the present results are lesser accurate than the 2012 results for high yields. The prediction with a tolerance of ±1 point increases from 38% to 50% of the experimental tests for this charge.

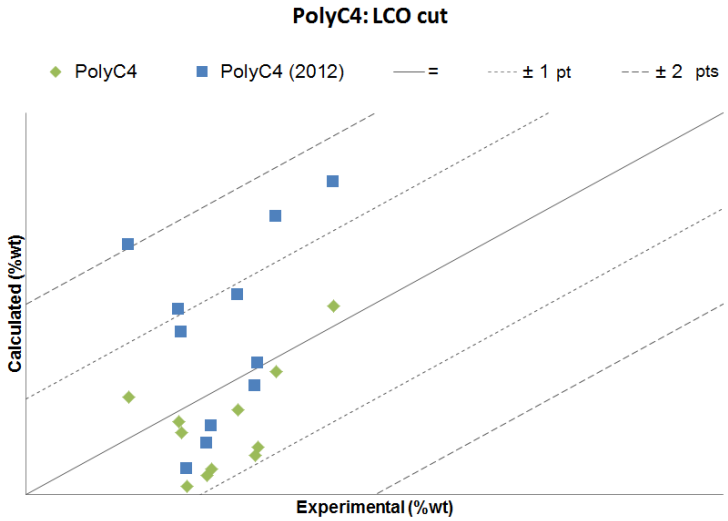

Figure 79 - Parity diagram of LCO cut for PolyC4 ($MSEP_{2012} = 1 \times 10^{-4}$; $MSEP_{2014} = 4 \times 10^{-5}$)

On the other hand, the results for PolyC4 are improved. Now, 55% of its experimental tests are predicted within a margin of ±0.5 points.

Table 23 - Absolute error tolerance intervals of LCO cut for the different feeds

% of yields within tolerance	Tolerance (pts)			
	±0.5	±1	±2	±4
Catalytic gasoline	9%	55%	100%	
Coker gasoline	25%	33%	92%	100%
PolyC3C4	44%	44%	89%	100%
PolyC4	55%	100%		

The best approach to predict the LCO yields with the new model is taking into account this reaction as first order. However, no better results were achieved.

5.6. Coke

The results of coke yields are presented in Figure 80 to Figure 82.

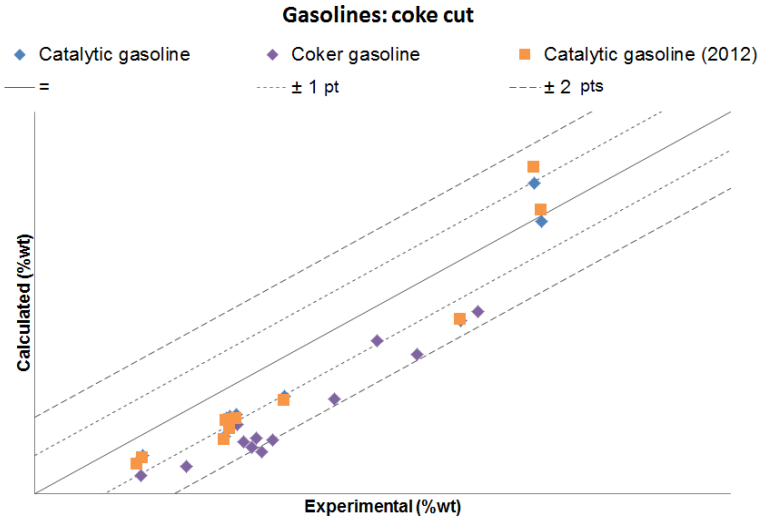

Figure 80 - Parity diagram of coke cut for catalytic and coker gasolines ($MSEP_{Catalytic\ gasol.2012} = 1 \times 10^{-4}$; $MSEP_{Catalytic\ gasol.2014} = 9 \times 10^{-5}$; $MSEP_{Coke\ gasol.2014} = 3 \times 10^{-4}$)

According to Figure 80, coke prediction for catalytic gasoline is slight improved for high yields. Regarding the coker gasoline, the prediction has lesser accuracy than catalytic gasoline. Only 17% of coker gasoline tests are estimated within a tolerance of ±1 point.

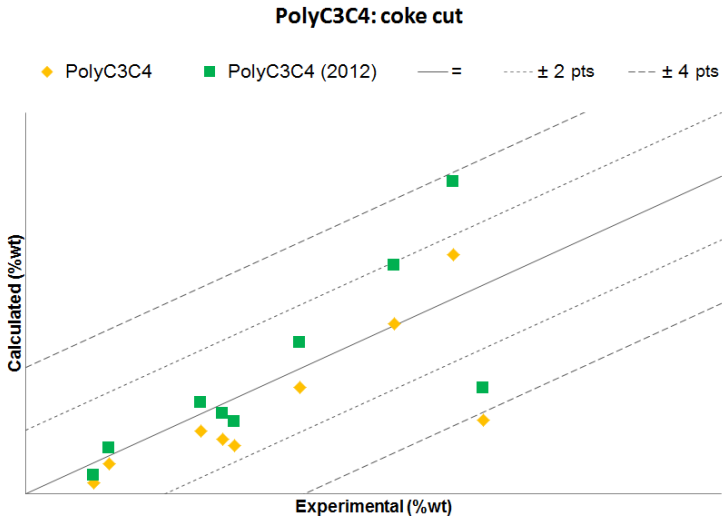

Figure 81 - Parity diagram of coke cut for PolyC3C4 ($MSEP_{2012} = 3.3 \times 10^{-4}$; $MSEP_{2014} = 2.7 \times 10^{-4}$)

Concerning PolyC3C4, coke yields are slightly lower and less accurate than the older ones. In this case, 55% of the results are predicted within a ±1 point tolerance and 89% within ±2 points tolerance.

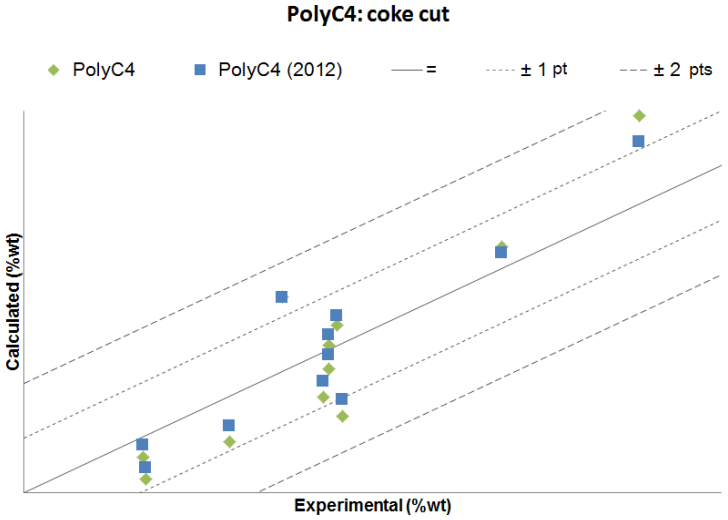

Figure 82 - Parity diagram of coke cut for PolyC4 ($MSEP_{2012} = 5 \times 10^{-5}$; $MSEP_{2014} = 8 \times 10^{-5}$)

The dispersion of coke results remains also in PolyC4. The accuracy of the results is lower comparing to the 2012 model.

Table 24 - Absolute error tolerance intervals of coke cut for the different feeds

% of yields within tolerance	Tolerance (pts)				
	±0.5	±1	±2	±4	±6
Catalytic gasoline	9%	64%	100%		
Coker gasoline	8%	17%	83%	100%	
PolyC3C4	22%	56%	89%	89%	100%
PolyC4	45%	73%	100%		

As presented in chapter 2.2.4, several authors propose different mechanisms to produce coke. One of them mechanism is the reaction between olefins or an aromatic and an olefins. The coke underestimation (mainly in gasolines feeds) can be explained by not having taken into consideration this type of reaction for its formation. As prospective, the coke formation by this type of mechanism should be analyzed.

The relative errors for each cut, as well as propylene, are presented in Appendix 2.

This page was intentionally left blank.

6. Sensitivity analysis

As explained in chapter 4.6, the activation energies were not optimized. The previous values were used and for the new reactions (isoparaffins catalytic and thermal cracking and isomerization) some assumptions were done. To understand the impact of its parameters, it was performed a sensitivity analysis. For that, the activation energies were changed on ±10% and ±20% of its value. The variation was tested separately for each reaction and after for groups of reactions.

The impact of alterations was assessed by the relative error of the objective function. The results are available in Table 25.

Table 25 – Sensitivity analysis results for ±10% and ±20% deviation of activation energies values

% relative error of objective function	**Activation energies deviation in the reaction(s) considered**			
	-20% Ea	**-10% Ea**	**+10% Ea**	**+20% Ea**
Olefins catalytic cracking	1.13%	0.55%	0.39%	0.71%
n-paraffins catalytic cracking	0.06%	0.23%	0.10%	0.06%
LCO formation	0.72%	0.35%	0.22%	0.67%
Coke formation	0.86%	0.51%	0.52%	1.01%
Olefins thermal cracking	0.37%	0.07%	1.47%	0.49%
n-paraffins thermal cracking	0.10%	0.12%	0.03%	0.17%
Oligomerization and cyclization	0.60%	0.21%	0.11%	0.50%
Isoparaffins catalytic cracking	1.26%	0.20%	0.02%	0.04%
Isoparaffins thermal cracking	0.92%	0.50%	0.55%	0.98%
Isomerization	1.40%	1.37%	0.21%	[20]
Catalytic Cracking reactions	1.01%	0.50%	0.48%	0.77%
Thermal cracking reactions	1.46%	0.66%	0.70%	1.54%
All reactions	0.65%	1.11%	0.06%	0.15%

The relative error was calculated according the follow equation:

$$Relative\ error\ (\%) = \frac{|ssq_{with\ the\ Ea\ deviation} - ssq_{without\ alterations}|}{ssq_{without\ alterations}} \quad \text{Eq. 45}$$

The maximum relative variation of this parameter in objective function is less than 2%. With that, it is possible to conclude that the assumptions made will not have a greater impact in the final results. However, the simulator performance changed with the variation of activation energy, especially in reactions that include equilibrium reactions (isomerization).

[20] The simulator does not converge for this modification

This page was intentionally left blank.

7. Conclusions

A kinetic model of naphtha catalytic cracking has been developed at IFPEN to be applied in a dual riser configuration. The main development that this work proposes is the distinction between linear and branched paraffins. For that, new components and reactions were introduced in the model in accordance with the considered assumptions. One of them was having considered the same kinetic expressions (with different kinetic parameters) as for linear paraffins cracking.

The model upgrade from PONA to PIONA introduced more variables and increased the simulator sensitivity. The problems to obtain convergence were more important for the mass balances obtained with more severe conditions, i.e. experimental tests that are obtained with higher/lesser temperature and/or C/O than the normal.

The structure parameters and ZSM-5 factors do not depend on the feedstock and for that reason they are considered the same for all feeds. Concerning the pre-exponential factor, the gasolines were grouped in the same set to reduce the number of these factors. The same procedure was tried with oligomer feeds without success. The use of different catalysts in the experimental tests can be responsible for the distinct reactivities of these feeds. The two set of pre-exponential factors obtained to describe the oligomers feeds were analyzed. However, without the full catalyst characterization it is difficult to understand their effect on it.

The molecule structure function was evaluated in order to compare the results between linear and branched paraffins. With the structure parameters that are calculated by the simulator, the function performs the expected effect for normal paraffins, a smooth normal distribution. However, the results for branched paraffins show a very abrupt normal distribution. This distribution predicts a high effect in the symmetric cracking and neglects the other cases. With that, it is possible to conclude that the present function is not suitable to be applied in isoparaffins catalytic cracking. The structure function should be reevaluated.

The results were evaluated by parity diagrams and compared with the previous model. Generally, the cuts' results did not change in a scale worth of consideration. The same can be noticed for the families. Looking to the work focus, the way to compare the new results to the previous ones is by the total paraffins yields. For the catalytic gasoline, the total paraffins yield is obtained with higher dispersion and much overestimation comparing to the 2012 model. The dispersion is also noticed in coker gasoline. Concerning the oligomers, the simulator predicts slight underestimated yields comparing to the 2012 results. The prediction of total paraffins was not improved.

With the results analysis of isoparaffins lump, it was possible to observe that some species are much over/underestimated than others. It is most notorious in gasolines, where iP_5 are overestimated and iP_4 and iP_6 are underestimated in catalytic gasoline results. On the other hand, for coker gasoline, the underestimation is related to iP_5 and iP_7. One of the causes for that can be the reaction network proposed. It was assumed that paraffins catalytic cracking do not produce branched paraffins, in order

to reduce the number of reactions. However, this assumption is not correct. According to the literature review, the cracking of a linear or a branched paraffin can produced a linear or branched species.

The ratio between the isoparaffins and total paraffins for the same carbon number is important to understand the implementation in terms of equilibrium. As expected the results for this ratio are more accurate for gasolines than for oligomers that can be explained by their composition in paraffins. The results also reveal that the simulator shows also a significant sensitivity to operation. The experimental tests obtained with a lower/higher temperature and/or higher C/O than the typical conditions have worst results and lower accuracy than the others. This sensitivity can be explained by the equilibrium data that are used that cannot be suitable for these severe operating conditions.

The distinction between normal and branched paraffin was implemented in this work, however, the global results did not show an improvement. The implementation was done without deteriorating overmuch the results that is a success for the first approach to introduce the new family. This model is able to achieve good results for each feed for PIONA composition. To improve the results it is necessary to develop the isoparaffins description. Some suggestions are described in future work.

Concerning overall the coker gasoline feed results, they have more dispersion and less accuracy than catalytic gasoline results. The coker gasoline results can get better by the description by a separated set of pre-exponential constants. Nevertheless, the goal of this model type is to obtain a single set of kinetic parameters that can describe all the possibilities and feeds. The improvements of the results should pass by the implementation of other changes (that will be discussed in the work prospective) and not by adding more set of parameters.

Finally, it was showed that the influence of activation energy is not significant and the assumption to use the previous values of activation energies did not increase too much the error. However, it was noticed again the simulator sensitivity in isomerization reactions. For this reason, a value of activation energy of isomerization reactions with more accuracy should be implemented.

8. Future work

In the following paragraphs it will be discussed several ways to improve the simulator and the results.

The simulator execution time increased five to eleven times, after isoparaffins implementation. This implies a limitation of tests that can be made. For that reason, the method to solve the mass balance should be reevaluated as well as the algorithm choice.

To improve the paraffins distinction more details are needed. In order to complete the reaction network, the paraffins cracking should predict the formation of branched paraffins that will mean more reactions and parameters. As concluded, the molecule structure function for isoparaffins catalytic cracking is not suitable for these molecules. So, it will be necessary a reevaluation of this effect and especially the symmetry assumptions (that cannot be appropriated for branched paraffins).

The equilibrium description should be also reconsidered once the actual results show a bad representation of that. The data used are from another IFPEN project that is not operating in the same conditions that second riser works. It is proposed the execution of experimental work at equilibrium conditions.

As explained, the components that are added to the model represent the isoparaffins by number of carbon atoms and do not take into account the type of isoparaffins (mono branched, di-branched, etc). Once mono and di-branched paraffins are the species most common in the feeds, the distinction can be made. Once again, with this type of alteration the number of components, reactions, and parameters will increase.

In order to understand the catalytic system to describe its effects in the model, it is necessary to have the full characterization of E-cat A and B. It would be also useful to test the different catalysts with the same feed to observe the different influences of them. With these data, the effects of the catalyst system can be modulated to complete the simulator. Consequently, the representation of the feeds in the same set of kinetic parameters it will be easily achieved.

Other modifications can be explored to describe better the reality but that may not improve the results so much:

- Catalyst deactivation by coke;
- Adsorption and desorption of the species;
- Temperature dependence in hydrogen transfer: according with Lee et al. (2011) the activation energy for this reaction are not neglected;
- Kinetic rate of oligomerization reaction according with Carabineiro's (2003) work that implies the chain length dependence;
- Distinction between the activation energies of β-scission and protolytic cracking (as explained in literature review);
- Distinction between linear and branched olefins.

Finally, the activation energy should be re-optimized or experimentally determined in order to increase the model fidelity. It is important to refer that the actual data was obtained with a small range of temperature that do not allow the calculation with some accuracy.

References

Caeiro, G. et al., 2006. Activation of C2–C4 alkanes over acid and bifunctional zeolite catalysts. *Journal of Molecular Catalysis ,* Volume Chemical 255, pp. 131-158.

Carabineiro, H., Pinheiro, C., Lemos, F. & Ribeiro, F., 2003. Transient microkinetic modelling of n-heptane catalytic cracking over H-USY zeolite. *Chemical Engineering Science,* pp. 1221-1232.

Cerqueira, H., Caeiro, G., Costa, L. & Ribeiro, F. R., 2008. Deactivation of FCC catalysts. *Journal of Molecular Catalysis A: Chemical,* Volume 292, pp. 1-13.

Concawe, 2013. *Oil refining in the EU in 2020, with perspectives to 2030,* Brussels: Concawe.

Corma, A. & Orchillés, A., 2000. Current views on the mechanism of catalytic cracking. *Microporous and Mesoporous Materials,* Volume 35-36, pp. 21-30.

Darouich, T. A., Béhar, F., Largeau, C. & Budzinski, H., 2005. Separation and Characterisation of the C15- Aromatic Fraction of Safaniya Crude Oil. *Oil & Gas Science and Technology – Rev. IFP,* 60(4), pp. 681-695.

Dasila, P. K. et al., 2012. Parametric Sensitivity Studies in a Commercial FCC Unit. *Advances in Chemical Engineering and Science,* Volume 2, pp. 136-149.

Do, M. P., 2009. *FCC – Flexible Responses to Market's Evolution.* Rueil-Malmaison: Axens.

Dupraz, C., 2012. *(R)FCC Product Flexibility with FlexEne.* Bangkok: Axens.

Dwyer, F. G. & Degnan, T. F., 1993. Studies in surface science and catalysis. In: J. Magee & M. Mitchell, eds. *Fluid catalytic cracking: science and technology.* Amesterdam: Elsevier, pp. 499-528.

Echard, M. & Feugnet, F., 2007. *Resid to Propylene Catalyst Selection,* Lyon: IFP Energies nouvelles.

Fahim, M. A., Alsahhaf, T. A. & Elkilani, A., 2010. *Fundamentals of Petroleum Refining.* 1st ed. Amsterdam: Elsevier.

Fernandes, J., 2007. *Nonlinear Modelling of Industrial Fluid Catalytic Cracking Processes for Model-Based Control and Optimization Studies.* Lisbon: Instituto Superior Técnico.

Fernandes, J., 2010. *Naphtha cracking modeling : New fit for HPFCC application,* Lyon: IFP Energies nouvelles.

Feugnet, F., 2008. *Naphtha cracking modelling,* Lyon: IFP Energies Nouvelles.

Feugnet, F. & Roux, R., 2011. *Process for catalytic cracking with a recycle of an olefinic cut removed upstream of the gas separation section in order to maximize propylene production.* US, Patent No. 0272326A1.

Figueiredo, J. & Ribeiro, F. R., 2007. *Catálise Heterogénea.* 2nd ed. Lisbon: Fundação Calouste Gulbenkian.

Fu, A., Hunt, D., Bonilla, J. A. & Batachari, A., 1998. *Deep catalytic cracking plant produces propylene in Thailand,* Houston: Oil & Gas Journal.

Gauthier, T., Bayle, J. & Leroy, P., 2000. FCC: Fluidization Phenomena and Technologies. *Oil & Gas Science and Technology – Rev. IFP,* 55(2), pp. 187-207.

Graça, I. P., 2010. *Influence of Oxygenated Compounds on the Properties of FCC Catalysts,* Lisbon: Instituto Superior Técnico.

Grace Davison, 1996. *Guide to Fluid Catalytic Cracking.* Maryland: W.R. Grace & Co.-Conn..

Guisnet, M. & Gilson, J.-P., 2002. *Zeolites for Cleaner Technologies.* 1st ed. London: Imperial College Press.

Guisnet, M. & Ribeiro, F., 2004. *Zeólitos, um nanomundo ao serviço da catálise.* 1st ed. Lisboa: Fundação Calouste gulbenkian.

Jiménez-Cruz, F. & Laredo, G. C., 2004. Molecular size evaluation of linear and branched paraffins from the gasoline pool by DFT quantum chemical calculations. *Fuel,* Volume 83, pp. 2183-2188.

Joly, J., Vleeming, J. & Galtier, P., 1997. *Isomerization of n-butane and isobutane with IS612A as catalyst. Results of the kinetic experiments,* Lyon: Institut Français du Pétrole.

Kano, M., Miyazaki, K., Hasebe, S. & Hashimoto, I., 2000. Inferential control system of distillation compositions using dynamic partial least squares regression. *Journal of Process Control,* Volume 10, pp. 157-166.

Kotre, S., Knozinger, H. & Gates, B., 2000. The Haag–Dessau mechanism of protolytic cracking of alkanes. *Microporous and Mesoporous Materials,* 35(36), pp. 11-20.

Leprince, P., 2001. *Petroleum Refining: Conversion processes.* Paris: Editions TECHNIP.

Longstaff, D., 2012. Development of a comprehensive naphtha catalytic cracking kinetic model. *Energy & Fuels,* Volume 26, pp. 801-809.

Nizamoff, A. J., 2013. *Propylene PERP 2013-1,* New York: Nexant.

Palma, A., 2012. *Kinetic Model for Gasoline Catalytic Cracking Based on a Lumped Molecular Approach.* Lisboa: Técnico Lisboa.

Pinheiro, C. I. C. et al., 2012. Fluid Catalytic Cracking (FCC) Process Modeling, Simulation, and Control. *Industrial & Engineering Chemistry Research,* Volume 51, pp. 1-29.

Pinheiro, C., Lemos, F. & Râmoa Ribeiro, F., 1999. Dynamic modelling and network simulation of n-heptane catalytic cracking: influence of kinetic parameters. *Chemical Engeneering Science,* pp. 1735-1750.

Rahimi, N. & Karimzadeh, R., 2011. Catalytic cracking of hydrocarbons over modified ZSM-5 zeolites to produce light olefins: A review. *Applied Catalysis,* General(398), pp. 1-17.

Sadeghbeigi, R., 2012. *Fluid Catalytic Cracking Handbook.* Butterworth: 3rd edition.

Sigma Aldrich, n.d. *Molecular Sieves.* [Online] Available at: http://www.sigmaaldrich.com/chemistry/chemical-synthesis/learning-center/technical-bulletins/al-1430/molecular-sieves.html
[Accessed 23 Abril 2014].

Wang, L., Yang, B. & Wang, Z., 2005. Lumps and kinetics for the secondary reactions in catalytically cracked gasoline. *Chemical Engineering Journal,* Volume 109, pp. 1-9.

Wan, V. Y., 2012. *Propylene production bt the JGC/MMC DTP process,* Santa Clara: IHS.

Williams, B. et al., 1999. The roles of acid strength and pore diffusion in the enhanced cracking activity of steamed Y zeolites. *Applied Catalysis A: General,* Volume 177, pp. 161-175.

This page was intentionally left blank.

Appendices

A1. Parity diagrams

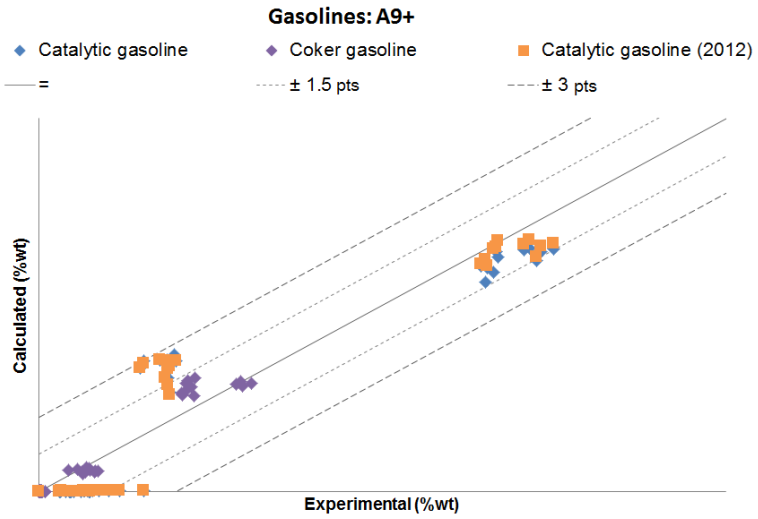

Figure 83 – Parity diagram of aromatic lump in gasoline cut for catalytic and coker gasolines

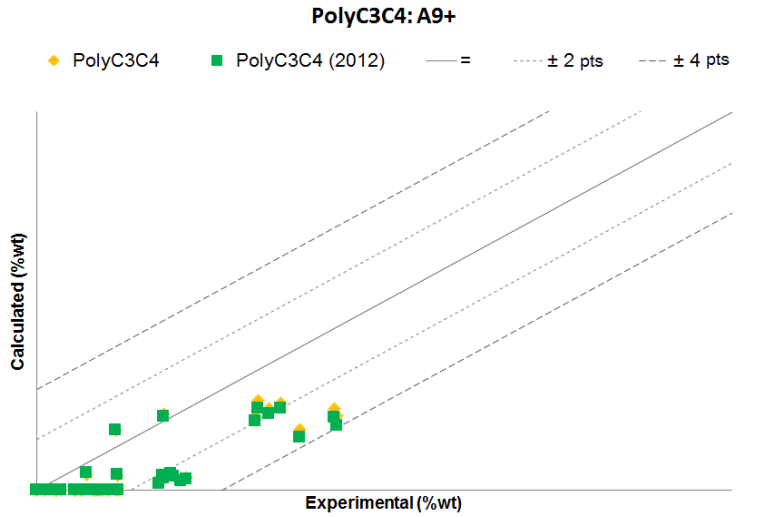

Figure 84 - Parity diagram of aromatic lump in gasoline cut for PolyC3C4

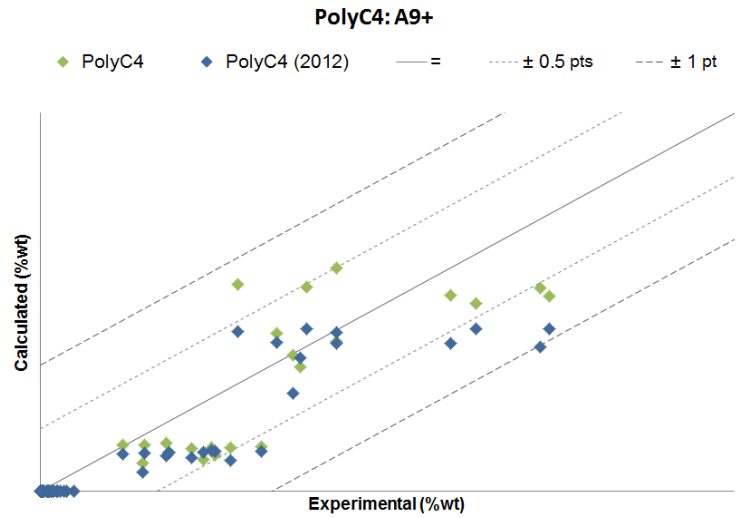

Figure 85 - Parity diagram of aromatic lump in gasoline cut for PolyC4

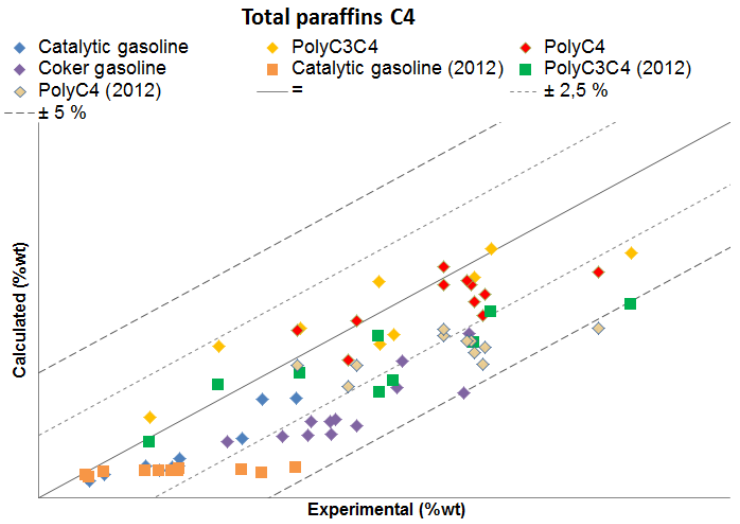

Figure 86 - Parity diagram of total paraffins C_4 for all feeds

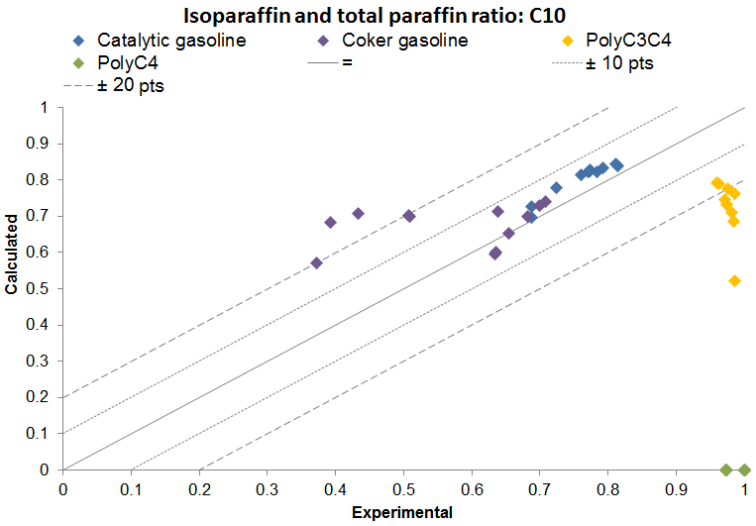

Figure 87 - Isoparaffin and total paraffins ratio for C_{10}

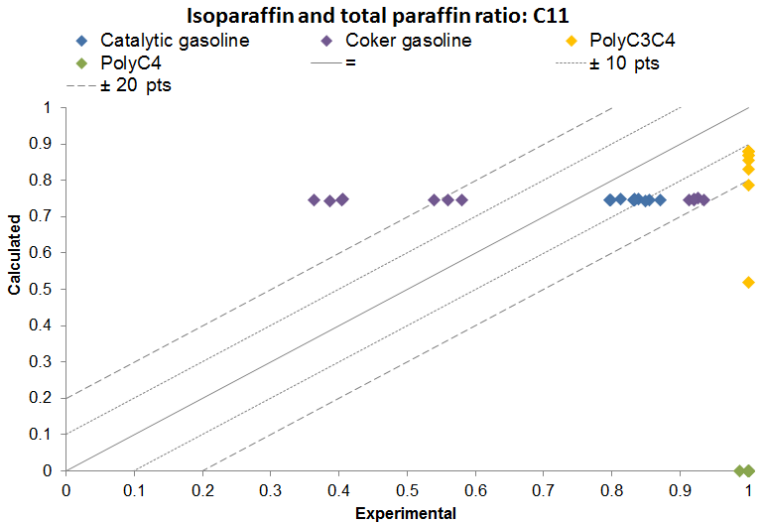

Figure 88 - Isoparaffin and total paraffins ratio for C_{11}

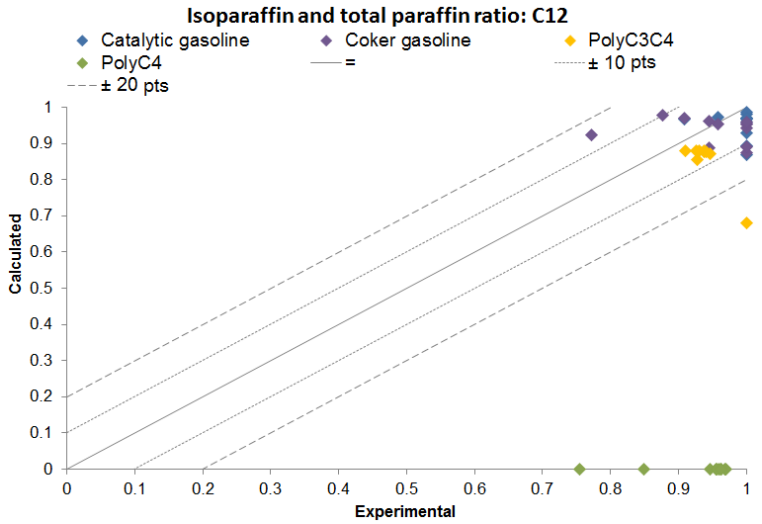

Figure 89 - Isoparaffin and total paraffins ratio for C_{12}

A2. Absolute errors for other species

Table 26 – Tolerance intervals of O_5 for all feeds

% of yields within tolerance	Tolerance (pts)					
	±0.5	±1	±2	±3	±4	±5%
Catalytic gasoline	55%	91%	91%	100%		
Coker gasoline	0%	0%	0%	25%	67%	100%
PolyC3C4	56%	78%	100%	100%		
PolyC4	18%	45%	91%	91%	100%	

Table 27 – Tolerance intervals of O_6 for all feeds

% of yields within tolerance	Tolerance (pts)					
	±0.5	±1	±1.5	±2	±2.5	±3
Catalytic gasoline	55%	55%	82%	100%		
Coker gasoline	33%	58%	75%	92%	100%	
PolyC3C4	11%	22%	67%	78%	89%	100%
PolyC4	36%	91%	91%	91%	91%	100%

Table 28 – Tolerance intervals of O_7 for all feeds

% of yields within tolerance	Tolerance (pts)				
	±0.25	±0.5	±0.75	±1	±1.5
Catalytic gasoline	100%				
Coker gasoline	25%	50%	75%	100%	
PolyC3C4	22%	22%	56%	78%	100%
PolyC4	27%	82%	100%		

Table 29 – Tolerance intervals of O_8 for all feeds

% of yields within tolerance	Tolerance (pts)				
	±0.25	±0.5	±0.75	±1	±1.5
Catalytic gasoline	73%	91%	100%		
Coker gasoline	8%	42%	50%	92%	100%
PolyC3C4	0%	22%	33%	67%	100%
PolyC4	0%	27%	55%	91%	100%

Table 30 – Tolerance intervals of O_9 for all feeds

% of yields within tolerance	Tolerance (pts)				
	±0.25	±0.5	±0.75	±1	±1.5
Catalytic gasoline	45%	100%			
Coker gasoline	8%	25%	67%	92%	100%
PolyC3C4	11%	44%	78%	89%	100%
PolyC4	100%	100%			

Table 31 – Tolerance intervals of N_6 for all feeds

% of yields within tolerance	Tolerance (pts)					
	±0.5	±0.75	±1	±1.5	±2	±2.5
Catalytic gasoline	45%	64%	82%	100%	100%	100%
Coker gasoline	75%	92%	100%	100%	100%	100%
PolyC3C4	0%	0%	11%	22%	56%	100%
PolyC4	100%	100%	100%	100%	100%	100%

Table 32 – Tolerance intervals of N_7 for all feeds

% of yields within tolerance	Tolerance (pts)				
	±0.25	±0.5	±0.75	±1	±1.5
Catalytic gasoline	18%	36%	73%	91%	100%
Coker gasoline	50%	75%	75%	100%	
PolyC3C4	89%	100%			
PolyC4	100%				

Table 33 – Tolerance intervals of N_8 for all feeds

% of yields within tolerance	Tolerance (pts)				
	±0.25	±0.5	±0.75	±1	±1.5
Catalytic gasoline	27%	91%	100%		
Coker gasoline	0%	17%	42%	58%	100%
PolyC3C4	56%	100%			
PolyC4	36%	91%	100%		

Table 34 – Tolerance intervals of iP_4 for all feeds

% of yields within tolerance	Tolerance (pts)				
	±1	±2	±3	±4	±5
Catalytic gasoline	27%	91%	100%		
Coker gasoline	25%	42%	75%	92%	100%
PolyC3C4	22%	44%	56%	89%	100%
PolyC4	9%	45%	91%	100%	

Table 35 – Tolerance intervals of iP_5 for all feeds

% of yields within tolerance	Tolerance (pts)					
	±0.5	±1	±2	±3	±4	±5
Catalytic gasoline	0%	0%	0%	36%	100%	
Coker gasoline	8%	17%	67%	92%	100%	
PolyC3C4	100%					
PolyC4	0%	9%	73%	100%		

Table 36 – Tolerance intervals of iP_6 for all feeds

% of yields within tolerance	Tolerance (pts)					
	±0.25	**±0.5**	**±0.75**	**±1**	**±2**	**±3**
Catalytic gasoline	27%	27%	45%	55%	91%	100%
Coker gasoline	75%	92%	100%			
PolyC3C4	67%	89%	100%			
PolyC4	100%	100%				

Table 37 – Tolerance intervals of iP_7 for all feeds

% of yields within tolerance	Tolerance (pts)					
	±0.5	**±0.75**	**±1**	**±2**	**±3**	**±4**
Catalytic gasoline	36%	91%	100%			
Coker gasoline	58%	92%	100%			
PolyC3C4	0%	11%	22%	33%	78%	100%
PolyC4	91%	100%				

Table 38 – Tolerance intervals of iP_8 for all feeds

% of yields within tolerance	Tolerance (pts)				
	±0.25	**±0.5**	**±0.75**	**±1**	**±1.5**
Catalytic gasoline	73%	100%			
Coker gasoline	50%	67%	92%	100%	
PolyC3C4	56%	78%	89%	89%	100%
PolyC4	82%	91%	91%	91%	100%

Table 39 – Tolerance intervals of iP_9 for all feeds

% of yields within tolerance	Tolerance (pts)				
	±0.25	**±0.5**	**±0.75**	**±1**	**±1.5**
Catalytic gasoline	100%	100%	100%	100%	100%
Coker gasoline	17%	33%	50%	75%	100%
PolyC3C4	22%	89%	100%	100%	100%
PolyC4	100%	100%	100%	100%	100%

A3. Relative error for propylene and second riser cuts

Table 40 - Relative error precision intervals of LPG cut for all feeds

% of yields within precision	Precision					
	5%	10%	15%	20%	25%	35%
Catalytic gasoline	36.36%	36.36%	54.55%	72.73%	90.91%	100.00%
Coker gasoline	16.67%	41.67%	66.67%	83.33%	83.33%	100.00%
PolyC3C4	33.33%	55.56%	88.89%	100.00%		
PolyC4	81.82%	100.00%				

Table 41 - Relative error precision intervals of gasoline cut for all feeds

% of yields within precision	Precision					
	10%	15%	20%	25%	30%	35%
Catalytic gasoline	90.91%	100.00%				
Coker gasoline	50.00%	66.67%	75.00%	100.00%		
PolyC3C4	55.56%	77.78%	77.78%	77.78%	88.89%	100.00%
PolyC4	72.73%	81.82%	100.00%			

Table 42 –Relative error precision intervals of LCO cut for all feeds

% of yields within precision	Precision					
	20%	30%	40%	50%	75%	100%
Catalytic gasoline	9.09%	27.27%	45.45%	54.55%	100.00%	
Coker gasoline	25.00%	25.00%	33.33%	33.33%	83.33%	100.00%
PolyC3C4	22.22%	33.33%	44.44%	55.56%	100.00%	
PolyC4	27.27%	45.45%	45.45%	45.45%	81.82%	100.00%

Table 43 - Relative error precision intervals of coke for all feeds

% of yields within precision	Precision					
	10%	20%	40%	50%	75%	100%
Catalytic gasoline	9.09%	18.18%	81.82%	100.00%		
Coker gasoline	0.00%	8.33%	25.00%	33.33%	100.00%	
PolyC3C4	11.11%	22.22%	66.67%	77.78%	100.00%	
PolyC4	18.18%	36.36%	63.64%	81.82%	90.91%	100.00%

Table 44 – Relative error precision intervals of O_3 for all feeds

% of yields within precision	Precision						
	5%	10%	15%	20%	30%	40%	50%
Catalytic gasoline	27.27%	36.36%	54.55%	72.73%	81.82%	90.91%	100.00%
Coker gasoline	58.33%	58.33%	66.67%	83.33%	100.00%		
PolyC3C4	66.67%	100.00%					
PolyC4	45.45%	90.91%	100.00%				

A4. Mean squared error of prediction

Table 45 – MSEP results summary

Cut/Molecular lump	Feed	2012	2014
Dry gas	Catalytic gasoline	6E-04	5E-05
	Coker gasoline	-	8E-05
	PolyC3C4	3E-04	2E-04
	PolyC4	2E-04	1E-04
P_1	Catalytic gasoline	1E-04	6E-06
	Coker gasoline	-	9E-05
	PolyC3C4	3E-05	4E-05
	PolyC4	6E-05	5E-05
P_2	Catalytic gasoline	8E-06	1E-05
	Coker gasoline	-	5E-05
	PolyC3C4	8E-05	3E-05
	PolyC4	9E-05	1E-04
LPG	Catalytic gasoline	6E-04	4E-04
	Coker gasoline	-	3E-03
	PolyC3C4	6E-04	3E-03
	PolyC4	5E-04	4E-04
O_3	Catalytic gasoline	1,0E-04	9,7E-05
	Coker gasoline	-	3E-04
	PolyC3C4	3E-04	1E-04
	PolyC4	1,6E-04	2,4E-04
O_4	Catalytic gasoline	8E-05	1E-04
	Coker gasoline	-	3E-04
	PolyC3C4	1,2E-03	9,7E-04
	PolyC4	1,7E-03	1,6E-03
Gasoline	Catalytic gasoline	8E-04	1E-03
	Coker gasoline	-	5E-03
	PolyC3C4	9E-04	2E-03
	PolyC4	6,3E-04	6,4E-04
Olefin lump O_{5^+}	Catalytic gasoline	1E-04	2E-05
	Coker gasoline	-	2E-04
	PolyC3C4	1E-04	7E-05
	PolyC4	4E-05	6E-05
A_6	Catalytic gasoline	3E-04	5E-05
	Coker gasoline	-	1E-04
	PolyC3C4	3E-04	1E-04
	PolyC4	2,8E-06	3,0E-06
A_7	Catalytic gasoline	2E-04	9E-04
	Coker gasoline	-	9E-04
	PolyC3C4	1,9E-05	1,9E-05
	PolyC4	3E-05	4E-05

Table 46 - MSEP results summary (continuation)

Cut/Molecular lump	Feed	2012	2014
A_8	Catalytic gasoline	3E-04	1E-03
	Coker gasoline	-	1E-03
	PolyC3C4	2,2E-04	1,6E-04
	PolyC4	6E-05	5E-05
Naphthene lump	Catalytic gasoline	2E-05	3E-05
	Coker gasoline	-	1E-04
	PolyC3C4	4E-05	9E-05
	PolyC4	2E-07	5E-06
Total paraffins lump C_{5+}	Catalytic gasoline	2E-04	4E-04
	Coker gasoline	-	3E-04
	PolyC3C4	1,8E-04	2,3E-04
	PolyC4	2E-04	6E-05
Isoparaffins lump ($C_4 - C_{12}$)	Catalytic gasoline	-	2E-04
	Coker gasoline	-	1E-04
	PolyC3C4	-	2E-04
	PolyC4	-	1E-04
LCO	Catalytic gasoline	2E-04	1E-04
	Coker gasoline	-	2E-04
	PolyC3C4	1,6E-04	1,7E-04
	PolyC4	1E-04	4E-05
Coke	Catalytic gasoline	1E-04	9E-05
	Coker gasoline	-	3E-04
	PolyC3C4	3,3E-04	2,7E-04
	PolyC4	5E-05	8E-05